



SERRI Report 70015-005

NUMERICAL MODELING OF BRIDGES SUBJECTED TO STORM SURGE FOR MITIGATION OF HURRICANE DAMAGE



SERRI Project: *Increasing Community
Disaster Resilience Through Targeted
Strengthening of Critical Infrastructure*

Project Principal Investigator:

Isaac L. Howard, PhD

Report Written and Performed By:

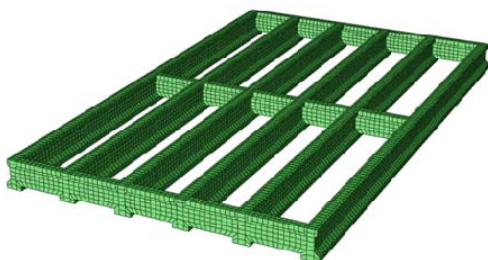
Philip M. Gullett - Mississippi State University

Mary-Margaret Dickey - Barter and Associates, Inc.

Isaac L. Howard - Mississippi State University



"An Industry, Agency & University Partnership"



This material is based upon work supported by the U.S. Department of Homeland Security under U.S. Department of Energy Interagency Agreement 43WT10301. The views and conclusions contained in this document are those of the authors and should not be interpreted as necessarily representing the official policies, either expressed or implied, of the U.S. Department of Homeland Security.

SERRI Project: Increasing Community Disaster Resilience
Through Targeted Strengthening of Critical Infrastructure

Performing Organization Report No. CMRC-10-02

**NUMERICAL MODELING OF BRIDGES SUBJECTED
TO STORM SURGE FOR MITIGATION OF HURRICANE DAMAGE**

Written By:

Philip M. Gullett, PhD, PE, Associate Professor, Mississippi State University
Mary-Margaret Dickey, PE, Design Engineer, Barter and Associates, Inc.
Isaac L. Howard, PhD, Associate Professor, Mississippi State University

Date Published:

August 2012

Prepared for
U.S. Department of Homeland Security
Under U.S. Department of Energy Interagency Agreement 43WT10301

Prepared by
OAK RIDGE NATIONAL LABORATORY
Oak Ridge, Tennessee 37831-6283
managed by
UT-BATTELLE, LLC
for the
U.S DEPARTMENT OF ENERGY
under contract DE-AC05-00OR22725

This page was intentionally left blank.

TABLE OF CONTENTS

LIST OF FIGURES	viii
LIST OF TABLES	x
ACKNOWLEDGEMENTS	xi
LIST OF SYMBOLS	xii
LIST OF ACRONYMS	xvii
EXECUTIVE SUMMARY	xviii

CHAPTER 1 – INTRODUCTION

1.1	General and Background Information	1
1.2	Objectives	2
1.3	Scope.....	2
1.4	Incorporation into the National Response Framework	3

CHAPTER 2 – LITERATURE AND PRACTICE REVIEW5

2.1	Overview of Literature and Practice Review.....	5
2.2	Storm Surge and Offshore Structures	5
2.2.1	Morison et al. (1950).....	5
2.2.2	Bea et al. (1999)	6
2.3	Storm Surge and Coastal Structures	7
2.3.1	Denson (1978, 1980, 1981).....	7
2.3.2	McConnell et al. (2003).....	7
2.3.3	Douglass et al. (2006, 2008).....	9
2.3.4	Ramey et al. (2008)	10
2.3.5	Sheppard and Marin (2009).....	13
2.3.6	AASHTO LRFD Specifications	15
2.3.7	AASHTO <i>Guide Specifications</i>	15
2.3.7.1	AASHTO <i>Guide Specifications</i> Maximum Vertical Load Case	15
2.3.7.2	AASHTO <i>Guide Specifications</i> Maximum Horizontal Load Case	16
2.3.8	Jin et al. (2008).....	17

2.3.9	Oregon State University	17
2.4	Damage Due to Storm Surge	20
2.5	Survey of Gulf Coast DOT's	21
2.5.1	Bridge Failures Attributed to Storm Surge and/or Hurricanes.....	21
2.5.2	DOT Design Procedures for Storm Surge on Bridges	23
2.6	Retrofit of Bridges for Storm Surge.....	24
 CHAPTER 3 – FINITE ELEMENT MODELING		27
3.1	Overview of Finite Element Modeling	27
3.2	Wave Load Modeling Approach.....	29
3.3	Idealized Wave Loads.....	30
3.3.1	Wave Theory Model	30
3.3.2	Wave Load Model Equations.....	32
3.4	FEM Wave Loads	33
3.4.1	Surface Impact Loading.....	34
3.4.2	Body Loads	35
3.5	Wave Load Model Verification	36
3.5.1	Verification Simulation Model	36
3.6	Wave Force Validation	37
3.6.1	FEM Structural Model	39
3.6.2	WLS Storm Models	39
3.6.3	Wave Force Coefficient Determination.....	41
3.6.4	Horizontal Drag and Inertia Coefficients.....	42
3.6.5	Vertical Force Coefficients	45
3.6.5.1	Buoyancy	46
3.6.5.2	Vertical Drag.....	49
3.6.5.3	Vertical Inertia	50
3.6.5.4	Vertical Drag Coefficient.....	50
3.7	Summary.....	52

CHAPTER 4 – FULL SCALE SIMULATIONS	53
4.1 Overview of Full Scale Simulations	53
4.2 Modeled Bridge Structure.....	53
4.3 Finite Element Model	54
4.3.1 Finite Element Mesh	54
4.3.2 Bridge Supports	54
4.3.3 Wave Profiles.....	55
4.3.3.1 Wave Profiles for Recent Hurricanes	55
4.3.3.2 Predicted Profiles for Storm Categories	55
4.3.4 Wave Force Coefficients.....	58
4.4 Maximum Total Reaction Forces.....	59
4.5 Maximum Force on a Single Beam	61
4.6 Comparison with AASHTO Loads.....	62
4.7 Comparison with AASHTO Single Girder Loads	64
CHAPTER 5 – RETROFIT DESIGN FOR STORM SURGE.....	68
5.1 Retrofit Design Overview	68
5.2 Examination of <i>Retrofit Manual</i> Strategies for Rapid Deployment	68
5.2.1 Reduction of Buoyancy Loads	68
5.2.2 Reduction of Wave Loads	69
5.2.3 Connection to Adjacent Spans	69
5.2.4 Connection of Bridge Superstructure to Substructure.....	69
5.3 Rapid Retrofit Options.....	70
5.3.1 Deck Venting Performed from Deck.....	70
5.3.2 Connection Between Substructure and Superstructure Installed from Deck	71
5.3.2.1 Design Loads	72
5.3.2.2 Design Load Evaluation.....	73
5.4 Rapid Retrofit Summary	74

CHAPTER 6 – SUMMARY CONCLUSIONS AND RECOMMENDATIONS.....	76
6.1 Summary	76
6.2 Conclusions.....	77
6.3 Recommendations.....	78
CHAPTER 7 – REFERENCES.....	79

LIST OF FIGURES

Figure 1.1.	Biloxi Bay Bridge-Hurricane Katrina-2005 Atlantic Hurricane Season	2
Figure 2.1.	Example of Fuse Element from <i>Retrofit Manual</i> (Used with Permission)	26
Figure 3.1.	The Geometric Complexity of the Girders and Diaphragm of a 1:5 Scale Bridge Model (Top) is Preserved in the Corresponding Finite Element Representation (Bottom).....	28
Figure 3.2.	Flow Chart Showing the Finite Element Based Wave Load Modeling Approach.....	29
Figure 3.3.	Wave Flow Variable Definitions	31
Figure 3.4.	Impact Surfaces (Left in Red) Represented by Individual Finite Element Faces (Right)	34
Figure 3.5.	An Element Face is Specified in Terms of Positions of Its Corners (Nodes).....	35
Figure 3.6.	Approximation of the Submerged Element Volume is Illustrated for the 2D Case.....	36
Figure 3.7.	Model Verification was Performed Using a Simple Block Geometry	36
Figure 3.8.	A Two Element Rectangular Box with Nodal Coordinates Shown was Used to Verify the Finite Element Implementation of the Wave Force Equations.....	37
Figure 3.9.	OSU Model of a Typical Escambia Bay Bridge Section Over Escambia Bay (Bradner 2008)	38
Figure 3.10.	OSU Bridge Cross Section.....	38
Figure 3.11.	OSU Girder Cross Section	38
Figure 3.12.	The Relative Size of the Simulated Wave Compared to the Bridge Structure for Periods: T=2.0 sec (Top),T=2.5 sec (Center) and T=3.0 sec (bottom)	41
Figure 3.13.	Experimentally Determined Maximum Horizontal Forces are Plotted Against Wave Height for the Three Wave Periods Considered	42
Figure 3.14.	The Velocity (Top) and Acceleration (Bottom) Vector Fields for One Wave Cycle	43
Figure 3.15.	The Relative Size of the Horizontal Reaction Force Scaled by Bridge Weight Due to Drag (CD), Inertia (CM), and the Additive Total (Tot)	44
Figure 3.16.	Experimentally Determined Maximum Vertical Reaction Forces are Plotted Against Wave Height for the Three Wave Periods Considered	46
Figure 3.17.	Uplift Due to Buoyancy for T=2.0 (Top), T=2.5 (Middle) and T=3.0 (bottom).....	47
Figure 3.18.	The Position of the Wave at Maximum Buoyancy for T=3.0, Between Times 0.9 (Bottom) and 1.1 sec (Top).....	48
Figure 3.19.	Maximum Buoyancy Forces as Function of Wave Height.....	48
Figure 3.20.	Computed Vertical Drag Forces are Shown for T=2.0.....	49
Figure 3.21.	Computed Vertical Drag Forces are Shown for T=2.5.....	49
Figure 3.22.	Computed Vertical Drag Forces are Shown for T=3.0 sec.....	50
Figure 4.1.	Biloxi Bay Bridge Typical Span and Girder Cross Sections	53
Figure 4.2.	Biloxi Bay Bridge Model.....	54
Figure 4.3.	Wave Profiles for Recent Hurricanes	55
Figure 4.4.	Modeled Category I Predicted Profiles.....	57

Figure 4.5.	Modeled Category II Predicted Profiles	57
Figure 4.6.	Modeled Category III Predicted Profiles	58
Figure 4.7.	Modeled Category IV Predicted Profiles	58
Figure 4.8.	Modeled Category V Predicted Profiles	58
Figure 4.9.	Shows the Data Used to Determine Wave Forcing Function Coefficients for the Full Scale Simulations	59
Figure 4.10.	Illustrates the Direction of Vertical Force Components With Respect to a Single Girder. F_y is the load caused by wave action, W is the Weight and R_y is the Reaction on the Bottom Surface of the Girder.....	60
Figure 4.11.	The Relationship Between AASHTO and WFS Predicted Vertical Loads for Various Levels of Percentage Entrapped Air are Shown. The Best Agreement was Found for %AIR = 20	64
Figure 4.12.	The Relationship Between AASHTO <i>Guide Specifications</i> and WFS Predicted Vertical Loads for Various Levels of Percentage Entrapped Air. The Best Agreement was Found for %AIR = 20	65
Figure 4.13.	The Relationship Between AASHTO and WFS Predicted Single Girder Maximum Loads for %AIR=20	67
Figure 5.1	Example Retrofit Schematic	71

LIST OF TABLES

Table 2.1.	Force Estimates Provided by Douglass et al. (2006)	9
Table 2.2.	Saffir-Simpson Hurricane Wind Scale.....	20
Table 2.3.	Notable Bridge Failures Attributed to Storm Surge/Hurricanes.....	22
Table 3.1.	Simulation Results Compared to Analytic Solutions for a Simple Verification Model	37
Table 3.2.	Simulation Load Cases for Oregon State Scaled Model.....	40
Table 3.3.	Wave Lengths and Wave Length to Depth Ratio's for Simulated Waves.....	40
Table 3.4.	Time for Crest to Reach Bridge Span Centerline	41
Table 3.5.	Horizontal Drag and Inertia Coefficients for Simulation Wave Periods and Wave Heights	44
Table 3.6.	Maximum Horizontal Reaction Forces from Simulations and Experiments	45
Table 3.7.	The Drag Coefficients Needed to Match the Measure Maximums When Only Drag and Buoyancy Forces Considered are Exceptionally Large	51
Table 3.8.	Summary of Buoyancy Constant, C_b , Needed to Match the Measured Maximums	51
Table 3.9.	Maximum Horizontal Reaction Forces from Simulations and Experiments	52
Table 4.1.	Wave Profiles for Recent Hurricanes	55
Table 4.2.	Galveston Causeway Extreme Wave Heights (ft) as Functions of Surge Height and Storm Category	56
Table 4.3.	Galveston Causeway Extreme Wave Periods (sec) as Functions of Surge Height and Storm Category	56
Table 4.4.	Extreme Wave and Storm Surge Estimations	57
Table 4.5.	Scaled Total Reaction Model Results	61
Table 4.6.	Scaled Maximum Beam Reaction Model Results	62
Table 4.7.	<i>Guide Specifications</i> Case I Extreme Event Limit State Loads by Type at Trailing Edge Far Side Girder	63
Table 4.8.	AASHTO Case I Extreme Event Vertical Wave Loads	64
Table 4.9.	Comparison of AASHTO Case I Extreme Event, and WFS Maximum Single Girder Loading.....	66
Table 5.1.	Maximum Calculated Total Anchorage and Girder Anchorage for Simply Supported Span.....	73
Table 5.2	The Approximate Number of Anchors Required Based on Steel Strength	74

ACKNOWLEDGEMENTS

Thanks are due to many for the successful completion of this project. The authors are especially grateful for the financial support provided by the *SERRI* program. In addition, due gratitude is extended to everyone employed at *DHS* and *ORNL* who worked diligently with the authors to make this project a success. A great deal of the success of this research can be attributed to the efforts of *DHS* and *ORNL* personnel.

State Departments of Transportation and the Federal Highway Administration were especially helpful during the research. The following individuals provided direct assistance to the research in the form of research data, technical guidance, and feedback. Many of the individuals indicated were also members of the *AASHTO/FHWA Wave Task Force* and provided data regarding those activities in addition to efforts within their respective DOT's. Their efforts were of the utmost importance in this research.

- **Dr. Firas I. Sheikh Ibrahim, PE**-Team Leader of Infrastructure
Inspection & Management-Federal Highway Administration
- **Mr. Buddy Black, PE**-Bridge Engineer-Alabama DOT
- **Mr. Mitchell K. Carr, PE**-Bridge Engineer-Mississippi DOT (Retired)
- **Mr. Dacio Marin III, PE**-Bridge Design Group Leader-Texas DOT
- **Mr. Greg Perfetti, PE**-State Bridge Design Engineer-North Carolina DOT
- **Mr. Rick Renna, PE**-State Hydraulics Engineer-Florida DOT
- **Mr. Steven Sibley, PE**-Bridge Inspection Engineer-Louisiana DOT

Dr. Daniel Cox and Dr. Solomon C. Yim of Oregon State University made considerable contributions to the research effort. Dr. Cox was gracious in hosting members of the MSU research team at the O.H Hinsdale Wave Research Laboratory, and both Dr. Cox and Dr. Yim provided substantial technical information by way of publications that were very useful to the research. Dr. D. Max Sheppard of the University of Florida was very helpful in providing information used during completion of this project. *Concrete Coring Company of Central Kentucky* provided technical assistance regarding coring concrete bridge decks. The efforts of all these individuals were essential to the success of this project and thanks are due as a result.

Special thanks to Dr. William McAnally for his technical review of this work and the helpful comments that he provided.

LIST OF SYMBOLS

Values in parenthesis indicate the equation where the symbol was used. To preserve continuity with the original sources, symbols were used as shown in the original text whenever possible. This resulted in the same symbol being used in more than one equation in some instances.

a	fluid acceleration (2.1)
a	water acceleration (2.6)
a	empirical parameter (2.11)
$a_0 - a_6$	AASHTO <i>Guide Specifications</i> Parameters (2.39)
a_m	AASHTO <i>Guide Specifications</i> Parameter (2.40)
b	empirical parameter (2.11)
b_h	element depth (2.8)
b_l	element length (2.8)
b_m	AASHTO <i>Guide Specifications</i> Parameter (2.40)
$b_0 - b_6$	AASHTO <i>Guide Specifications</i> Parameters (2.37)
b_w	element width that is normal to direction of wave attack (2.8 to 2.10)
c_h^{mc}	an empirical coefficient from McConnell's work, 1.0 (2.25)
c_l	clearance between soffit level and still water level (2.9, 2.10)
c_m	AASHTO <i>Guide Specifications</i> Parameter (2.40)
<i>coords</i>	position of the current element integration point by the array (---)
c_r	reduction coefficient for reduced horizontal load on the internal girders (2.13)
c_r	reduction coefficient for reduced horizontal load on half of the girders beyond the seaward girder, 0.33 (2.25)
c_{v-va}	empirical coefficient for the vertical varying load (2.12, 2.13)
c_v^{mc}	empirical coefficient from McConnell's work, 1.0 (2.24)
d	water depth (---)
d	still water elevation (3.1, 3.3 to 3.6)
d_b	maximum storm surge elevation (2.18, 2.19)
d_b	girder height plus slab thickness for girder bridges, slab thickness plus deck thickness for slab bridges (2.40)
d_s	depth of water at toe of wall (2.20, 2.21)
d_s	area of bridge projection into the horizontal plane (2.23)
d_s	water depth at or near the bridge including surge, astronomical tide, and local wind setup (2.37)
f	force (---)
f_b	buoyancy force per unit volume (---)
f_{brkw}	total breaking wave load per unit length of wall acting at the SWL (2.23)
g	gravity (2.36, 3.1, 3.8, 3.12)
h	wetted height (2.17, 2.19)
h	wave height (---)
h_{bd}	deck plus railing height (2.19)
h_c	lesser of 0.78*maximum wave height or bridge depth (2.18)
h_{bd}	deck plus railing height (2.21)

$h_{element}$	element height (3.12)
$h_{submerged}$	submerged height (3.12)
h_{wd}	bridge height (2.21)
$jltyp$	type of force (---)
k	$2\pi/L$ wave number (3.2 to 3.6)
m_e	effective mass (2.33, 2.35)
$noel$	unique number identifying current element (---)
p_1	pressure at the top of the element (2.8 to 2.10)
p_2	pressure at the bottom of the element (2.8 to 2.10)
q	force per unit length (2.1)
r	rail height (2.40)
t	current time (3.2 to 3.6, 3.12)
u	fluid velocity (2.1, 2.3 to 2.5)
u	horizontal fluid velocity (2.32, 2.33)
u	horizontal velocity field (3.3, 3.9a, 3.10a)
\dot{u}	horizontal acceleration field (3.4, 3.10a)
w	wetted width (2.17)
w	vertical velocity field or vertical fluid velocity (2.35, 3.5, 3.9b, 3.10b)
\dot{w}	vertical acceleration field (3.5, 3.10b)
x	AASHTO <i>Guide Specifications</i> Parameter (2.37, 2.39)
x	horizontal position (3.2 to 3.6)
x	half bridge width (3.12)
y	AASHTO <i>Guide Specifications</i> Parameter (2.37, 2.39)
z	vertical position relative to the still water elevation (3.3 to 3.6)
A	vertical deck area (2.3 to 2.6)
A	AASHTO <i>Guide Specifications</i> Parameter (2.38)
A_h	area of bridge projection into the vertical plane (2.15, 2.27)
A_X	horizontal deck area (2.32)
A_x	projected area of wave crest impact in horizontal plane (3.9a, 3.10a)
A_v	area of bridge projection into the horizontal plane (2.14, 2.26)
A_y	projected area of wave crest impact in vertical plane (3.9b, 3.10b)
A_Z	vertical deck area (2.34)
B	AASHTO <i>Guide Specifications</i> Parameter (2.38)
BC	boundary condition (---)
CD	simulation used for determination of C_{dx} (---)
C_D	friction drag coefficient (2.1)
C_d	drag coefficient (2.4)
C_{DX}	horizontal drag coefficient (2.32)
C_{dx}	horizontal drag coefficient (3.10a)
C_{dy}	vertical drag coefficient (3.10b)
C_{DZ}	vertical drag coefficient (2.34)
C_l	lifting coefficient (2.5)
C_I	inertia coefficient (2.35)
CM	simulation used for determination of C_m (---)
C_M	inertia coefficient (2.1)

C_m	inertia coefficient (2.6)
C_{mx}	horizontal inertia coefficient (3.11a)
C_{my}	vertical inertia coefficient (3.11b)
C_p	dynamic pressure coefficient (2.23)
C_s	slamming coefficient (2.3, 3.9a, 3.9b)
D	cylinder diameter (2.1)
D	depth of water one wavelength from wall (2.20, 2.21)
F_A	force due to acceleration of the body (---)
F_B	buoyancy force (2.31)
F_b	buoyancy force (2.2, 3.7)
f_b	buoyancy force (3.12)
F_{brkw}	total breaking wave load acting at the still water level (2.22)
F_d	drag force (2.2, 3.7)
F_d/W	drag force divided bridge weight (---)
F_{dx}	horizontal drag force (3.10a)
F_{dy}	vertical drag force (3.10b)
F_{DX}	horizontal drag force (2.30)
F_{DZ}	vertical drag force (2.31)
F_e	dynamic loading factor (2.7)
F_{exp}/W	force measured during OSU experiments divided by bridge weight (---)
F^*	basic wave force, either F_v^* or F_h^* (2.11)
F_g	gravitational load (positive down) (---)
F_h	horizontal force (2.13)
F_h	horizontal wave force (2.16, 2.18, 2.20)
F_h^*	horizontal basic wave force (2.9, 2.10)
F_h^*	reference horizontal load (2.13, 2.25)
F_{H-AV}	horizontal force associated with F_{V-MAX} (2.39)
F_{hqst+}	horizontal landward acting force caused by the wave impacting the beam (---)
F_{H-MAX}	horizontal quasi-static hydrostatic and hydrodynamic force (2.41)
F_{hqst-}	horizontal landward force caused by the wave impacting the back of the beam due to trapping of the wave by the deck (---)
F_i	inertia force (2.2, 3.7)
F_{ix}	inertial drag (3.11a)
F_{iy}	inertial drag (3.11b)
F_l	vertical lift force (2.2)
F_{max}	transient impact force with relatively large magnitude (---)
F_{qs}	equivalent quasi-static design force (2.11)
F_{qs+}	maximum vertical or horizontal positive quasi-static force (---)
F_{qs-}	maximum vertical or horizontal negative quasi-static force (---)
F_s	slamming force (2.2, 2.7, 3.7)
F_s	vertical slamming force (2.38)
F_{sx}	transient slamming force (3.9a)
F_{sy}	transient slamming force (3.9b)
F_s'	effective slamming force (2.7)
F_{tw}	total force from a wave crest impact (2.2, 3.7)

F_x/W	force in x-direction divided by bridge weight (---)
F_y/W	force in y-direction divided by bridge weight (---)
F_v	vertical force (2.12)
F_v	vertical wave force (2.17, 2.19, 2.21)
F_{V-AH}	vertical force associated with F_{H-MAX} (2.42)
F_{V-MAX}	vertical quasi-static hydrostatic and hydrodynamic force (2.37, 2.40)
F_{vqs+}	vertical upward acting force caused by the slam of the deck or beam (---)
F_{vqs-}	vertical downward acting force caused by inundation of the deck (---)
F_v^*	vertical basic wave force (2.8)
F_v^*	reference vertical load (2.12, 2.24)
F_X	total horizontal quasi-static force from a wave crest impact (2.30)
$F_{x-Inertia}$	horizontal inertia force (2.30)
F_Z	total vertical quasi-static force from a wave crest impact (2.31)
$F_{z-Inertia}$	vertical inertia force (2.31)
H	wave height (3.2 to 3.6)
H/D	bridge height to water depth ratio (---)
H_b	maximum wave height (2.20, 2.21)
H_{max}	maximum probable wave height (2.37 to 2.40)
H_s	significant wave height (2.11)
K	relative amplitude of the Keulegan-Carpenter number
L	length, perpendicular to wave action (2.17 to 2.21)
L	wave length (3.1, 3.12)
L	wall length (---)
LC	load case (---)
L_B	length of bridge (2.28, 2.29)
L_D	wave length in water depth of D (2.20, 2.21)
M_{T-AH}	overturning moment associated with F_{H-MAX} (2.43)
M_{T-AV}	overturning moment associated with F_{V-MAX} (2.40)
N	number of girders supporting the bridge span deck (2.13, 2.25)
R	total vertical reaction (---)
Re	Reynolds number (---)
R_x/W	reaction force in x-direction divided by bridge weight (---)
R_y/W	reaction force in y-direction divided by bridge weight (---)
R_z/W	reaction force in z-direction divided by bridge weight (---)
Sim	result from finite element simulation
T	wave period (3.1, 3.12)
TAF	trapped air factor (2.37)
Tot	horizontal reactions from additive (---)
T_p	period of the waves with the greatest energy exhibited in a spectrum (2.37)
V_s	submerged volume (2.36, 3.8, 3.11a, 3.11b)
V	Volume (3.12)
W	total width of bridge, in the direction of wave propagation (2.39)
W	total bridge weight (---)
W^*	effective bridge width (2.40)
W_B	width of bridge (2.28, 2.29)
\bar{W}	AASHTO <i>Guide Specifications</i> Parameter (2.37)

α	adjusted bridge width (2.41)
β	AASHTO <i>Guide Specifications</i> Parameter (2.37)
Δz_h	elevation difference of maximum wave crest and the centroid of A_h (2.15)
Δz_h	elevation difference of maximum wave crest and elevation of the centroid of A_h or elevation difference between the elevation of the top of the solid portion of the guard rail and elevation of centroid of A_h , whichever is smaller (2.27)
Δz_v	elevation difference of maximum wave crest and bridge deck underside (2.14)
Δz_v	elevation difference of maximum wave crest and bottom of the end diaphragms or elevation difference of the top of the solid portion of the guard rail and bottom of the end diaphragms, whichever is smaller (2.26)
η	wave surface elevation (3.2)
λ	wave length (2.38 to 2.40)
η_{max}	maximum crest height
ω	adjusted bridge width (2.41)
ω	$2\pi/T$ is the radian frequency (3.2 to 3.6)
ρ	fluid density (2.1)
ρ	mass density of seawater (2.3 to 2.6, 2.36, 3.8, 3.9a, 3.9b, 3.10a, 3.10b, 3.11a, 3.11b, 3.12)
ρ_{water}	mass density of seawater (---)
$\rho_{concrete}$	mass density of concrete (---)
γ	unit weight of water (2.14, 2.15, 2.16, 2.18, 2.19, 2.20, 2.21, 2.23, 2.26, 2.27)
γ_w	unit weight of water (2.37 to 2.39)

LIST OF ACRONYMS

AASHTO	American Association of State Highway and Transportation Officials
ADCIRC	Advanced Circulation Model for Coastal Ocean Hydrodynamics
ADT	Average Daily Traffic
ASCE	American Society of Civil Engineers
ASTM	American Society for Testing and Materials
BC	Boundary Condition
CEE	Civil and Environmental Engineering
CI	Criticality Index
DHS	Department of Homeland Security
DOT	Department of Transportation
ESF	Emergency Support Function
FEM	Finite Element Method or Finite Element Modeling
FEMA	Federal Emergency Management Agency
FHWA	Federal Highway Administration
HLT	Hurricane Liaison Team
LRFD	Load Resistance Factor Design
MDOT	Mississippi Department of Transportation
MSU	Mississippi State University
NRF	National Response Framework
NICC	National Infrastructure Coordinating Center
ORNL	Oak Ridge National Laboratory
OSU	Oregon State University
RMA2	Resource Management Associates 2
SERRI	Southeast Region Research Initiative
SWAN	Simulating Waves Nearshore
SWE	Still Water Elevation
SWL	Still Water Level
US	United States
USACE	United States Army Corps of Engineers
WLS	Wave Load Software

EXECUTIVE SUMMARY

This report is a standalone document that was performed through Task Order 4000064719. Ten additional reports with unique content were also part of this task order that were related to other aspects of disaster response and recovery.

The primary objective of the research presented in this report was to perform finite element modeling to determine forces on highway bridges as a result of storm surge and wave action and use these forces to investigate the feasibility of rapid retrofit techniques to prevent failure. Both objectives were met. The retrofit evaluation performed is a fairly traditional assessment that makes use of fundamental principles. The finite element modeling (FEM) approach, however, is fairly unique and has applications beyond those presented in this report.

A three component FEM approach was developed and used in this research; the components are a structural model, a wave load model, and an element data transfer model. The structural model is comprehensive but is not unique and can be performed with a variety of commercially available FEM software packages (Abaqus was used in this project). The wave load model (named wave load software (WLS) by the authors) is much more unique and is a key component to this project. The WLS was written in Fortran (other languages could be used) and is a set of software routines that generates wave based surface and body forces based on a wave theory model that has core functionality that is independent of the FEM model. The element data transfer model was also written in Fortran (other languages could be used) to communicate problem specific information between the FEM structural model and the WLS. A third program (Python) was used to submit the multiple load cases and to extract numerical results in an automated manner.

The WLS was calibrated using measured data provided by Oregon State University. The calibrated model was compared to a fairly recently released American Association of State Highway and Transportation Officials (AASHTO) document for storm surge on coastal highway bridges. The model compared well with the AASHTO document and has many appealing uses.

Research results showed rapid retrofit of a highway bridge to resist uplift forces due to storm surge appears to be feasible for some storm events depending on the retrofit method employed. Venting the bridge deck to reduce forces due to entrapped air appears to be the most viable rapid retrofit approach. Anchoring the superstructure to the substructure in a rapid manner appears more useful for lower category storms than for higher category storms.

CHAPTER 1 – INTRODUCTION

1.1 General and Background Information

The work presented in this report was developed in partial fulfillment of the requirements of Task Order 4000064719 sponsored by the *Department of Homeland Security (DHS)* through its *Southeast Region Research Initiative (SERRI)* program administered by *UT-Battelle* at the *Oak Ridge National Laboratory (ORNL)* in Oak Ridge, Tennessee. The research was proposed by members of the *Department of Civil and Environmental Engineering (CEE)* at *Mississippi State University (MSU)* to *SERRI* in a document dated 1 June 2007. The proposed research was authorized by *UT-Battelle* in its task order dated 10 December 2007. This task order included a scope of work defined through joint discussions between *MSU* and *SERRI*. Work on the project was initiated on 1 January 2008. A modification of Task Order 4000064719 was proposed on 9 September 2008 and agreed upon on 29 September 2008. A second Task Order modification dated 22 June 2010 was also performed, which is the Task Order used to generate this report.

The scope of work associated with Task Order 4000064719 included several related components. The general objectives of the project were to investigate means for rapidly using on-site materials and methods in ways that would most effectively enable local communities to rebuild in the wake of a flooding disaster. Within this general framework, several key work components were associated with Task Order 4000064719. Specifically, the scope of work dated 22 June 2010 includes research efforts in the following six task groups:

Task 1: Erosion Control-Erosion Protection for Earthen Levees.

Task 2: Bridge Stability-Lateral & Uplift Stability of Gravity-Supported Bridge Decks.

Task 3: Levee Breach Repair-Closure of Breaches in Flood Protection Systems.

Task 4: Pavement Characterization and Repair.

Task 5: Emergency Construction Material Development-Staging Platform Construction.

Task 6: Fresh Water Reservoir-Restoration of Fresh Water Supplies.

The work contained herein was associated with Task 2. The report of this work was the 5th deliverable of the research project, hence the designation of the report as *SERRI Report 70015-005* of Task Order 4000064719. The research contract was delivered in a series of reports to allow users to more efficiently obtain the information of interest.

Research within Task 2 was motivated by past occurrences where storm surge from events such as hurricanes destroyed bridges. Figure 1.1 is an example from the 2005 Atlantic Hurricane Season. Many other examples are available such as the bridges destroyed during Hurricane Dolly during the 2008 Atlantic Hurricane Season. Bridge failures where the deck and supporting beams (often called girders), referred to collectively as superstructure, are lifted from the substructure often occur in storm surge conditions as evidenced by Figure 1.1.



Figure 1.1. Biloxi Bay Bridge-Hurricane Katrina-2005 Atlantic Hurricane Season.

1.2 Objectives

A key component of this research was to develop solutions which may be rapidly deployed to achieve maximum benefit to the community, typically through the use of on-site materials, pre-engineered components, and innovative construction materials and techniques. This research aimed to develop solutions for protecting and/or expeditiously reconstituting critical civil infrastructure components. In this context, the specific objective of the total effort of Task Order 4000064719 was to develop specialty materials and design and construction procedures which may be rapidly deployed to protect and restore selected key civil infrastructure components.

The primary objective of the research presented in this report was to perform finite element modeling to determine forces on highway bridges as a result of storm surge and use these forces to investigate the feasibility of rapid retrofit techniques to prevent failure. To accomplish the objective a finite element modeling framework had to be developed where auxiliary routines specific to this research were written. The purpose of the retrofit techniques is to provide additional lateral and/or uplift stability to prevent bridge decks from being destroyed during hurricanes or similar events.

1.3 Scope

For the specific research component described in this report (Task 2), the revised scope of work dated 22 June 2010 includes the six subtasks summarized below. These six subtasks are the full deliverable of Task 2; this report fully addresses all six subtasks.

- a) Contact Departments of Transportation in the southeastern US to obtain feedback and information related to storm surge on bridges. Also identify, contact, and potentially visit key research groups dealing with storm surge.

- b) Define the geometry of the bridge as it will be incorporated into the numerical models.
- c) Develop conventional records of wave forces versus time using significant storms that have ravaged portions of the southeastern U.S.
- d) Simulate the behavior of the prototype bridge during application of the wave force records and investigate various retrofit methods to prevent failure, and determine a set of properties (e.g., material strength and stiffness, member geometry, connection type) required to provide an acceptable level of restraint for the prototypical bridge during application of the wave force records.
- e) Use the required properties from d) as a performance specification to determine if commercially available materials and equipment could successfully restrain the bridge under the wave force records. Information related to retrofit will be obtained from the *AASHTO Subcommittee on Bridges and Structures*. The retrofit technique and the integrity of the bridge are both considerations.
- f) Assess the construction feasibility of any solutions deemed feasible in e).

The focus of this research was highway bridges. Railway bridges are a notable infrastructure component but evidence from Hurricane Katrina placed their performance above highway bridges. DesRoches (2006) noted that railroad bridges remained standing in Lake Pontchartrain and the Biloxi Bay while adjacent highway bridges lost their superstructure. It is notable that railway bridges are designed for much heavier loads than are highway bridges.

A visit to the Mississippi coast following Hurricane Katrina prompted members of the research team to begin studying storm surge on bridges beginning in 2006. Funding from the current research allowed those initial investigations to be developed into a more comprehensive study where substantial efforts initiated in the summer of 2009.

1.4 Incorporation into the National Response Framework

The National Response Framework (*NRF*) is a document that guides the United States when conducting all-hazards response (response refers to immediate actions to save lives, protect property and the environment, and meet basic human needs. This framework is entailed in *NRF* (2008), which has complimentary material found in print and online. The *NRF* is a continuation of previous federal level planning documents (e.g. Federal Response Plan of 1992), and serves as the state of the art in responding to disaster events. The following paragraphs summarize how Task 2 performed as part of Task Order 4000064719 could be applicable to the *NRF* and in what manner. The tone of the paragraphs assumes the reader is at least casually familiar with the *NRF* and supporting documentation.

The goals of Task 2 seemingly align with the needs of the *Hurricane Liaison Team (HLT)*, whose goal is to enhance hurricane disaster response. The *NRF* is not specific as to whether response refers to actions immediately prior to an event that temporarily strengthen key infrastructure (e.g. Task 2 - gravity supported bridges). The work of Task 2 would seem to align since the work would be performed immediately prior to an event and is in response to an anticipated event. The aforementioned discussion also aligns with *Scenario 10: National Disaster-Major Hurricane* of the National Planning Scenarios that have been established in *NRF* (2008).

“The National Infrastructure Coordinating Center (*NICC*) monitors the Nation’s critical infrastructure and key resources on an ongoing basis. During an incident, the *NICC* provides a coordinating forum to share information across infrastructure and key resources sectors through appropriate information-sharing entities such as the Information Sharing and Analysis Centers and the Sector Coordinating Councils.” A potential Task 2 application of the *NICC* would be to select which bridges to temporarily strengthen.

Fifteen Emergency Support Functions (*ESF*’s) have been established under *FEMA* coordination. Of the fifteen *ESF*’s, *ESF #1-Transportation*, and *ESF #3-Public Works and Engineering* are applicable to the research conducted under Task Order 4000064719. This research effort is primarily applicable to Regions IV (Atlanta headquarters) and VI (Denton headquarters) of the ten *FEMA* regions. *ESF #3* has a primary coordinator of the *USACE* who is tasked as a support agency for multiple functions including restoring transportation infrastructure. *ESF #3* includes: 1) conducting pre-incident and post-incident public works and infrastructure assessments; 2) providing technical and engineering expertise including repair of damaged public infrastructure; 3) construction management; and 4) other scenarios outside the scope of this research. Task 2 focuses on the prevention of damage to bridges and thus aligns with *ESF #3*.

CHAPTER 2 – LITERATURE AND PRACTICE REVIEW

2.1 Overview of Literature and Practice Review

The first key item of the literature and practice review was to determine wave force characterization techniques. Select research related to analytic methods for calculating forces imparted to offshore and coastal structures subjected to surge and wave loading is presented. Although precise mathematical modeling of the physical interactions between large bridge structures and surge and wave action represents a complex multiphysics challenge, many problems involving wave impacts can be satisfactorily addressed using simplified deterministic models. While the development of such models for wave loading on components of offshore platform structures has received considerable attention (e.g. Sarpkaya et al.1981), guidance for wave loads on coastal structures, such as highway bridges, could be enhanced by studying coastal bridges with a similar comprehensiveness as offshore platform structures. This chapter reviews selected work related to wave loading on offshore structures and bridge superstructures. Sheppard and Marin (2009) provide more extensive wave loading research reviews.

The next component of the literature and practice review was to assess the damage that has occurred due to storm surge. Thereafter, a survey was sent to select departments of transportation (DOTs) to obtain guidance from experienced field engineers. The final component of the literature and practice review dealt with retrofit of highway bridges with the intent of providing storm surge resistance.

2.2 Storm Surge and Offshore Structures

2.2.1 Morison et al. (1950)

One of the first deterministic models to gain wide application is the Morison equation. Morison et al. (1950) proposed this semi-empirical equation for computing the wave loads on stationary cylindrical structures in which the wave loading was written as the sum of “a drag force proportional to the square of the velocity which may be represented by a drag coefficient having substantially the same value as for the steady flow” and “a virtual mass force proportional to the horizontal component of the accelerative force exerted on the mass of water displaced by the pile”:

$$q = C_D \rho \frac{D}{2} |u| u + C_M \rho \frac{D^2}{4} a \quad (2.1)$$

where

- q force per unit length
- ρ fluid density
- D cylinder diameter
- C_D friction drag coefficient
- C_M inertia coefficient

u fluid velocity
 a fluid acceleration

The approach was extended to include horizontal components (e.g. Kaplan and Silbert 1976) and platform decks (Bea et al. 2001).

2.2.2 Bea et al. (1999)

Bea et al. (1999) investigated forces generated by wave crests for offshore oil platform decks. Experimental results were examined as well as performance of platforms during past hurricanes. The wave load equation was formulated after Isaacson and Prasad (1994), Kaplan (1992) and writes the total platform deck force as the superposition of forces from several contributing sources.

$$F_{tw} = F_b + F_s + F_d + F_l + F_i \quad (2.2)$$

where

F_{tw} total force from a wave crest impact
 F_b buoyancy force
 F_s slamming force
 F_d drag force
 F_l vertical lift force
 F_i inertia force

As in the Morison equation, the contributing forces are written as functions of particle velocity or acceleration:

$$F_s = 0.5C_s\rho Au^2 \quad (2.3)$$

$$F_d = 0.5\rho C_d Au^2 \quad (2.4)$$

$$F_l = 0.5\rho C_l Au^2 \quad (2.5)$$

$$F_i = \rho C_m Aa \quad (2.6)$$

where

C_s slamming coefficient
 ρ mass density of seawater
 A vertical deck area
 u horizontal fluid velocity
 C_d drag coefficient
 C_l lifting coefficient
 C_m inertia coefficient
 a water acceleration

Because the slamming force is the result of transient dynamic wave action, a dynamic load factor is provided to account for possible load increase loads due to dynamic excitation.

$$F'_s = F_e F_s \quad (2.7)$$

where

F'_s effective slamming force
 F_e dynamic loading factor

2.3 Storm Surge and Coastal Structures

2.3.1 Denson (1978, 1980, 1981)

Research addressing wave loading on bridge structures and surge resistant bridge design was initiated in response to extensive damage to the Bay St. Louis Bridge and the Biloxi Bay Bridge by Hurricane Camille in 1969 (Denson 1978, Denson 1980, Denson 1981). The experimental effort investigated the magnitude of lift, drag and overturning moment that resulted from a variety of wave loading conditions.

Denson (1978) and Denson (1980) present the results of an experimental evaluation of wave impacts on a scale model of a Bay St. Louis Bridge section. The wave flume experiments included a variety of wave heights, water depths, and bridge heights for a fixed wave period of three seconds. The 1978 study included a normal wave impact angle and the 1980 study examined impact angles from 30 to 90 degrees. The bridge supports were instrumented to measure lift, drag, and rolling moment loads. The collected data was used to generate a series of charts that relate the bridge height to water depth ratio (H/D) with the non-dimensional force or moment reactions. Third order polynomials were fit to the experimental data using a least squares minimization to generate curves that were meant to supply loading guidance for the design structural support loads as a function of wave height and water depth.

Denson (1981) measured fluid pressures parallel to wave action along the width of the bridge model for a variety of wave heights and depths. Deck pressure was observed to be a linear function of wave height and included positive uplift from the crest's passing, followed by a down-pull (suction) from the trough's passing. Over wash of the seaward lane was observed to be a function of the bridge height to water depth ratio. Dimensionless curves were created to allow the design engineer to enter the curves with the appropriate H/D ratio and select the peak positive and negative pressures.

Denson's work would be difficult to extend to bridges with significantly different cross sections. Douglass et al. (2006) found that the scaled wave period used is not realistic for Biloxi Bay hurricane induced wave profiles.

2.3.2 McConnell et al. (2003)

McConnell et al. (2003) examined exposed jetties without breakwater protection. The research included wave basin testing of a scaled deck with and without beams. The scaled deck included features typical of a jetty head supported by cylindrical piles, and was fitted with four force transducers. The wave flume was capable of random wave generation and was used to test a range of wave conditions, water depths and deck heights.

A review of the force histories resulted in the identification of key force characteristics: 1) a transient impact force with relatively large magnitude (F_{max}); 2) maximum vertical or horizontal positive quasi-static force (F_{qs+}); and 3) maximum vertical or horizontal negative quasi-static force (F_{qs-}). Determination of wave forces were proposed as a scaling of vertical and horizontal force equations that were termed basic wave forces:

$$F_v^* = b_w b_l p_2 \quad (2.8)$$

$$F_h^* = b_w (\eta_{max} - c_l) \frac{p_2}{2} \quad \text{for } \eta_{max} \leq c_l + b_h \quad (2.9)$$

$$F_h^* = b_w b_h \frac{(p_1 + p_2)}{2} \quad \text{for } \eta_{max} > c_l + b_h \quad (2.10)$$

where

F_v^*	vertical basic wave force
F_h^*	horizontal basic wave force
b_w	element width that is normal to direction of wave attack
b_l	element length
b_h	element depth
η_{max}	maximum crest height
c_l	clearance between soffit level and still water level (SWL)
p_1	pressure at the top of the element
p_2	pressure at the bottom of the element

The equivalent quasi-static design force, F_{qs} , is found by scaling the basic vertical or horizontal wave force using the equation

$$\frac{F_{qs}}{F^*} = \frac{a}{\left[\frac{(\eta_{max} - c_l)}{H_s} \right]^b} \quad (2.11)$$

where

F^*	basic wave force, either F_v^* or F_h^*
a, b	empirical parameters
H_s	significant wave height

Using these equations, the work provides analysis for four types of wave loads: 1) vertical upward acting force (F_{vqs+}) caused by the slam of the bottom of the deck or beam; 2) vertical downward acting force (F_{vqs-}) caused by inundation of the deck; 3) horizontal landward acting force (F_{hqs+}) caused by the wave impacting the beam; and 4) horizontal landward force (F_{hqs-}) caused by the wave impacting the back of the beam due to trapping of the wave by the deck. The work mentions but does not include dynamic transient forces due to wave slamming.

2.3.3 Douglass et al. (2006, 2008)

Douglass et al. (2006) and Douglass et al. (2008) give a history of previous work related to wave forces and provide simple-to-apply and interim guidance for calculating wave loads on bridge structures. This work modifies McConnell et al. (2003) and provides loads to bridge structural components in terms of horizontal and vertical force components as:

$$F_v = c_{v-va} F_v^* \quad (2.12)$$

$$F_h = [1 + c_r(N - 1)] c_{h-va} F_h^* \quad (2.13)$$

where

F_v	vertical force
F_h	horizontal force
F_v^*	reference vertical load
F_h^*	reference horizontal load
c_{v-va}	empirical coefficient for the vertical varying load
c_r	reduction coefficient for reduced horizontal load on the internal girders
N	number of girders supporting the bridge span deck

The vertical and horizontal references forces have the form:

$$F_v^* = \gamma \Delta z_v A_v \quad (2.14)$$

$$F_h^* = \gamma \Delta z_h A_h \quad (2.15)$$

where

γ	unit weight of water
A_v	area of bridge projection into the horizontal plane
A_h	area of bridge projection into the vertical plane
Δz_v	elevation difference of maximum wave crest and bridge deck underside
Δz_h	elevation difference of maximum wave crest and the centroid of A_h

Douglass used the Biloxi Bay Bridge as a case study at 8:00 AM on August 29, 2005 and compared the force calculations based on several methods. Force estimates (summarized in Table 2.1) were made based on a significant wave height of 6.2 ft, wave period of 6 seconds, water depth of 16 ft, and storm surge of 12 ft.

Table 2.1. Force estimates provided by Douglass et al. (2006)

Method	Vertical Force (kip)	Horizontal Force (kip)
Bea et al. (1999)	40*, 420**, 250***	n/a
Denson (1978)	50	9
Denson (1980)	710	150
McConnell et al. (2003)	520	165
Douglass et al. (2006)	440	220

Note: Biloxi Bay Bridge: August 29, 2005 at 8:00 AM

*Drag, **Inertia, *** Impact

Douglass suggests the Table 2.1 values account for the Biloxi Bay Bridge damage, given span self-weight was 340 kips (value could vary slightly from span to span). The report also suggests that entrapped air added to its buoyancy. Douglass et al. (2006) also describes the vertical loading as a slowly varying force able to move the spans in the direction of flow.

2.3.4 Ramey et al. (2008)

Ramey et al. (2008) studied the I-10 Bridge over Mobile Bay. From the literature, the authors determined three design hurricane sea states at the bridge site and selected wave force calculation methods that best suited the coastal bridge. Wave force calculations were made for each and retrofits were proposed.

The design hurricane sea states were based on two actual events, Hurricane Frederic and Hurricane Katrina, and a scenario of Hurricane Katrina making landfall near Mobile, AL, Mock-Hurricane Katrina.

For wave force calculations, McConnell and Douglass, reviewed in the previous sections, were both used. At the time of this work, AASHTO's *Guide Specifications for Bridges Vulnerable to Coastal Storms* had not been completed; however there were tentative equations available to the authors. Although not directly applicable to bridges, wave force equations from the Shore Protection Manual were used. The equations from the Shore Protection Manual (Coastal Engineering Research Center 1984) covered non-breaking, broken, and breaking waves. The Coastal Construction Manual (FEMA 2005) was also used to define breaking wave loading on a vertical wall.

From the Shore Protection Manual, Ramey adjusted the wave force equations for a variety of conditions. For Unbroken Wave Forces on a Wall, the components are:

$$F_h = \frac{1}{2} \gamma h^2 L \quad (2.16)$$

$$F_v = \rho g w h L \quad (2.17)$$

where

F_h	horizontal wave force
F_v	vertical wave force
γ	unit weight of water
h	wetted height
w	wetted width
L	length, perpendicular to wave action

For Broken Wave Forces on a Wall, the components are:

$$F_h = \left(\frac{\gamma d_b h_c}{2} + \frac{\gamma h_c^2}{2} \right) L \quad (2.18)$$

$$F_v = \left(\frac{\gamma d_b w}{2} + \gamma h_b d w \right) L \quad (2.19)$$

where

F_h	horizontal wave force
F_v	vertical wave force
γ	unit weight of water
d_b	maximum storm surge elevation
h_c	lesser of 0.78 *maximum wave height or bridge depth
w	wetted width
h_{bd}	deck plus railing height
L	length, perpendicular to wave action

For Breaking Wave Forces on a Wall, the components are:

$$F_h = \left(\frac{1}{3} \left(10.1 \gamma \frac{H_b d_s}{L_D D} (D + d_s) \right) h_{wb} + \frac{\gamma (h_{wb})^2}{2} \right) L \quad (2.20)$$

$$F_v = \left(\left(\frac{h_{bd}}{h_{wb}} \right)^2 \left(10.1 \gamma \frac{H_b d_s}{L_D D} (D + d_s) \right) h_{bd} + \frac{\gamma (h_{bd})^2}{2} \right) L \quad (2.21)$$

where

F_h	horizontal wave force
F_v	vertical wave force
γ	unit weight of water
H_b	maximum wave height
L_D	wave length in water depth of D
d_s	depth of water at toe of wall
D	depth of water one wavelength from wall
h_{wd}	bridge height
h_{bd}	deck plus railing height
L	length, perpendicular to wave action

From the FEMA Coastal Construction Manual, the Breaking Wave Load on a Vertical Walls is:

$$F_{brkw} = f_{brkw} * L \quad (2.22)$$

$$f_{brkw} = 1.1 C_p \gamma d_s^2 + 2.41 \gamma d_s^2 \quad (2.23)$$

where

F_{brkw}	total breaking wave load acting at the still water level
f_{brkw}	total breaking wave load per unit length of wall acting at the still water level
C_p	dynamic pressure coefficient
γ	unit weight of water
d_s	area of bridge projection into the horizontal plane
L	wall length

The authors also provided proposed modifications to the Douglass et al. (2006) equations. The modifications were intended to refine the computed results while maintaining the overall approach to wave load calculation. Following Douglass, Ramey specifies the design vertical and horizontal loads in term of reference loads:

$$F_v = c_v^{mc} F_v^* \quad (2.24)$$

$$F_h = \left[1 + c_r \frac{(N-1)}{2} \right] c_h^{mc} F_h^* \quad (2.25)$$

where

F_v^*	reference vertical load
F_h^*	reference horizontal load
c_v^{mc}	empirical coefficient from McConnell's work, 1.0
c_r	reduction coefficient for reduced horizontal load on half of the girders beyond the seaward girder, 0.33
N	the number of girders supporting the bridge deck span
c_h^{mc}	an empirical coefficient from McConnell's work, 1.0

The reference forces are written as elevation and projected area as

$$F_v^* = \gamma \Delta z_v A_v \quad (2.26)$$

$$F_h^* = \gamma \Delta z_h A_h \quad (2.27)$$

where

γ	unit weight of water
A_v	area of bridge projection into the horizontal plane
A_h	area of bridge projection into the vertical plane
Δz_v	elevation difference of maximum wave crest and bottom of the end diaphragms or elevation difference of the top of the solid portion of the guard rail and bottom of the end diaphragms, whichever is smaller
Δz_h	elevation difference of maximum wave crest and elevation of the centroid of A_h or elevation difference between the elevation of the top of the solid portion of the guard rail and elevation of centroid of A_h , whichever is smaller

The projected area is written as:

$$A_v = L_B * \frac{W_B}{2} \text{ for } W_B > 20 \text{ ft} \quad (2.28)$$

$$A_v = L_B * W_B \text{ for } W_B \leq 20 \text{ ft} \quad (2.29)$$

where

L_B	length of bridge
W_B	width of bridge

These equations, along with McConnell, Douglass, and AASHTO's preliminary *Guide Specifications*, were used by the authors to determine the magnitude of wave forces for three storm scenarios given above. From these calculations, the author concluded that Douglass et al. 2008 gave the largest vertical force and the Breaking Wave equation from the Shore Protection Manual gave the largest horizontal force. The report concluded that the I-10 Bridge at the north end of Mobile Bay would fail due to the wave forces from a storm surge greater than 16 ft. This report went on to make some recommendations based on their findings, suggesting the use of ductile connections to tie “spans together longitudinally to allow spans to better distribute wave loads to adjacent spans and bents” and to tie spans to bent caps or piles “to better transmit vertical and horizontal surge/surface wave forces.”

2.3.5 Sheppard and Marin (2009)

Sheppard and Marin (2009) carried out physical testing of wave-bridge interaction at the University of Florida. The physical testing included a 1:8 scale polypropylene bridge model being impacted by monochromatic waves in an air/sea wave tank. Along with the testing, a theoretical model for predicting the quasi-static forces was developed. The theoretical model used the work of Kaplan (1992), Kaplan et al. (1995) and Morison et al. (1950). The physical model was developed to determine the coefficients of drag and inertia for the theoretical model.

In the development of the theoretical model, some assumptions were made by the authors. First, the structure was assumed to be horizontal and rigid. Second, the waves were assumed monochromatic, non-breaking, 2D, and normal to the structure's length. Third, the wave-structure interaction was assumed to be accounted for by drag and inertia coefficients. Fourth, the total force was assumed uniform along the structures length and to be the summation of the forcing components. The quasi-static forces are as follows:

$$F_X = F_{DX} + F_{x-Inertia} \quad (2.30)$$

$$F_Z = F_{DZ} + F_{z-Inertia} + F_B \quad (2.31)$$

where

F_X	total horizontal quasi-static force from a wave crest impact
F_Z	total vertical quasi-static force from a wave crest impact
F_{DX}	horizontal drag force
$F_{x-Inertia}$	horizontal inertia force
F_{DZ}	vertical drag force
$F_{z-Inertia}$	vertical inertia force
F_B	buoyancy force

The individual force components are as follows:

$$F_{DX} = \frac{1}{2} \rho C_{DX} A_X u |u| \quad (2.32)$$

$$F_{x-Inertia} = \left(C_I m_e \frac{du}{dt} + C_M u \frac{dm_e}{dt} \right) \quad (2.33)$$

$$F_{DZ} = \frac{1}{2} \rho C_{DZ} A_Z w |w| \quad (2.34)$$

$$F_{Z-Inertia} = \left(C_I m_e \frac{dw}{dt} + C_M W \frac{dm_e}{dt} \right) \quad (2.35)$$

$$F_B = \rho g V_s \quad (2.36)$$

where

ρ	mass density of seawater
C_{DX}	horizontal drag coefficient
A_X	horizontal deck area
u	horizontal fluid velocity
C_I	inertia coefficient
C_m	mass coefficient
m_e	effective mass
C_{DZ}	vertical drag coefficient
A_Z	vertical deck area
w	vertical fluid velocity
g	gravity
V_s	submerged volume

The physical modeling was carried out in a wave tank basin. The wave tank was 6 ft wide by 6 ft deep by 120 ft long. The wave tank was outfitted with a piston wave maker and wave absorbers. The wave absorbers were located at both ends of the tank to reduce wave reflection. For the trails, the water depths ranged from 1.5 to 3.0 ft with wave periods and wave heights ranging from 1 sec to 3.5 sec and 0 ft to 1.16 ft, respectively. Only monochromatic waves were studied.

The bridge slab was modeled by three, 1:8 scale, flat plates. The plates were made up of 1 in thick polypropylene sheets. The plates were 48 in wide by 24 in long by 7 in thick. The final dimensions of the slab were 48 in wide by 72 in long by 7 in thick. The slab was supported by a carriage system from above to reduce the blockage of flow and to make it easier to change the span elevation. The carriage system was made up of a rigid steel frame that connected to steel channels on top of the walls of the wave tank. The carriage system was connected to the slab by twelve steel pipe columns with bolted bearing plates on both ends. The steel pipes connected to the interior plate were outfitted with four load cells, one per pipe. The load cells were capable of measuring forces in all directions. Ten pressure transducers were mounted flush to the bottom of the deck along its length.

To better represent the geometry of a bridge superstructure, the slab was added in two stages; beams were added first and overhangs were added second. Railings were added along with additional pressure transducers thereafter. Finally, three beams were removed and the girder spacing was changed. Trails were run for each stage to determine what effects the components had on the measured loads. Along with the water depths, wave period and wave height, the clearance height was varied from -8 ft to 4.0 ft. In total 1,200 trails were completed.

The authors determined that the vertical quasi-static force was reduced when the number of beams was reduced (i.e. when the beam spacing increased). The behavior was attributed to less air being trapped for the wider spacing. For the vertical slamming force, entrapped air reduced the magnitude of the force while lengthening its duration. Also, the number of slamming pulses exhibited in the force readings is equal to the number of spaces

between beams. The authors found that the quasi-static force has a lower frequency than the slamming force, which is usually the frequency of the dominant wave, and that the slamming force is usually at or greater than the magnitude of the quasi-static force.

Sheppard and Marin (2009) stated the damage seen at I-10 Escambia Bay bridge during Hurricane Ivan was predicted by the empirical coefficients and the equations determined by this research using hind casted conditions. However, neither the values of the coefficient or the magnitude of these forces were given in the report.

2.3.6 AASHTO LRFD Specifications

The American Association of State Highway and Transportation Officials (AASHTO) Load Resistance Factor Design (LRFD) Bridge Design Specifications states: “Wave action on bridge structures shall be considered for exposed structures where the development of significant wave forces may occur” (AASHTO 2010). The Shore Protection Manual is referenced by AASHTO 2010 for computing the wave forces using site-specific conditions (Ramey et al. 2008). The manual provides guidelines for computing forces created by waves on pilings and walls but gives no specific bridge superstructure guidance.

2.3.7 AASHTO Guide Specifications

AASHTO recently published *Guide Specifications for Bridges Vulnerable to Coastal Storms* (AASHTO 2008), which defines parametric equations for calculating the design loads on bridges due to waves. This document is referred to herein as the *Guide Specifications*. This was one of two documents developed through efforts led by a task force established in May of 2006 by the *AASHTO Subcommittee on Bridges and Structures*. The development of the two documents was performed with pooled funds under Study Number TPF-5(130) initiated in September 2006 with \$590,000 from the Federal Highway Administration (FHWA) and eleven state DOTs. The equations were developed using experimental and theoretical research carried out at the University of Florida (See Sheppard and Marin 2009).

The guide specifies evaluation of bridge structures with three separate load cases. The first and second load cases correspond to maximum vertical load and maximum horizontal loading. The third load case is provided for the evaluation of bridge overhang components that uses a prorated combination of the maximum vertical and horizontal loads. For each load case, equations for vertical, horizontal and overturning moments are provided which consider bridge geometry (e.g. span type – slab or girder and girder type), wave characteristics, as well as entrapped air in the determination of the load magnitude.

2.3.7.1 AASHTO Guide Specifications Maximum Vertical Load Case

When considering the structural response to the maximum vertical load, the specification provides the following equations (AASHTO §6.1.2.2):

$$F_{V-MAX} = \gamma_w \bar{W} \beta \left(-1.3 \frac{H_{max}}{d_s} + 1.8 \right) \cdot [1.35 + 0.35 \tanh(1.2(T_p) - 8.5)] \cdot \left(b_0 + b_1 x + \frac{b_2}{y} + b_3 x^2 + \frac{b_4}{y^2} + \frac{b_5 x}{y} + b_6 x^3 \right) \cdot TAF \quad (2.37)$$

For this case, the slamming and horizontal forces are:

$$F_s = A\gamma_w H_{max}^2 \left(\frac{H_{max}}{\lambda}\right)^B \quad (2.38)$$

$$F_{H-AV} = \gamma_w H_{max}^2 \cdot (a_0 + a_1x + a_2x^2 + a_3x^3 + a_4x^4 + a_5x^5 + a_6 \ln(y)) \left[a_7 + a_8 \left(\frac{W}{\lambda}\right) \right] \quad (2.39)$$

and the overturning moment is:

$$M_{T-AV} = [F_{V-MAX}W^* + F_{H-AV}(d_b + r)] \left\{ a_m + \frac{b_m}{\left(\frac{W}{\lambda}\right)} + \frac{c_m}{\left(\frac{H_{max}}{\lambda}\right)} \right\} + \frac{2F_s W^*}{3} \quad (2.40)$$

where

F_{V-MAX}	vertical quasi-static hydrostatic and hydrodynamic force
F_s	vertical slamming force
F_{H-AV}	horizontal force associated with F_{V-MAX}
M_{T-AV}	overturning moment associated with F_{V-MAX}
γ_w	unit weight of water
H_{max}	maximum probable wave height
d_s	water depth at or near the bridge including surge, astronomical tide, and local wind setup
T_p	period of the waves with the greatest energy exhibited in a spectrum
TAF	trapped air factor
λ	wave length
W	total width of bridge, in the direction of wave propagation
W^*	effective bridge width
d_b	girder height plus slab thickness for girder bridges, slab thickness plus deck thickness for slab bridges
r	rail height
\bar{W}, β, x, y	given in specification
a_m, b_m, c_m	given in specification
A, B	variables given in specification
$a_0 - a_6$	coefficients given in specification
$b_0 - b_6$	coefficients given in specification

2.3.7.2 AASHTO Guide Specifications Maximum Horizontal Load Case

The maximum quasi-static horizontal load case uses the same slamming force as the maximum vertical case. The equations for horizontal, vertical and over moment are (AASHTO §6.1.2.3):

$$F_{H-MAX} = \gamma_w \pi (d_b + r) \left(\omega + \frac{1}{2} H_{max} \right) \left(\frac{H_{max}}{\lambda} \right) e^{\left[-3.18 + 3.76 e^{\left(-\frac{\omega}{\lambda} \right)} - 0.95 \left[\ln \left(\frac{\eta_{max} - Z_c}{d_b + r} \right) \right]^2 \right]} \quad (2.41)$$

$$F_{V-AH} = \gamma_w \alpha (\eta_{max} - Z_c) e^{\left[-0.30 + 2.04 e^{\left(-9.01 \frac{\alpha}{\lambda} \right)} - 0.16 \left(\frac{\eta_{max} - Z_c}{d_b} \right)^2 \right]} \quad (2.42)$$

$$M_{T-AH} = \left[F_{H-MAX}(d_b + r) + \frac{2}{3}(F_{V-AH} + F_s)W \right] 1.37 \tanh\left(\frac{d_b}{\eta_{max}-z_c}\right) \quad (2.43)$$

where

F_{H-MAX}	horizontal quasi-static hydrostatic and hydrodynamic force
F_{V-AH}	vertical force associated with F_{H-MAX}
M_{T-AH}	overturning moment associated with F_{H-MAX}
ω, α	adjusted bridge widths

Bradner (2008) determined that the horizontal and vertical quasi-static forces compared well to measured forces. However, the total vertical force, adding the quasi-static force with the slamming force, over-predicted the measured vertical force, see Section 2.3.9 for further information.

2.3.8 Jin et al. (2008)

Jin et al. (2008) computed site-specific design wave parameters for four different coastal bridges in Texas. Water levels were simulated by the Advanced Circulation Model for Coastal Ocean Hydrodynamics (ADCIRC), while wave parameters were simulated by Simulating Waves Nearshore (SWAN). Simulations were performed for varying storm surge and wind speed levels. During the project, Hurricane Ike made landfall near Galveston, Texas, and according to this reports finding, ADCIRC and SWAN provide accurate predictions of extreme wave conditions when compared to the measured wave height and high water marks from Hurricane Ike.

2.3.9 Oregon State University

Testing at Oregon State University (Schumacher et al. 2008; Schumacher et al. 2008b; Bradner et al. 2008; Bradner 2008; Bradner et al. 2011) included wave flume experiments of a detailed, 1:5 scale, reinforced concrete model impacted by regular and random waves. Details of the experiments have been provided first as they apply to all documents, with additional pertinent findings of each document provided thereafter. The goal of the research was to model and measure wave induced forces on coastal bridges.

The experiments were carried out in a large wave flume using wave characteristics and water depths that represent conditions typical in the Gulf of Mexico region during hurricane events. The bridge support substructure was modeled for three conditions: rigid, flexible, and unconstrained. The published work only discusses the data from the rigid case. Detailed representation of the flexible bridge structure and the extensive data acquisition are significant components of this work.

The coastal environment was modeled in a 2D large wave flume that is 342 ft long by 12 ft wide and 15 ft deep. The flat bottom of the wave flume was adjusted to mimic the near shore environment. To do so, three sections of slabs were mounted to the bottom of the wave flume. The main section of slab, 95 ft long, was mounted 4.8 ft above the bottom of the wave flume at mid-span. The other two sections were on a 1:12 slope (positive) and were located just before and after the main sections to provide transitions. The first section provided a transition between the wave flume's bottom and the main slab section. The

second section provided a transition between the main slab section and free surface (SWE). The wave conditions experienced during Hurricanes in the Gulf of Mexico were produced with a flap-type wave maker, capable of producing waves with a period of 3.5 s and a maximum wave height of 5.2 ft. Both regular and random waves were studied.

A steel frame reaction system was bolted to the side walls of the wave flume. The system was made of two wide flange beams (W18x76), steel guide rails, ball bearing rollers, and six load cells. One W18x76 beam was attached to each side of the wave flume. A guide rail was attached to the top of each wide flange beam. Three load cells were used per wide flange beam. One load cell was used to measure the horizontal reaction and was attached on the “off-shore” end of the beam to an anchorage block that was bolted to the flume wall. The other two load cells measured the vertical force and were placed so that when the specimen was on the frame, the load cells would be directly under the “off-shore” and “on-shore” girders. The vertical load cells were attached to ball bearing rollers that could slide on the guide rail.

The bridge specimen was a 1:5 scale of a typical highway coastal bridge span (I-10 over Escambia Bay). The bridge’s superstructure consisted of a deck, six AASHTO Type III girders, and four diaphragms. The bridge was constructed of reinforced concrete. The girders and diaphragms were cast together. The deck was attached to the girders and diaphragms with No. 4 threaded rods, spaced at 12 in o.c. and 18 in o.c. for the edges and center, respectively. All of the seams between the girders and the deck were sealed with silicone. Two pier caps, HSS 7x5x1/2, were attached to the bottom of the girders at both ends. The pier caps were then mounted to the load cells on the steel frame reaction system. For the connection between the horizontal load cells and anchorage blocks, three different anchorage setups were provided: free, rigid, and flexible. The free scheme was only used to determine the friction force. For the fixed setup, the pier cap was bolted to a steel angle that was bolted to the wide flange beam. For the flexible setup, two different springs, soft and stiff, were used to connect the bent cap to the anchorage block. The bridge specimen was 74 in above the main section of slab and about 150 ft from the wave maker.

The 1:5 scale bridge testing was instrumented to measure wave conditions, forces acting on the specimen, pressures acting on the specimen, and specimen response. Ten surface piercing wave gauges were used to measure water surface elevation. Six tension-compression load cells were used to measure overall specimen forces. Thirteen pressure transducers were used to measure pressure distribution. Strain gages were placed on each girder at mid-span to measure flexural response. Linear position transducers and analog accelerometers were also used in some test configurations.

Schumacher et al. (2008) discussed the data from a target wave height of 2.95 ft and a wave period of 3.1 s. Wave gage readings showed that the bridge specimen acted as a breakwater and reduced the wave heights by about 20%. Pressure transducer readings varied from one girder to the next. The first girder (i.e. “off-shore” girder) readings showed a constant value of 0.49 psi over 0.7 s and then dropped to zero for 0.4 s. The second girder (i.e. next to the “off-shore” girder) readings showed a steep spike in pressure of 3.26 psi with a short duration followed by a negative pressure of 0.36 psi with a long duration. These findings were credited to the pressure transducers sensitivity to entrapped air or breaking waves. The readings from the two girders showed a time delay of about 0.23 s.

Strain gage readings from two sensors were also discussed by Schumacher et al. (2008). These sensors were located on the bottom flange of the girders for the exterior “off-

shore” girder and the exterior “on-shore” girder. There was no time delay in the response. The researchers concluded that “the specimen seems to respond as a unit to the passing wave front, activating all girders in bending action at the same time.” The maximum strain reading corresponds to a concrete surface stress of 1740 psi. Readings from both horizontal load cells were similar (only horizontal forces were discussed), indicating that the loading was uniform across the bridge. Also, no impulsive spike was recorded. The peak horizontal force on the specimen was 1800 lbs.

Schumacher et al. (2008b) compared the findings from the rigid and the flexible setup for a water depth of 6.2 ft (74 in). This water depth was considered to produce the highest forces. Regular waves were studied with a target wave height of 2.05 ft and a wave period of 2.5 s. The data was filtered, rejecting any frequencies above 50 Hz. The horizontal load measured on either side of the frame reaction system was similar for the rigid and flexible setups, and therefore they could be added to get the total force. The flexible setup produced greater horizontal forces than the rigid setup. The vertical loads measured on the “on-shore” side varied from the “off-shore” side for the rigid and flexible setups. The maximum vertical force measured on the “on-shore” side was 67% of the total force. The vertical forces were also greater for the flexible case. The vertical response is similar for both cases. However, the horizontal response for both cases is different. For the rigid setup, maximum horizontal and vertical forces occurred simultaneously with no negative horizontal forces measured. For the flexible setup, the maximum horizontal and vertical forces occurred at different instants and there were both positive and negative horizontal forces measured.

Bradner et al. (2008) found that wave height has the greatest effect on force followed by water level. In this paper water level was a function of both bridge-water clearance and water depth, so it is not certain which of these has the greatest effect on the force. The wave period was also found to effect the force. The relationship between wave height and force was fit by using a 2nd order polynomial function.

Pressure spikes were found located between girders but not on the outside face of the “off-shore” girder. Bradner et al. (2008) attributed these spikes to compression of air. The spikes did not lead to a simultaneous spike in the load cell data and therefore these spikes had little effect on the supporting structure. The author concluded the short duration spike was not great enough to overcome the inertial force of the bridge specimen and that the spike was not uniform over the girder and produced a phase-lag.

Overall the vertical forces measured and reported by Bradner et al. (2008) were three to five times the corresponding horizontal force. No comparison was made between the maximum horizontal or vertical forces. It was noted, for wave heights of approximately 2 ft, as the water level approached the bottom of the girders the force increased until the water level was equal to the bottom of the girders then the force tended to level off or even decrease which “suggests that the forces can be related to particle velocity and acceleration”; meaning that the bridge has limited effects on the wave.

Bradner (2008) studied a rigid structural configuration. While Bradner (2008) did not find evidence of a spike in the load cell data that was found in the pressure readings, large spikes were found within the quasi-steady vertical force that represented the passing wave striking all six girders, which is similar to Sheppard’s findings. Bradner also found a directly proportional relationship between force and momentum flux for regular and random wave trails. Bradner (2008) also determined that the horizontal and vertical quasi-static forces (F_{H-MAX} and F_{V-MAX}) computed by the *Guide Specifications* compared well to measured

forces. However, the total vertical force, adding the quasi-static force with the slamming force (F_{V-MAX} plus F_S), over-predicted the measured vertical force by a factor of 1.6 to 2.2 in some conditions.

2.4 Damage Due to Storm Surge

Hurricane damage potential is routinely characterized by the Saffir-Simpson Wind Scale used by the National Hurricane Center. The scale is intended to quantify a hurricane's potential damage and flooding caused at landfall. It was used in this report to classify the category of hurricanes. Wind speeds and storm surge are given in Table 2.2 for each category.

Table 2.2. Saffir-Simpson hurricane wind scale

Category	Wind Speed (mph)	Storm Surge (ft)
I	74-95	4-5
II	96-110	6-8
III	111-130	9-12
IV	131-155	13-18
V	≥156	>18

Infrastructure damage caused by Hurricane Katrina led to the initiation of significant research and development activity. DesRoches (2006) provides an assessment of the transportation system during Hurricane Katrina performed for the American Society of Civil Engineers (ASCE). Wind speeds in excess of 140 mph and storm surges of 25 to 35 ft occurred in parts of Mississippi and Louisiana. Approximately 45 bridges were damaged in Alabama, Louisiana, and Mississippi ranging from minor damage to bridge collapse. The overall economic damage from Hurricane Katrina was estimated at 40 to 120 billion dollars, approximately double the damage of Hurricane Andrew. The overall cost to repair or replace bridges damaged during Hurricane Katrina was over one billion dollars. Notable expenses reported by DesRoches (2006) were \$267 million for US90 Bay St. Louis Bridge, \$275 million for US90 Biloxi Bay Bridge, and an estimated \$600 million to construct replacement I-10 twin spans over Lake Pontchartrain. Note Bergeron (2007) reported an estimated \$338 million to replace the Biloxi Bay Bridge.

The I-10 twin spans crossing Lake Pontchartrain were simply supported, 65 ft long, supported by six girders, and resting on steel/bronze bearings. The top of the bridge deck was approximately 15 ft above the mean water level in the low lying approach spans where the damage occurred. A total of 473 spans shifted off supports and 64 spans shifted to an extent where they fell into the water. The damage was reported to occur through a combination of buoyant forces and lateral water hammering. Each 65 ft long span was calculated to weigh 500 kips and surge produced uplift forces of approximately 900 kips according to the Louisiana DOT.

Connection type between decks and bents appears to be a key factor in hurricane performance. For example, DesRoches (2006) reported that many simply supported bridges on I-10 either failed or sustained significant damage while nearby rigidly connected bridges on US-11 were not damaged. Since Hurricane Katrina the Alabama DOT has begun to

provide more secure anchorage between girder and bent caps for storm surge resistance. DesRoches (2006) provides dialogue from a Louisiana DOT bridge engineer indicating the *FHWA* is to require a storm surge analysis to be conducted for all new bridges over coastal waterways where surge loads are explicitly considered in design. Bridges with vent holes were noted by DesRoches (2006) to mitigate buoyant forces. Vertical resistance devices such as steel cables were noted as a potential retrofit technique. Additionally, transverse shear keys were recommended.

White et al. (2006) reported on a site visit to the damaged Mississippi coast in October of 2005 following Hurricane Katrina; select authors of this report were present for the site visit. A key observation related to this research was that many simply supported horizontal structures (e.g. bridge decks and parking garage slabs) failed during the storm. Wind driven waves were stated to be perhaps the most severe structural load during the storm. The Bay St. Louis and Biloxi Bay bridges were especially noted; their bearings did not constrain the deck and girders, which is the likely cause of failure of the bridges.

Robertson et al. (2007) suggests that friction from the Biloxi Bay Bridge self-weight and small thick steel angles were the only restraints to the lateral movement. The lack of restraint plus the forces of uplift and buoyancy allowed the structure to move off of its substructure. Douglass et al. (2006) suggests that the damaging agent was the wave-induced loads from the wave crest hitting the un-submerged bridge deck. Both documents agreed that the simply supported design of the Biloxi Bay Bridge led to its failure.

The loading created by Hurricane Katrina's wave surge caused significant numbers of the Biloxi Bay Bridge spans to be displaced. Some were completely moved off of the pile caps and came to rest 16 to 47 ft away (O'Connor 2005). In some cases, the girders and the deck sustained significant fracturing. The elevated spans that led to the drawbridge were the only ones not damaged or moved, as they were out of the reach of the waves.

2.5 Survey of Gulf Coast DOT's

The Texas, Louisiana, Mississippi, Alabama and Florida DOT's were contacted to: 1) obtain information related to storm surge in the context of bridge design; 2) determine the amount of research funded related to storm surge effects on bridges (performed either internal to the DOT or through external contract); 3) provide a medium for experienced engineers to give guidance to the research; and 4) make bridge engineers at DOT's along the Gulf Coast aware of the research so they can obtain any information relevant to their activities that is approved by the sponsor for public release. The survey asked if and/or how the DOT considered storm surge in design of bridges, what research had been conducted for the DOT related to storm surge on bridges with an emphasis on finite element modeling, if any large scale bridges had failed and could be attributed to storm surge, and for any other feedback the DOT wished to provide related to storm surge and bridges.

2.5.1 Bridge Failures Attributed to Storm Surge and/or Hurricanes

Table 2.3 summarizes bridge failures identified during survey of state DOT's. It is notable that the failures encompass multiple states over a period of several decades. Specific information obtained from the DOT's is summarized in the following paragraphs.

Table 2.3. Notable bridge failures attributed to storm surge/hurricanes

State	Hurricane	Year	Bridge	Route
Mississippi	Camille	1969	Bay St. Louis	US 90
Mississippi	Camille	1969	Biloxi Bay	US 90
Alabama	Fredric	1979	Dauphin Island	SR 193
Florida	Ivan	2004	Escambia Bay	I-10
Mississippi	Katrina	2005	Bay St. Louis	US 90
Mississippi	Katrina	2005	Biloxi Bay	US 90
Louisiana	Katrina	2005	I-10 Twin Spans	I-10

Five spans were lost on a bridge in Alabama during Hurricane Katrina. The connection details for the replacement spans included girder anchorage at each girder line and each end, concrete diaphragm venting to reduce entrapped air pockets. Additionally, continuous decks were used whereas previous practice would have been to use simple spans with open joints.

The Florida DOT noted the damage to the Escambia Bay Bridge during Hurricane Ivan. This was a well publicized situation that resulted in damage of 58 spans each 60 ft long. The Louisiana DOT noted the damage to the I-10 twin spans crossing Lake Pontchartrain due to wave action atop the surge on a bridge with minimal connectivity.

The Mississippi DOT provided information on four bridges that failed due to storm surge and/or hurricane events. They are presented below nearly verbatim as provided.

- a. US 90 bridge over Bay St. Louis – This 2 mile long bridge was originally a low-level bridge with 41 ft concrete T beams (simple spans) with a low level bascule span. The entire superstructure was destroyed along with much of the substructure. Spans and debris were found as far away as 220 ft from the existing alignment. The bridge was replaced with high level prestressed concrete beam spans and post-tensioned drop-in prestressed Bulb-T concrete spans.
- b. US 90 bridge over Biloxi Bay – This 1.6 mile bridge was originally a low to mid-level bridge with 52 ft prestressed concrete beam spans (simple spans) with a mid-level bascule span. Most of the superstructure was destroyed along with some of the substructure. The bridge was replaced with high level prestressed concrete beam spans and post-tensioned drop-in prestressed Bulb-T concrete spans.
- c. US 90 over the CSX Railroad near Henderson Point in Pass Christian – The end span was knocked off the west bound bridge and several spans were displaced. The bridge was repaired with two 125 ft prestressed concrete Bulb-T spans alongside repositioning and repairing four additional spans.
- d. Pops Ferry Road over Biloxi Bay - This bridge, which is locally owned by the City of Biloxi, was severely damaged by the storm. It consists of low level prestressed concrete beams spans and a low level bascule span. Spans appeared to float and drop, walking across the caps breaking the caps beams, slabs, and cracking piling. Twelve spans were replaced and 9 spans were repositioned and repaired. Eight bent caps were replaced. The bascule span

required significant repair and rehabilitation of motors, alongside repair of electrical machinery, mechanical machinery, and the submarine cable.

According to the Texas DOT, no large bridges have failed that have been directly attributed to storm surge. However, a small structure, Rollover Pass, was damaged by Hurricane Ike. The bridge was a box beam structure topped with an asphalt overlay, 72 ft wide by 240 ft long (five spans of 45 to 50 ft). The storm surge caused some of the beams to shift towards the bay side. Some of the beams that shifted also fell into the bay. The boxes were reset and made composite by epoxy anchoring bars into the boxes and casting a slab on top of the boxes. In addition, Texas DOT added anchor rods to protect against storm surge.

2.5.2 DOT Design Procedures for Storm Surge on Bridges

The Alabama DOT considers storm surge in bridge design. Storm surge elevations from Hurricane Fredric were used to establish profile elevations for the replacement structure. Storm surge was also considered in establishing profile elevations on the I-10 Bayway bridges. The Alabama DOT does not currently perform structural calculations on a bridge specifically for storm surge. Alabama DOT representatives indicated the most effective manner to address storm surge was to clear the anticipated surge elevation, though it was noted this can be impractical due to approaches and tie-ins. When spans are vulnerable to storm surge forces, better anchorage, continuity, and less surface area exposed to storm surge (e.g. shallow depth girders, open barrier rails) were considered important parameters by Alabama DOT representatives.

The Florida DOT uses storm surge analysis to obtain bridge hydraulics on all its coastal bridges during design; wave heights are evaluated. Typically, surge is numerically modeled using either ADCIRC or RMA2 and driven by design hurricane hydrographs located at the open coast. ADCIRC and RMA2 use finite element modeling to characterize hurricane hydraulics. When wave forces are relevant, a near field wave model, typically SWAN, is employed to predict the design wave climate at the bridge. Wave forces are then computed if the bridge cannot be elevated above the waves. Bridge response is addressed using LRFD code rather than modeling bridge response.

The Florida DOT is pursuing a statewide screening of its existing bridges using a refined process based on in depth hurricane hindcasting of the Tampa area. This same effort is planned for use to refine LRFD load factors associated with wave forces on bridges. Florida DOT also uses coastal engineers exclusively to perform hurricane hydraulic analyses in they feel it is essential for properly estimating surge and wave hydraulics.

According to DOT representatives Louisiana does not currently have many bridges vulnerable to storm surge. Louisiana considers storm surge in bridge design. It is considered by placing the superstructure at an elevation higher than the maximum predicted storm surge elevation (including associated wave heights).

Post Hurricane Katrina, the Mississippi DOT considers the effects of storm surge. Mississippi considers practical parameters that can be easily performed based on lessons learned from Hurricane Katrina damage. Examples include: 1) placing the majority of the bridge superstructure above the predicted storm surge and maximum wave height; 2) utilizing multiple prestressed concrete beam spans made continuous for live loads which, due to the dead load resulting from the length, offers great resistance to overturning and wave attack; and 3) possibly utilizing open type diaphragms at the end of spans to allow air to pass

in an attempt to assist with buoyancy. Research was conducted by *Ocean Engineering Associates, Inc* to determine needed elevations to exceed storm surge and maximum wave heights for the superstructure of the Biloxi Bay and Bay St. Louis replacement bridges.

The Texas DOT historically has not considered storm surge in the design of bridges, but noted they would design for storm surge per the *Guide Specifications* of AASHTO (2008). No bridges have been designed in Texas since Hurricane Ike that would be affected by storm surge. The preponderance of Texas DOT bridges, even along the coastline, are not affected by most storm surges since they are set at elevations where it is uncommon for there to be any problems. Elevations of most bridges in Texas have been dictated by factors (e.g. geometric design, commercial waterways) that have indirectly avoided storm surge parameters.

2.6 Retrofit of Bridges for Storm Surge

The second document developed through efforts led by a task force established in May of 2006 by the *AASHTO Subcommittee on Bridges and Structures* has been referred to as the *Retrofit Manual*, which is a working document under development that was provided to the research team for use (Modjeski and Masters 2008). The development of the two documents (the *Guide Specifications* of Section 2.3.7 being the other document) was performed with pooled funds under Study Number TPF-5(130) initiated in September 2006 with \$590,000 from the FHWA and eleven state DOTs.

Current practice does not typically retrofit bridges to improve resistance to surge produced by coastal storms. The most comprehensive investigation of storm surge retrofit techniques identified during literature and practice review was the *Retrofit Manual* which represents the state of the art for bridges and was the only document considered in this report. Review of the document indicates there is a considerable amount of work required to implement rapid retrofit techniques. The *Retrofit Manual* does not provide design procedures, rather conceptual guidance and potentially problematic situations to be mindful of when considering retrofit.

Quoting Modjeski and Masters (2008): “Each bridge will present a unique set of vulnerabilities and constraints, and each project must be approached individually. Due to the magnitude of the wave loads that may be determined at a given site and the difficulty in retrofitting some bridges, it is entirely possible that the best strategy for a given bridge will be to do nothing to the existing bridge, and plan for its eventual replacement after a coastal event.”

A screening procedure that compares the dead load of the bridge to a simplified vertical force is used to determine the vulnerability of a coastal bridge when impacted by a storm event and whether to retrofit the bridge. The screening procedure takes into consideration the importance and economic implications of the bridge. The bridge is evaluated based on a 100-year return period design event and largely follows the *Guide Specifications* (AASHTO 2008) for analysis. There are three levels of analysis. Level I is the most conservative because it allows the use of published information as opposed to measured or modeled information. It assumes the storm surge, wind setup, current, wave height, and period are all maximums simultaneously. For a Level II analysis, the design parameters have been reassessed from the Level I parameters. Where bridges are deemed

critical, a Level III analysis is required. This analysis is more extensive and requires computer modeling and analysis.

The screening procedure also includes a Criticality Index (CI). CI values ranged from one for minor economic or emergency need impact to four for extreme economic or emergency need impact. The work performed in this research would be for CI equal to four.

Retrofit strategies were divided into seven categories. It was stated that each bridge presents unique vulnerabilities and constraints that require each project to be approached individually. The seven categories provided in the retrofit manual were: 1) buoyancy load reduction; 2) wave load reduction; 3) adjacent span connection; 4) strengthening connection of superstructure to substructure; 5) strengthening substructure; 6) strengthening foundation; and 7) accepting loss of superstructure to protect substructure.

According to the authors of the *Retrofit Manual*, trapped air underneath a bridge deck when compressed according to the ideal gas law could produce buoyancy forces on the order of the dead load of the bridge when submerged in static sea water up to the level of the top of the sidewalk. The Biloxi Bay Bridge and I-10 Lake Ponchartrain Bridge were said to have buoyancy loads on a span equal to 86% and 104% of their dead load, respectively. The authors recommended vents to alleviate trapped air. Coring of 150 mm diameter holes in a bridge deck could be performed in a rapid response strategy, though care should be taken not to saw the reinforcing bars in the bridge.

Wave load reduction requires time intensive activities such as construction of artificial reefs and is not feasible for rapid response. Connection of adjacent spans would provide additional resistance to surge provided the wave loading was not uniformly developed along all connected spans. The use of cables and the use of shear transfer rods inserted between the spans were discussed in the *Retrofit Manual* as options to connect adjacent spans. Cables would require considerable deflection prior to mobilization, which could result in damage when the superstructure comes back into contact with the substructure. Shear transfer rods would require less movement for mobilization which should minimize damage after the wave has passed.

Strengthening of the connection between the superstructure and substructure is conceivably feasible. The *Retrofit Manual* contains methods such as earwalls, shear blocks, and cable restraints to strengthen the superstructure and substructure connection. These methods would not lend themselves well to rapid retrofit in the form they were described in the manual, though other approaches could be used for rapid retrofit. The key parameter to consider in this situation are stresses that occur due to the retrofit (e.g. negative midspan bending) and ensuring the retrofit does not cause unintended consequences. The *Retrofit Manual* states that for bridges with a bottom of superstructure elevation significantly below the top of wave crest elevation, the *Guide Specifications* (AASHTO 2008) predicted vertical forces can become large enough to preclude any strategy that includes resisting the forces by structural means.

Fuse elements were recommended to limit unintended consequences when connecting the substructure to the superstructure. Fuse elements are components made from highly predictable material that have a specified minimum and maximum load. The *Retrofit Manual* provides example drawings of some types of fuse elements; one of these drawings is shown in Figure 2.1. It was noted that multiple fuse elements designed to work in parallel could be problematic if they require differential movement prior to being engaged and that construction tolerances should be considered. If some elements become more engaged than

others due to a variety of factors the elements will not act in parallel as intended, which could result in undesired performance.

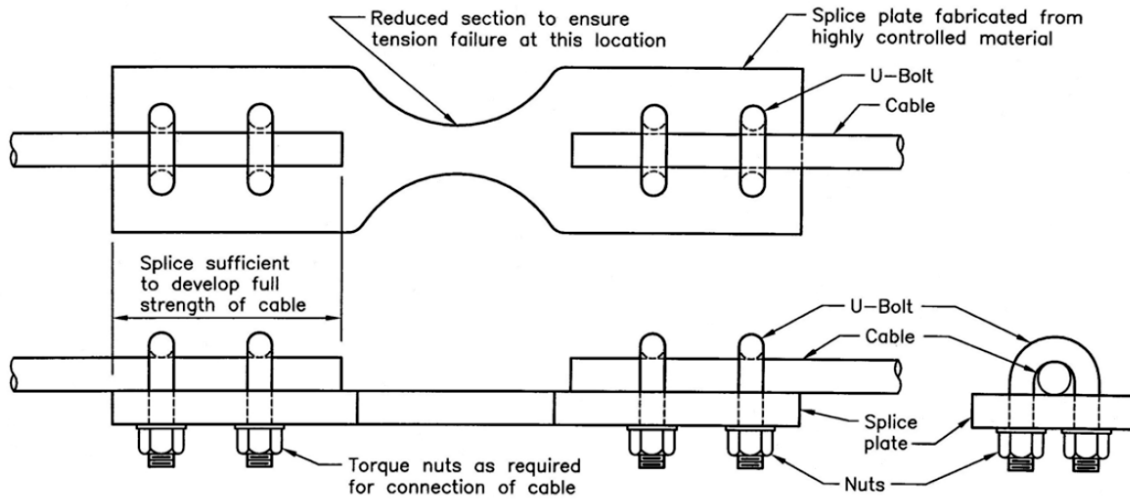


Figure 2.1. Example of fuse element from *Retrofit Manual* (used with permission)

Strengthening the substructure and the foundation are not feasible for a rapid retrofit. Accepting loss of the superstructure to protect the substructure could be the most feasible alternative for a very large storm, especially if the bridge is at a low elevation. Fuse elements could allow this approach to be coupled with strengthening the connection between the superstructure and substructure.

CHAPTER 3 – FINITE ELEMENT MODELING

3.1 Overview of Finite Element Modeling

The finite element method (FEM) has become one of the primary means of generating and solving mathematical models for problems in solid and structural mechanics. The predominance of the FEM stems from its multifaceted appeal: the procedure is highly intuitive and allows for representation of complex structural geometries, material properties, and boundary conditions with precision. This chapter provides a brief overview of the components of a finite element model that demonstrates many of these features, with a primary focus on the application of complex boundary conditions capable of simulating the dynamic forces due to storm surge and wave action on bridge superstructures.

A finite element analysis generally begins with the creation of an idealized structural representation called a finite element mesh. Figure 3.1 shows an example of a structural system and a corresponding finite element mesh. The mesh is a collection of elements that have simple shapes (brick shaped hexadrons are common), that when combined provide a geometrically accurate representation of the overall structural geometry. This single step accounts for the fundamental appeal of the finite element method as a numerical solution technique because the generally intuitive step of creating a mesh representation of the known structural geometry simultaneously defines the more abstract mathematical representation of the structure, its boundaries, and the equations used to describe internal stresses, strains, and displacements. This link between mesh and the mathematical model results in two particularly notable features of the FEM approximation: the actual geometry of the modeled structure can be represented with a high degree of mathematical precision, and the resulting mathematical equations are well suited for powerful computer based solution schemes.

After construction of a finite element mesh, boundary conditions representing the applied forces and displacements must be specified. Force type boundary conditions can include static and/or transient loads applied to points, surfaces or volumes. Displacement type boundary conditions range from simple specified zero or non-zero displacements to more complex conditions such as solution dependent contact interactions. Application of boundary conditions in the FEM is conceptually straightforward in that known force and displacement type conditions are mathematically modeled by specification of the conditions on individual elements or on groups of elements. The association of forces with individual elements provides a convenient means of mathematically representing force and displacement conditions that vary in spatially complex ways.

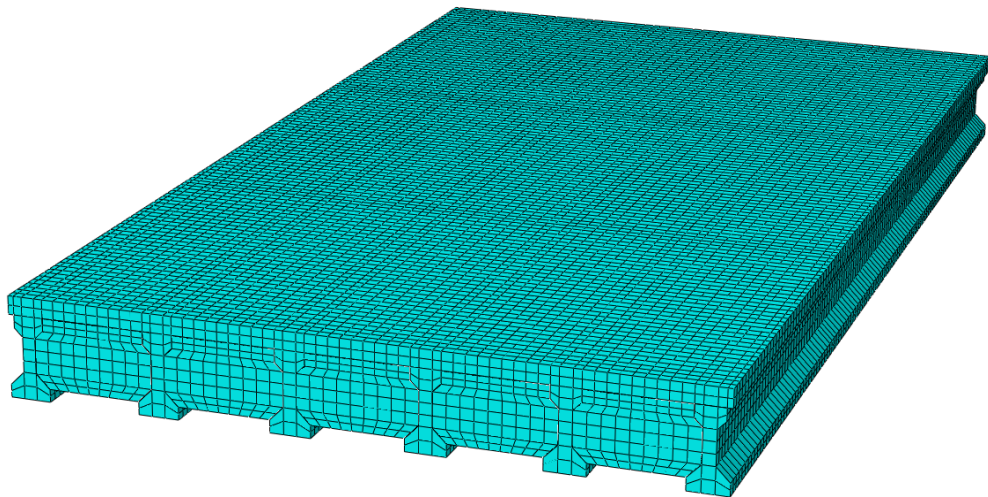
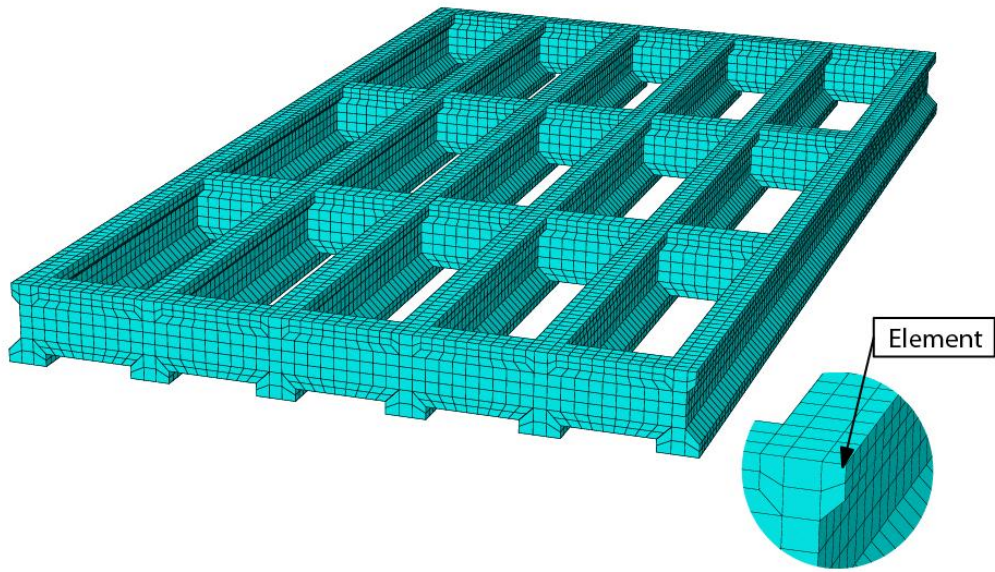


Figure 3.1. The geometric complexity of the girders and diaphragm of a 1:5 scale bridge model (top) is preserved in the corresponding finite element representation (bottom).
Note: The last image shows the finite element mesh after the deck was installed. The model shown is from Oregon State Universities 1:5 scale model of an Escambia Bay Bridge span.

3.2 Wave Load Modeling Approach

Because the FEM provides a convenient means for simulating the response of geometrically complex structures subjected to transient loading conditions, it is well suited for the simulation of structural response due to wave and surge forces. Figure 3.2 shows the framework of the approach used to incorporate wave loading into the FEM simulations. There are three primary components in this approach: a generic FEM structural model (indicated on the left), a wave load model (shown on the right), and a data transfer mechanism (shown in the middle).

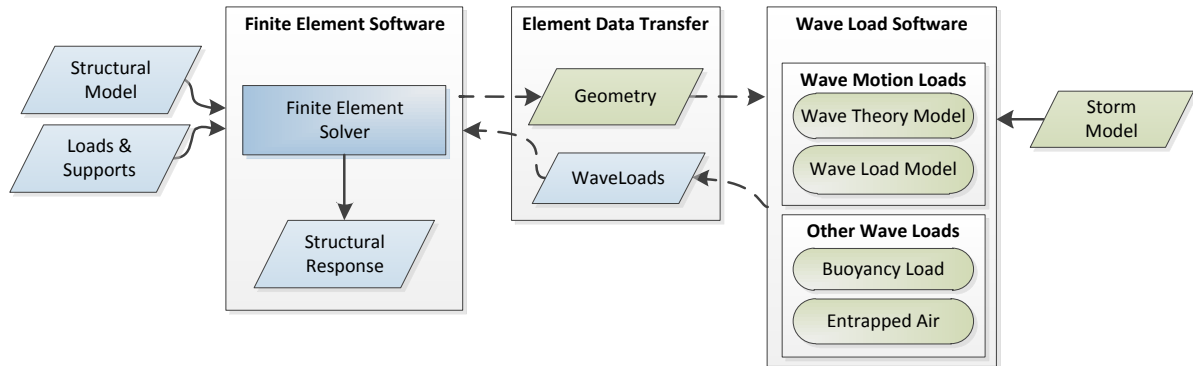


Figure 3.2. Flow chart showing the finite element based wave load modeling approach.

Note: The structural body and surfaces forces induced by the wave depend on the position and geometry of the structure relative to the wave motion.

The finite element software box in Figure 3.2 represents a “generic” finite element simulation in the sense that it includes as inputs a structural geometry model in the form of a mesh along with displacement/support boundary conditions, and non-wave related surface and body loads. The FEM software, structural model, and non-wave loads are entirely independent of the wave loading simulation, and can be performed with variety of commercially available FEM software packages (Abaqus is suitable but is not required).

The wave load software (WLS) (right side of Figure 3.2) is a set of software routines that generate wave based surface and body forces caused by buoyancy, drag, and inertia effects. The WLS’s core functionality is independent of the FEM model and requires specification of a wave theory model that predicts wave particle kinematics, and a wave load model that relates wave particle motion to surface and body loads. In this modeling approach, the WLS can accommodate a variety of methods for predicting wave particle kinematics, including simple analytic expressions such as linear gravity wave theory to complex numerical solutions of nonlinear wind-generated wave theories (e.g. output from predictive software such as SWAN).

The element data transfer box represents software routines that communicate problem specific information between the FEM and WLS. For a given FEM model, the element geometric information required for wave based load prediction includes geometric information such as position relative to the wave flow field, surface sizes, surface orientations, and structural volume. This information is transferred from the FEM model to the WLS at the element level. The WLS uses the FEM data, combined with model storm data

to generate surface and body forces that are communicated back to the FEM analysis. This portion of the approach must be adjusted for the specific FEM software.

The approach developed herein incorporates the use of robust, commercially available FEM software to handle the typical modeling tasks (mesh creation, boundary condition application and analysis), and separate software tools that provide approximate wave and surge forces.

Many commercial FEM software packages provide a means of interacting with external programs. In this work, FEM development was performed using Abaqus. Abaqus is a general purpose finite element program able to model static and dynamic problems involving large displacements and transient loads. It has large libraries of element types, material constitutive models, and sophisticated boundary conditions. Critical to the modeling of surge and wave loading, Abaqus has the capability of linking externally generated, time varying structural loading to the FEM model. This feature was utilized to link a finite element mesh of a bridge span generated within Abaqus to simulated wave and surge loadings produced by the WLS.

3.3 Idealized Wave Loads

For this work, wave interactions are coupled to the structural model in one direction. That is, while the structure is loaded by the wave motion, the wave is assumed to propagate unhindered by the presence of the bridge structure. As a result, the computation of wave loads requires:

1. Selection of a wave motion model that provides wave particle position, velocity and acceleration fields.
2. Selection of a wave force model that relates the wave particle motion to forces.
3. Structural model geometric data necessary for computation of wave particle velocities and buoyancy forces.

Selection of idealized wave force model is independent of the finite element method or specific structural model. The calculations throughout this report use specific choices for wave kinematics, and resulting forces, but the approach and software framework is general, and can easily accommodate virtually any analytic formulations, tabulated field data, or data generated by external numerical simulations (a useful attribute to incorporate future approaches).

3.3.1 Wave Theory Model

The wave model used in this work is a linear wave theory, propagating harmonic wave (Dean 1991) depicted in Figure 3.3. The dispersion relationship for a small-amplitude based approximation, provides a nonlinear relationship between wave length and period

$$L = \frac{g}{2\pi} T^2 \tanh \frac{2\pi}{L} d, \quad (3.1)$$

where L is the wave length, g is the gravitational acceleration, T is the wave period; and d is the still water elevation (SWE). The wave surface elevation is given by

$$\eta = \frac{H}{2} \sin(\omega t - kx), \quad (3.2)$$

where H is the wave height, $\omega = 2\pi/T$ is the radian frequency; $k = 2\pi/L$ is the wave number, t is the current time and x is the horizontal position. The horizontal velocity and acceleration fields are given by:

$$u = \frac{\omega H}{2} \frac{\cosh k(z+d)}{\sinh kd} \cos(\omega t - kx) \quad (3.3)$$

$$\dot{u} = \frac{\omega^2 H}{2} \frac{\cosh k(z+d)}{\sinh kd} \sin(\omega t - kx) \quad (3.4)$$

where z is the vertical position relative to d , and the vertical velocity and acceleration fields are:

$$w = \frac{\omega H}{2} \frac{\sinh k(z+d)}{\sinh kd} \sin(\omega t - kx) \quad (3.5)$$

$$\dot{w} = -\frac{\omega^2 H}{2} \frac{\sinh k(z+d)}{\sinh kd} \cos(\omega t - kx) \quad (3.6)$$

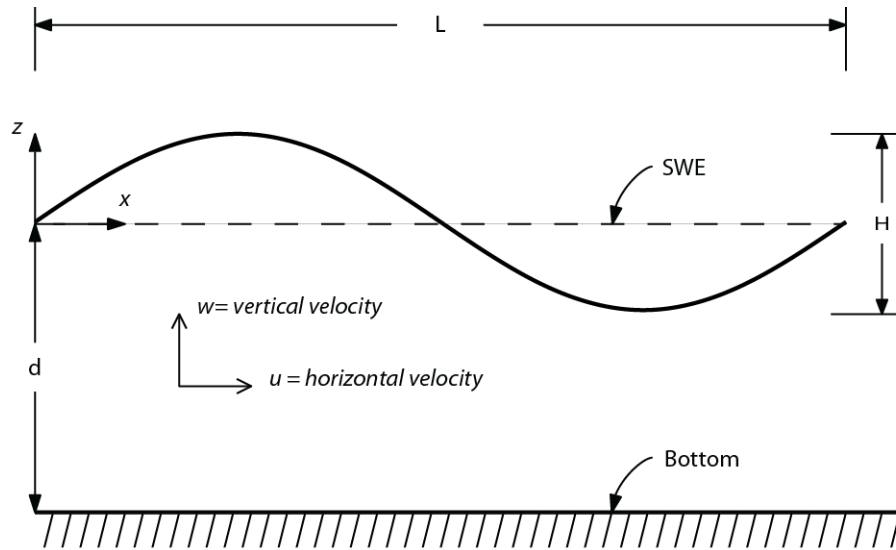


Figure 3.3. Wave flow variable definitions.

With this kinematic theory, a wave is completely parameterized specifying the SWE, wave height, and either the wave length or period. Calculation of particle velocity and acceleration requires specification of a position and time. When the wave kinematic theory is

combined with the wave load model, local wave forces are parameterized by wave model parameters combined with wave load coefficients.

In the FEM context, once the wave profile parameters and wave load coefficients have been specified, determination of local, time varying wave forces on a specific finite element requires communication of the current time, element position, surface size and orientation to the wave load routines. Surface and body forces are then computed and returned to the FEM analysis routines to be incorporated into the wave load simulation.

3.3.2 Wave Load Model Equations

Analytic wave force intensity equations chosen for this work follow those presented in Bea et al. (1999) with some modifications presented in Sheppard and Marin (2009). This formulation has been widely used in the design of offshore platforms, and has been found to predict forces that correspond well with empirical measurements of wave impact events. This method specifies loading as a function of time and position, and as such is well suited for the development of surface based finite element loads.

The wave load representation used by Bea et al. (1999) that is based on Isaacson and Prasad (1994) expresses the total wave force applied to a platform deck as the sum of several forces:

$$F_{tw} = F_b + F_s + F_d + F_i \quad (3.7)$$

where F_{tw} : total force from a wave crest impact; F_b : buoyancy force; F_s : slamming force; F_d : drag force; F_i : inertia force. The size and duration of each force depends on profile characteristics of the modeled wave as well as the modeled structure.

The buoyancy force is the vertical body force of magnitude equal to the weight of the water displaced by the bridge structure, and may be written in the form

$$F_b = \rho g V_s \quad (3.8)$$

where V_s is the submerged structural volume. The transient slamming force (Kjeldsen and Myrhang 1979) has the form:

$$F_{sx} = 0.5 C_s \rho A_x u^2 \quad (3.9a)$$

$$F_{sy} = 0.5 C_s \rho A_y w^2 \quad (3.9b)$$

where C_s : slamming coefficient (Isaacson and Prasad 1994); ρ : mass density of seawater; A_x, A_y : the projected area of wave crest impact in the vertical and horizontal planes; and u, w : horizontal and vertical fluid velocities. In static analyses, this expression is generally modified to account for dynamic aspects of the transient load, however because this dynamic analysis directly represents the wave transients, dynamic impact factors are not necessarily required.

The submerged portions of the structure are subject to steady-state and inertial drag forces caused by flow associated with surge inundation. The horizontal and vertical drag forces are written in the form (Sheppard and Marin 2009)

$$F_{dx} = 0.5\rho C_{dx}A_x u^2 \quad (3.10a)$$

$$F_{dy} = 0.5\rho C_{dy}A_y w^2 \quad (3.10b)$$

where C_{dx} and C_{dy} are the horizontal and vertical drag coefficients. A simple form of inertial drag (drag associated with the change of velocity of fluid around the structure) was used

$$F_{ix} = \rho C_{mx} V_s \dot{u} \quad (3.11a)$$

$$F_{iy} = \rho C_{my} V_s \dot{w} \quad (3.11b)$$

where C_m is the inertia coefficient, V_s is the submerged volume, and \dot{u}, \dot{w} are the horizontal and vertical water particle accelerations.

Application of these wave forces, in the context of FEM, is performed on an element by element basis. Wave forces on a specific element depend on wave particle motion at the location of the element as well as the size and orientation of element surfaces and the submerged volume of the element. Thus, as indicated in Figure 3.2, structural geometry information must be communicated from the FEM model to the WLS. This data is then combined with a wave theory model to determine the local wave kinematics from which the local surface and body forces are determined and returned to the FEM model.

3.4 FEM Wave Loads

In an FEM model, the structural geometry is represented by a collection of elements. The member volumes and surfaces loaded by wave action, such as the bridge girder with seaward face highlighted in Figure 3.4 (left), is represented by elements and exposed element surfaces shown in Figure 3.4 (right). As a result, wave loading in the FEM model is specified on an element by element basis (element based loading). Element geometric data, including position, volume, and surface area and orientations must be passed from the FEM model to the WLS for determination of element loading.

Interaction between the FEM software and WLS for element loads is accomplished by user defined Element Data Transfer routines. User defined routines are often written in common programming languages (e.g. Fortran) and link the FEM software to external routines and/or programs. Abaqus provides an interface structure that allows incorporation of externally generated element surface and body loads into the FEM analysis. The data transfer routines may be written in the Fortran programming language using the following interface format:

```

subroutine dload(f, kstep, kinc, time, noel, npt, layer, kspt,
1          coords, jltyp, sname)
user code here

return
end

```

where the subroutine `dload`, is any user defined Fortran code that returns a force, f , to the FEM simulation. The force, f , may represent a surface or body load, and may be the result of computations coded into the `dload` subroutine or by interaction with external programs.

Information about the FEM model that is provided to the subroutine includes the simulation time, `time`, a unique number identifying the current element, `noel`, the position of the current element integration point by the array, `coords`, and the type of force (surface or body), `jltyp`.

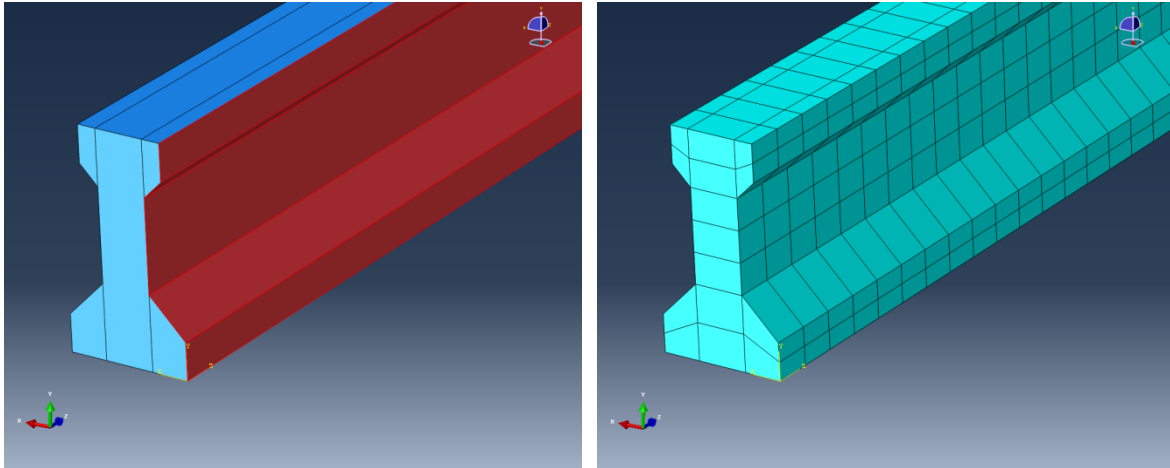


Figure 3.4. Impact surfaces (left in red) represented by individual finite element faces (right).

This functionality allows a user to specify structural loading on an element by element basis having been provided simulation time, element number and position. The structural loading due to wave and surge forces is the result of wave velocity, acceleration, and structural buoyancy. Wave velocity generates surface loads on elements while buoyancy and wave acceleration generate body loads.

3.4.1 Surface Impact Loading

Determination of wave impact loading on a single element surface (face) requires position of the element face in the water particle velocity field and the orientation of the face with respect to wave motion. While the wave particle velocity fields are continuous functions of position, the FEM only allows specification of load intensity at specific locations (integration points) on each element face. Finite element software such as Abaqus, provide access to integration point locations, making determination of the instantaneous velocity field data using wave equations such as Equations 3.3 through 3.6 trivial. Care must be taken to assure that integration point locations (commonly specified with respect to the model's global coordinate system) and the wave particle velocity field coordinate system share a common datum.

Calculation of the surface force associated with the particle velocity, requires the surface orientation with respect to the flow field. Finite Element analysis software may not provide user defined load routines with information sufficient for determining surface orientation (e.g. element number and integration point coordinates only). Thus determination of the element orientation for surface impact forces requires additional effort.

The surfaces of structural components impacted by the wave may be arbitrarily oriented with respect to the wave motion. In finite element meshes, the geometry of each element is defined by specification of element nodes. Nodes, in turn, are defined by position

vectors (nodal coordinates). The nodal position vectors may be used to determine the orientation of element faces by computing the element face normal vector as the cross product of vectors aligned along any two element edges (Figure 3.5). Determination of element face normal vector can be performed during a FEM simulation if the software provides access to nodal coordinates, if access is not provided, as is the case with Abaqus, surface normal vectors may be determined by processing the mesh geometry externally, and developing a database of surface normal vectors. Once the correct element face orientation has been identified, the vertical and horizontal components of the surface forces are determined using Equations 3.9 and 3.10.

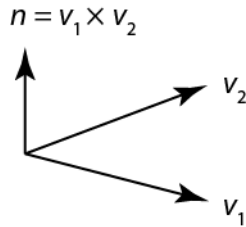


Figure 3.5. An element face is specified in terms of positions of its corners (nodes).
Note: The surface normal vector n , is easily found as the cross product of vectors v_1 and v_2 .

3.4.2 Body Loads

Body loads are induced by particle acceleration (inertia loading) and buoyancy. The inertia loads given by Equation 3.11 depend on the wave particle acceleration at the element integration point coordinate, which for linear gravity waves is computed directly using Equations 3.4 and 3.6, and the result returned to the FEM simulation.

Precise determination of the buoyancy force requires determination of the volume fraction of a finite element (an arbitrary polygonal solid) below the wave surface (an oriented curved surface in three dimensions, Figure 3.6 left). Because of the nontrivial nature of the required geometric computations, the first order approximation illustrated in 2D by Figure 3.6 (right) was taken. The element volume is approximated by a minimum enclosing box oriented along the global coordinate axes. The water height is determined at the vertical edges of the enclosing box using the wave profile elevation from Equation 3.2.

The local wave elevation is computed as the linear average of the edge elevations. The submerged volume fraction is then approximated by the submerged height fraction (Figure 3.6 right). The resulting buoyancy force load per unit volume, is then given by:

$$f_b = \rho g(V_s/V) \approx \rho g(h_{submerged}/h_{element}) \quad (3.12)$$

with the fractional height restricted to values between 0 and 1.

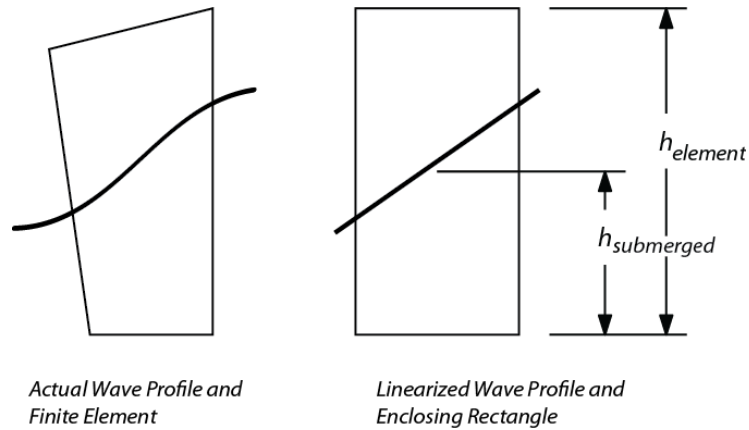


Figure 3.6. Approximation of the submerged element volume is illustrated for the 2D case.
Note: The actual wave profile and polygonal element (left) are approximated by the linear wave profile and enclosing rectangle (right). The ratio of the volume submerged to total volume is approximated by the ratio of the average height submerged to the total element height.

3.5 Wave Load Model Verification

The FEM based wave load simulation approach was implemented within Abaqus. In order to verify that the wave load equations were correctly implemented, simulations were performed using a geometrically simple block structure shown in Figure 3.7. The simulation results were checked against closed form solutions to assess the accuracy of the FEM approach used.

3.5.1 Verification Simulation Model

To verify the implementation of the linear wave theory and wave force equations, a simple simulation was performed. The structure modeled is a rectangular box with dimensions 4 x 2 x 2 ft in the x, y and z, directions respectively. The FEM mesh consisted of two elements with nodal coordinates show in Figure 3.8. The base of the box (x,0,z) was fixed in x, y, and z directions, and was aligned to the still water level.

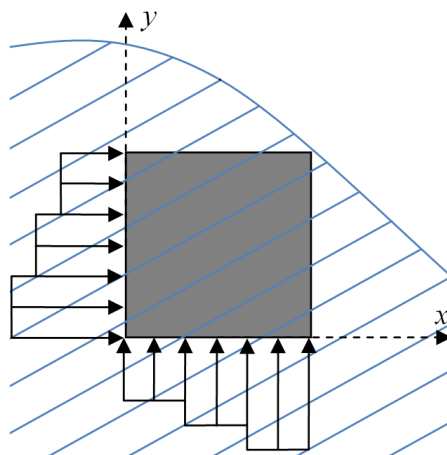


Figure 3.7. Model verification was performed using a simple block geometry.

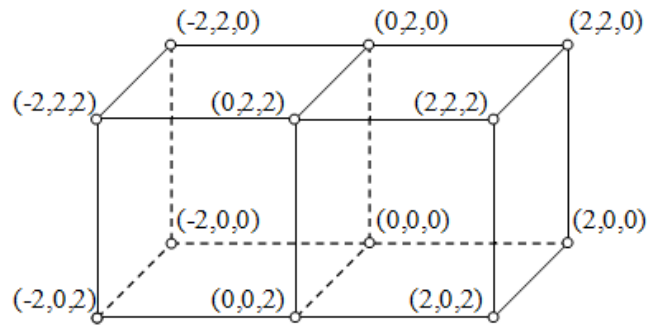


Figure 3.8. A two element rectangular box with nodal coordinates shown was used to verify the finite element implementation of the wave force equations.

For this simulation, the assumed wave conditions resemble those of the U.S. 90 Biloxi Bay Bridge (Douglass et al. 2006), with: water depth (d) of 16 ft, wave height (H) of 10 ft, and wave period (T) of 6 sec.

The simulation results were divided into: horizontal surface, vertical surface, and body loads. Dynamic effects and gravity were not accounted for so that a comparison could be made between the reactions taken from the Abaqus simulations and hand calculations. Table 3.1 provides results of the comparison.

Table 3.1. Simulation results compared to analytic solutions for a simple verification model

Component	Simulation (lb)	Hand Calculations (lb)
Horizontal Surface	606	605
Vertical Surface	1089	1089
Body	1030	1030

3.6 Wave Force Validation

In order to establish the validity of the modeling approach, and assign values to wave force model constants, simulations were developed that correspond to wave impact experiments conducted at Oregon State University (OSU). The OSU experiments (Bradner, 2008; Bradner et. al. 2011) consisted of subjecting a geometrically precise scaled bridge span model to a variety of wave conditions. The geometric details of test specimen were based on a 1:5 scale replication of a typical section of the I-10, Escambia Bay Bridge near Pensacola, Florida. Figure 3.9 shows the specimen girders and diaphragms, while Figures 3.10 and 3.11 show the geometric measurements of the model components. The prototype bridge span was 11.3 ft long.



Figure 3.9. OSU Model of a typical Escambia Bay Bridge Section Over Escambia Bay (Bradner 2008).

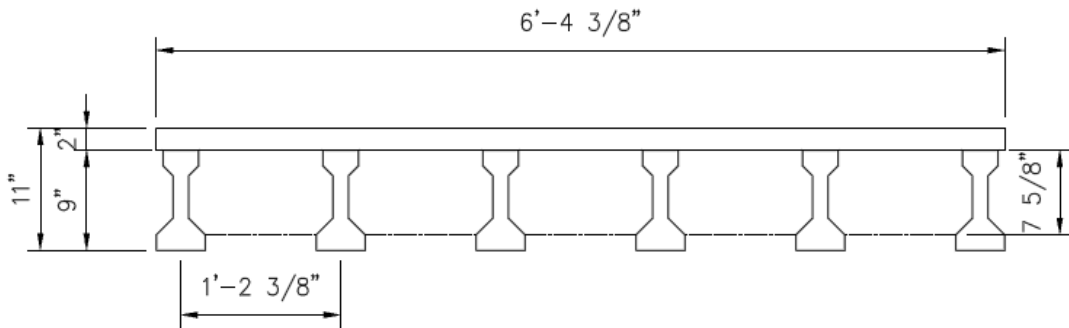


Figure 3.10. OSU Bridge cross section.

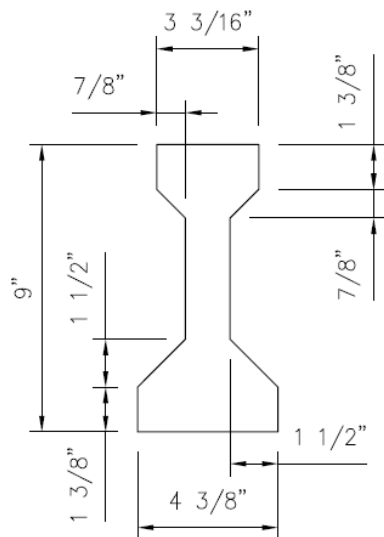


Figure 3.11. OSU Girder cross section.

The OSU scale model was placed in the Large Wave Flume at the O.H. Hinsdale Wave Research Laboratory. The model was supported by attaching the specimen girders to reaction frames. The reaction frames were instrumented to record a variety of force and displacement measurements.

The model was subjected to a variety of regular and random wave conditions that were chosen to correspond to conditions likely to occur to Gulf Coast bridges during hurricane events. These included still-water elevations (SWE) ranging from 5.3 ft (1.61 m) to 7.1 ft (2.17 m). The bottom height of the bridge girders was 6.2 ft (1.89 m), making the SWE vary from -0.9 ft (-0.28 m) below to 0.9 ft (+0.28 m) above the bottom of the bridge girders. Wave heights ranged from 0.8 ft (0.25 m) to 3.4 ft (1.0 m), and wave periods ranged from 2.0 to 3.0 seconds.

For regular wave trials, the experimental results were analyzed to establish relationships between peak structural reaction force and wave height, water depth, bridge clearance, and wave period. The total number of trials performed was 144.

The evaluation determined that a SWL located at the bottom of the bridge girders corresponded to the most consistent force measurements (see Bradner 2008 p. 31). As such, this data was used for the purpose of model validation.

3.6.1 FEM Structural Model

The FEM structural model of the OSU test specimen is shown in Figure 3.1. The deck is removed in a portion of the figure to expose the bridge girders and diaphragms and to highlight their resemblance to those of the actual test specimen shown in Figure 3.9. The finite element mesh consisted of a relatively coarse discretization of the 28,680, eight-node hexahedral elements in representation of bridge deck, girders, and diaphragms. The purpose of this evaluation was to examine qualitative structural behavior and extraction of support reactions. For this purpose, a course mesh is acceptable. The structural supports were modeled by fixing the translational degrees of freedom of the nodes located at the bottom of the girder ends, leaving a free span of 10.9 ft (3.32 m). The concrete was modeled as a linear elastic material with a density of 163 lb/ft³, which allowed the total weight of the FEM structural model to match the reported 4270 lb weight of the OSU model.

3.6.2 WLS Storm Models

For the purposes of model validation, experimental results for simply supported bridge girders with a still water elevation (SWE) located at the bottom of the bridge girders were considered. Table 3.2 shows the storm model, wave profile data simulated along with equivalent full scale profiles under Froude scaling. The wave heights range from 0.5 ft to 2.0 ft, and correspond to full scale wave heights from 2.5 to 10 feet. The modeled wave periods were 2.0, 2.5, and 3.0 seconds. These wave periods correspond to full scale wave periods of 4.5, 5.6, and 6.7 seconds. This range of wave heights and periods includes estimated conditions at the Biloxi Bay Bridge during Hurricane Katrina (Chen et al. 2009). The wave lengths were determined as the root of Equation 3.1.

Table 3.2. Simulation load cases for Oregon State Scaled Model

Load Case	Model				Full Scale			
	T (sec)	D (ft)	L (ft)	H (ft)	T(sec)	D (ft)	L (ft)	H (ft)
1	2.0	6.2	19.7	0.5	10.0	31.0	98.5	2.5
2	2.0	6.2	19.7	1.0	10.0	31.0	98.5	5.0
3	2.0	6.2	19.7	1.5	10.0	31.0	98.5	7.5
4	2.0	6.2	19.7	2.0	10.0	31.0	98.5	10.0
5	2.5	6.2	28.2	1.0	12.5	31.0	141.0	5.0
6	2.5	6.2	28.2	1.5	12.5	31.0	141.0	7.5
7	2.5	6.2	28.2	2.0	12.5	31.0	141.0	10.0
8	2.5	6.2	28.2	2.5	12.5	31.0	141.0	12.5
9	3.0	6.2	36.4	1.0	15.0	31.0	182.0	5.0
10	3.0	6.2	36.4	1.5	15.0	31.0	182.0	7.5
11	3.0	6.2	36.4	2.0	15.0	31.0	182.0	10.0
12	3.0	6.2	36.4	2.5	15.0	31.0	182.0	12.5

Note: T is wave period; D is SWE; H is wave height; L is wave length

Table 3.3 shows the resulting wave lengths along with the corresponding wave length to water depth ratio. The ratios confirm the conditions correspond to intermediate or transitional water depths.

Table 3.3. Wave lengths and wave length to depth ratio's for simulated waves

T (sec)	L (ft)	L/d
2.0	19.72	0.30
2.5	28.22	0.22
3.0	36.41	0.17

Figure 3.12 provides a scaled view of the wave profiles plotted relative to the bridge dimensions when the wave crest is centered on the bridge span. The scale view shows that most wave period and height combinations correspond to partial submersion of the bridge span. Three cases include partial submersion of the bridge deck, and two cases correspond to full submersion of the span.

The time the wave crest initially reaches the center of the bridge is given by:

$$\frac{2\pi}{T}t - \frac{2\pi}{L}x = \frac{\pi}{2} \tag{3.12}$$

where x is half the bridge width. From this equation the time at which this will occur is given in Table 3.4.

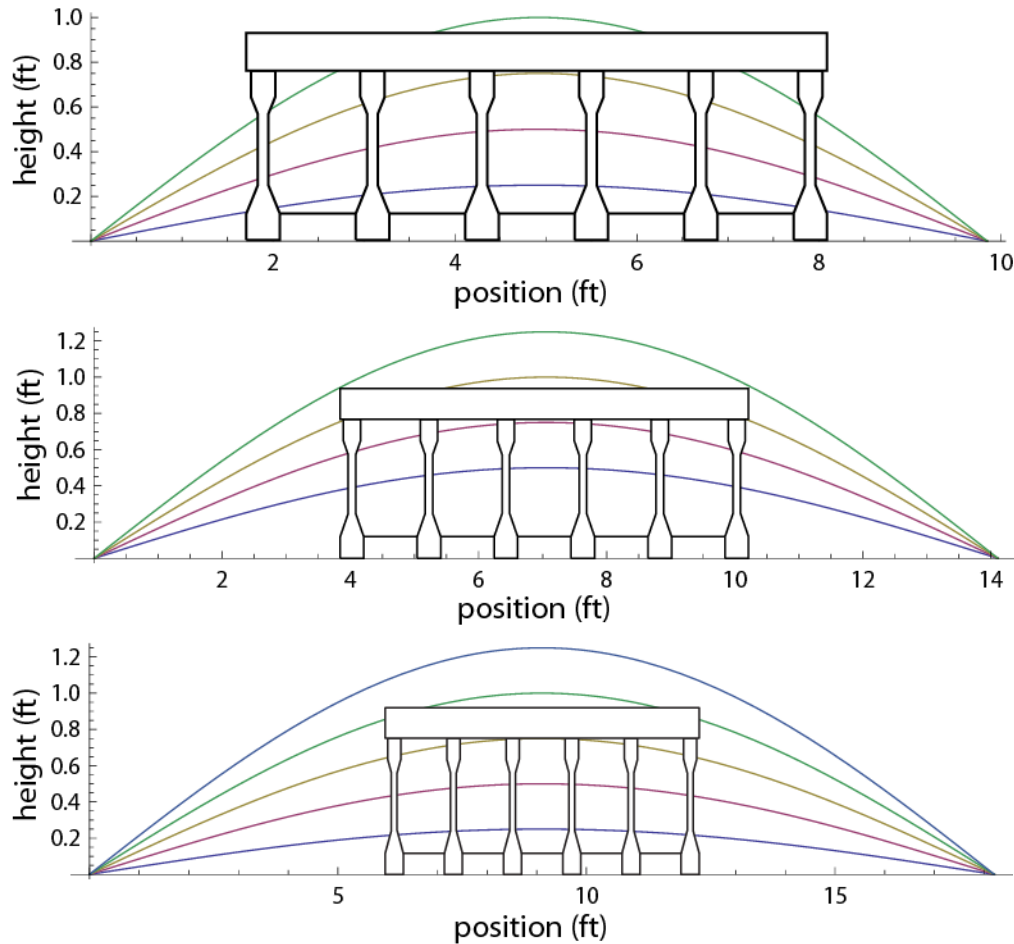


Figure 3.12. The relative size of the simulated wave compared to the bridge structure for periods: $T = 2.0$ sec (top), $T = 2.5$ sec (center) and $T = 3.0$ sec (bottom).

Table 3.4. Time for crest to reach bridge span centerline

Period-T (sec)	Time (sec)
2.0	0.82
2.5	0.91
3.0	1.01

3.6.3 Wave Force Coefficient Determination

The calculation of wave forces according to the chosen model requires determination of drag and inertia coefficients, C_d and C_m in the wave force expressions in Equations 3.9 through 3.11. There is considerable uncertainty regarding the appropriate coefficient values because they depend on the Reynolds number ($Re = UmD/\nu$) and the relative amplitude of the Keulegan-Carpenter number K (see Sarpkaya 2010, p.73), and while values can be established for simple flows and target geometries, precise determination of coefficient values for complex structural shapes subjected harmonic flow may not be possible.

The approach taken in this work was to choose values that optimize the consistency between computed maximum structural reaction forces and experimental reactions reported by Bradner (2008).

3.6.4 Horizontal Drag and Inertia Coefficients

Figure 3.13 shows the experimentally determined maximum horizontal structural reactions plotted as functions of wave height for the three wave periods considered. The plot shows that the maximum reaction is strongly dependent on wave height. For wave heights smaller than approximately 1.5 feet, the wave period has little effect on the maximum reaction, and for wave heights greater than 1.5 feet, the maximum reaction force shows a small but noticeable increase with increasing wave period.

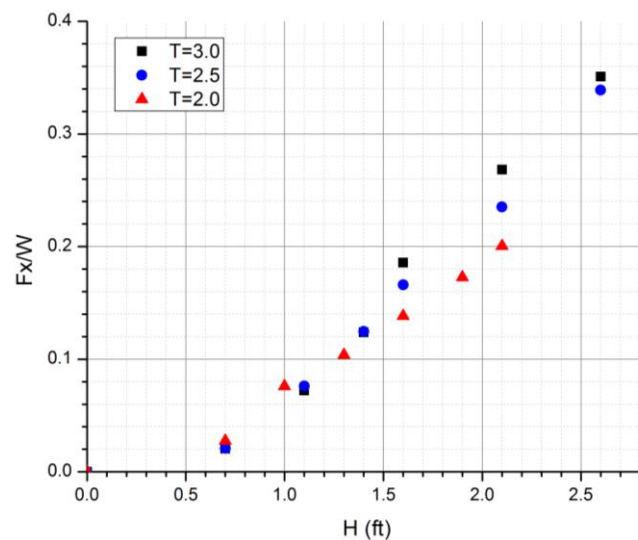


Figure 3.13. The experimentally determined maximum horizontal forces are plotted against wave height for the three wave periods considered.

The drag and inertia coefficients were sought such that the maximum horizontal reaction matched the experimental data. To understand the relative contributions of the drag and inertia force terms, the velocity and acceleration vector fields are plotted in Figure 3.14 for Load Case 2, with $T = 2$ sec and $H = 1$ ft. The right hand edge represents the wave position relative to the bridge structure at time = 0 sec. The plot shows that the horizontal component of the velocity and acceleration fields are not in phase, thus the peak drag and inertia forces have to be considered independently. The horizontal component of the velocity and acceleration vectors are in the same direction for the first (blue square) and third (green square) quarters of the cycle, and of opposite direction otherwise. In addition, with a bottom of the bridge girders at height of 6.2 ft., only the first half cycle will load the bridge super structure.

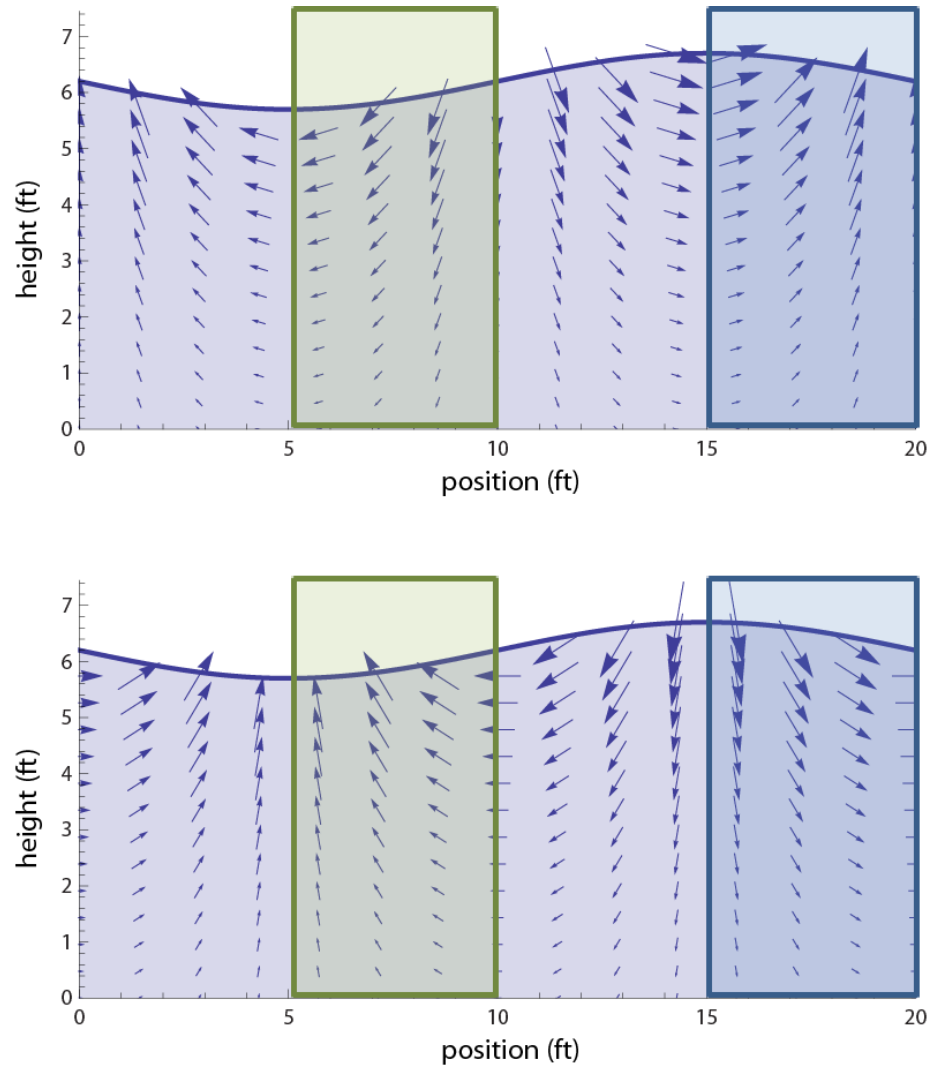


Figure 3.14. Velocity (top) and acceleration (bottom) vector fields for one wave cycle.

Note: The in-phase action is indicated by the squares, with blue in the initial impact direction and green the load reversal.

Figure 3.15 shows the time history of computed horizontal reactions from individual action of drag (CD), inertia (CM), and the additive (Tot). The reaction time histories CD, CM, and Tot are determined from two separate simulations: the first considered on the action of the drag force with ($C_d=1$, $C_m=0$), while the second considered only the inertia force ($C_d=0$, $C_m=1$). The maximum reaction due to the inertia term is 56% of the maximum due to the drag. The peak inertia reaction occurs at 0.5 sec, while the peak drag induced reaction occurs at 0.8 sec, or roughly when the wave peak is at the center line of the bridge cross-section.

The drag and inertia coefficients are chosen such that the peak reaction matches the experimental results contained in Figure 3.13. Because no other information regarding the experimental reaction (e.g. time) was available, there are an infinite number of combinations of C_d and C_m , that can provide the desired maximum. Unique values of C_d and C_m were found by assuming the maximum reaction due to inertia and drag were approximately equal.

Thus the drag coefficient C_d was assumed to be one half of C_m . This relative sizing was motivated by published values indicating that the inertia coefficient is often larger than the drag coefficient. While somewhat arbitrary, the choice will not affect the computed maximum reactions, the aim of the current work, but will affect the distribution of internal forces within structural members. A more refined approach may be required for determination of member internal force distributions.

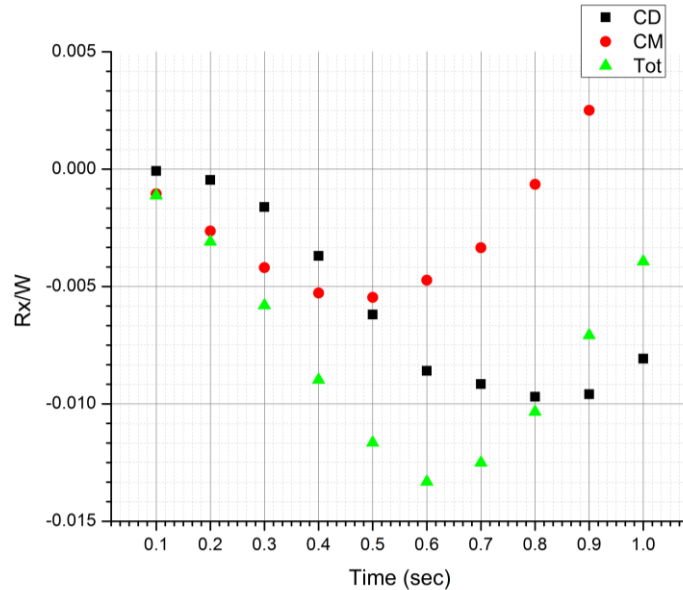


Figure 3.15. The relative size of the horizontal reaction force scaled by bridge weight due to drag (CD), inertia (CM), and the additive total (Tot).

Table 3.5 lists the coefficients determined for all the OSU simulations. The coefficients determined using this procedure depend on wave height and period. The coefficient values were largest for the small wave heights, and tended to decrease with increasing wave height for all wave periods. For wave heights greater than 1.0 ft, the coefficients increase with wave period. For the 1.0 wave height, the coefficients decrease with period.

Table 3.5. Horizontal drag and inertia coefficients for simulation wave periods and wave heights

H (ft)	T=2.0 sec		T=2.5 sec		T=3.0 sec	
	C_{dx}	C_{mx}	C_{dx}	C_{mx}	C_{dx}	C_{mx}
1.0	4.7	9.3	4.4	8.7	4.0	8.0
1.5	2.5	5.0	3.0	5.9	3.5	6.9
2.0	1.6	3.1	2.2	4.4	2.9	5.8
2.5	---	---	1.9	3.8	2.9	5.7

The resulting simulation maximum reaction forces are compared to the experimental results in Table 3.6. The differences between the simulated and experimental are much smaller than the expected accuracy of the experimentally determined reactions.

Table 3.6. Maximum horizontal reaction forces from simulations and experiments

T (sec)	H (ft)	Load Case	Rx/W		% Diff
			Sim	OSU	
2.0	0.5	C01	0.023	NA	---
	1.0	C02	0.084	0.084	6.13E-04
	1.5	C03	0.126	0.126	2.21E-05
	2.0	C04	0.168	0.168	7.00E-06
2.5	0.5	C05	0.004	NA	---
	1.0	C06	0.073	0.073	8.83E-06
	1.5	C07	0.135	0.135	7.90E-06
	2.0	C08	0.215	0.215	2.38E-06
	2.5	C09	0.311	0.311	4.87E-06
3.0	0.5	C10	0.028	NA	---
	1.0	C11	0.059	0.059	1.45E-05
	1.5	C12	0.140	0.140	8.94E-06
	2.0	C13	0.257	0.257	1.08E-06
	2.5	C14	0.408	0.408	4.15E-06

Note: T is wave period; H is wave height

3.6.5 Vertical Force Coefficients

A similar approach was taken to determine the vertical force coefficients. The normalized, experimentally determined vertical forces are shown in Figure 3.16 for the wave periods and heights under consideration. There are several vertical forces acting on the structural system:

$$F_b + F_d + F_i + F_a - W + R = 0$$

where F_b is the buoyancy force, F_d is the drag force, F_i is the inertial force, W is the gravitational load (positive down), R is the total vertical reaction, and F_a is the force due to acceleration of the body. Simulations were run to determine the size of each force contribution to the total reaction.

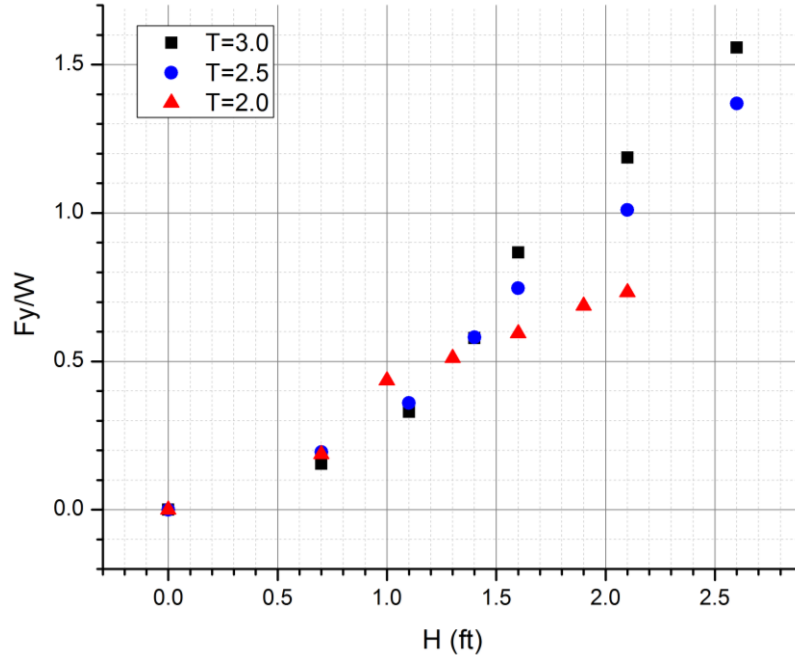


Figure 3.16. The experimentally determined maximum vertical reaction forces are plotted against wave height for the three wave periods considered.

3.6.5.1 Buoyancy

The computed reaction force due to buoyancy loading was examined by setting all other wave forces to zero. Figure 3.17 contains plots of the reaction time histories grouped by wave period. The peak reaction increases with wave period and height. For all periods, the largest increase occurs between wave heights of 1.5 and 2.0 ft. Examination of Figure 3.17 shows that the jump corresponds to initial submersion of the deck section located at 1.6 ft. For most cases, the maximum uplift occurs when the wave peak reaches the center of the bridge structure. For the case of T=3.0 sec, H=2.5 ft, the maximum reaction initially occurs at 0.9 sec and remains nearly constant until 1.1 sec. The reason that this case differs from the others is illustrated in Figure 3.18 which plots wave profiles. The plots show that under these conditions the the bridge section is completely submerged resulting in a maximum plateau between 0.9 and 1.1 sec.

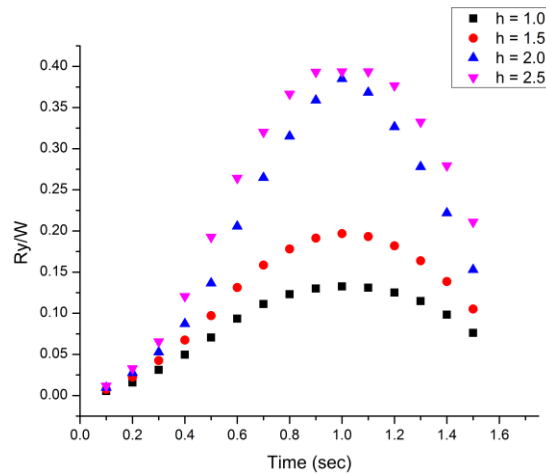
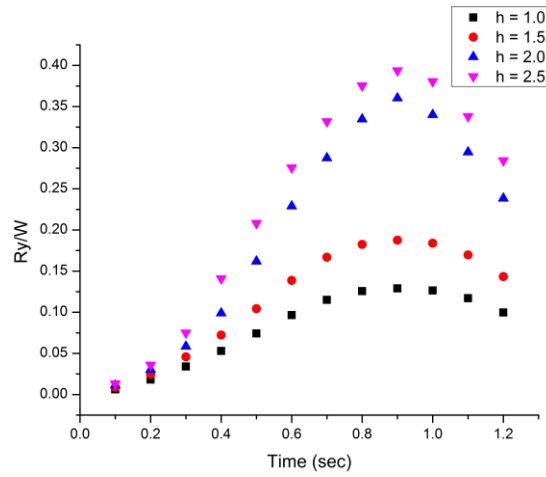
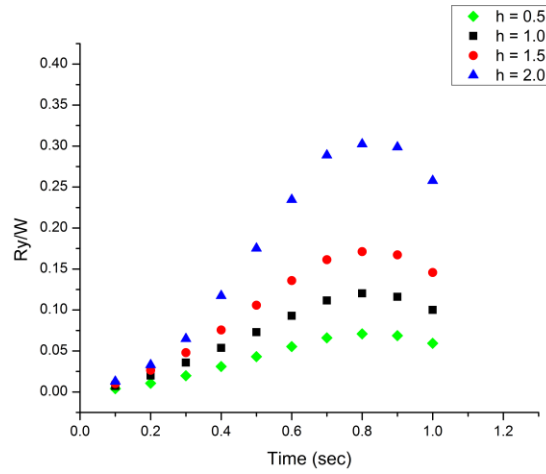


Figure 3.17. shows the uplift due to buoyancy for $T=2.0$ (top), $T=2.5$ (middle) and $T=3.0$ (bottom).
 Note: Periods $T=2.5$ and $T=3.0$ include a full submersion condition.

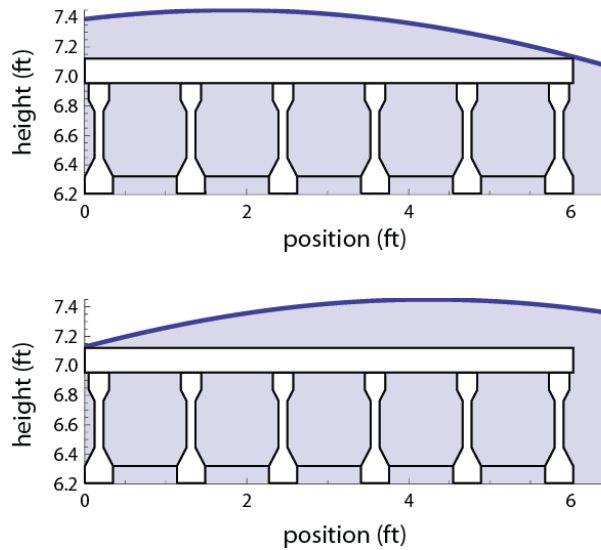


Figure 3.18. The position of the wave at maximum buoyancy for $T=3.0$, between times 0.9 (bottom) and 1.1 sec (top).

Figure 3.19 shows a plot of the maximum buoyancy loads scaled by bridge weight plotted against wave height. These values represent approximately 40% of the experimentally measured uplift forces (Figure 3.16) for wave heights below 2 ft, and as low as 25% of the experimentally measured maximum for waves exceeding 2 ft. The absolute maximum buoyancy force for simulation cases was approximately 39% of the bridge weight which compares favorably with the material density ratio used in this model:

$$\frac{\rho_{water}}{\rho_{concrete}} = \frac{2.0 \text{ slugs/ft}^3}{5.1 \text{ slugs/ft}^3} = 0.39.$$

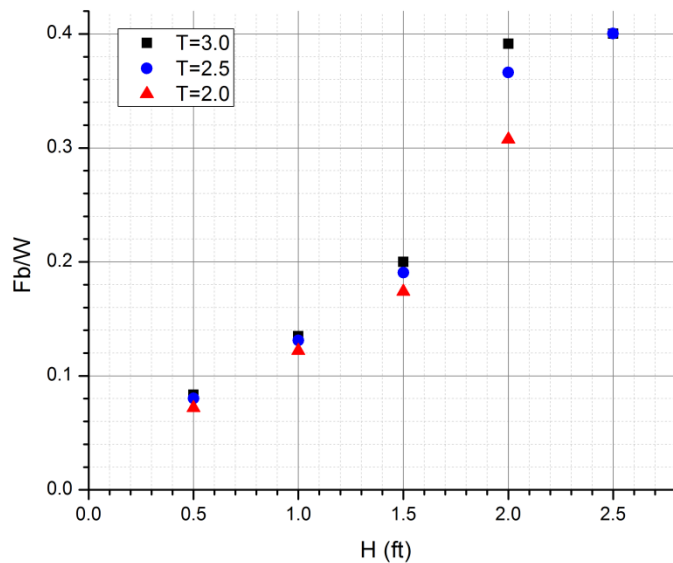


Figure 3.19. Maximum buoyancy forces as function of wave height.
Note: The buoyancy force jumps for wave heights greater than 1.5 feet which corresponds to submersion of the bridge roadway.

3.6.5.2 Vertical Drag

Simulations were run with buoyancy and vertical drag forces ($C_d=1$, $C_m=0$). Figures 3.20 through 3.22 show the computed reactions with buoyancy forces subtracted. In all cases, the maximum vertical drag occurs before maximum buoyancy force is reached. The peak lift occurred at approximately 0.4 sec for $T=2.0$, and 0.6 sec for $T=2.5$ and 3.0 sec. In all cases, vertical drag exhibited strong dependence on wave height, with a jump between 1.5 and 2.0 ft. The drag forces were significantly smaller than the buoyancy, and ranged from a minimum of 0.2% of the bridge weight for $T=2.0$, $H=1.0$, to 5.5% for $T=2.5$, $H=2.5$.

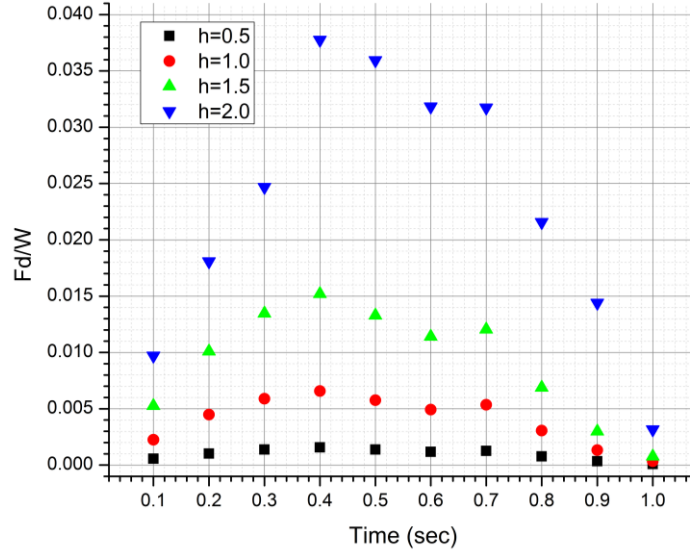


Figure 3.20. The computed vertical drag forces are shown for $T=2.0$.
Note: The maximum lift occurs at $t = 0.4$ seconds for all wave heights.

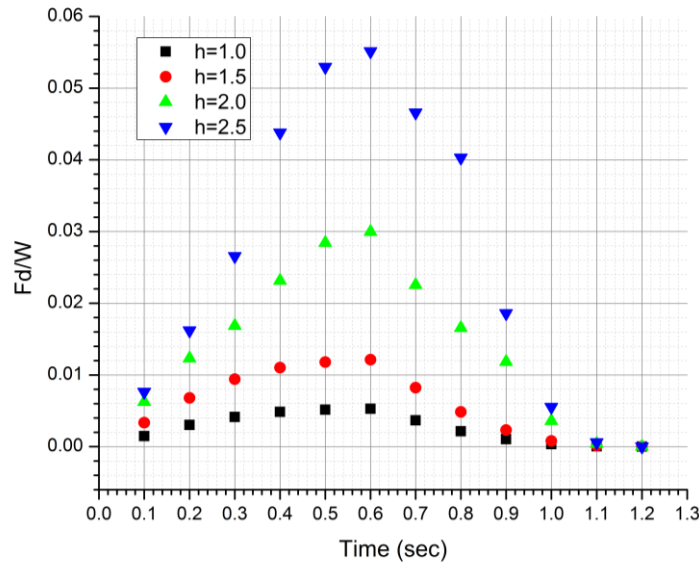


Figure 3.21. The computed vertical drag forces are shown for $T=2.5$.
Note: The maximum occurs at approximately 0.6 seconds for all wave heights.

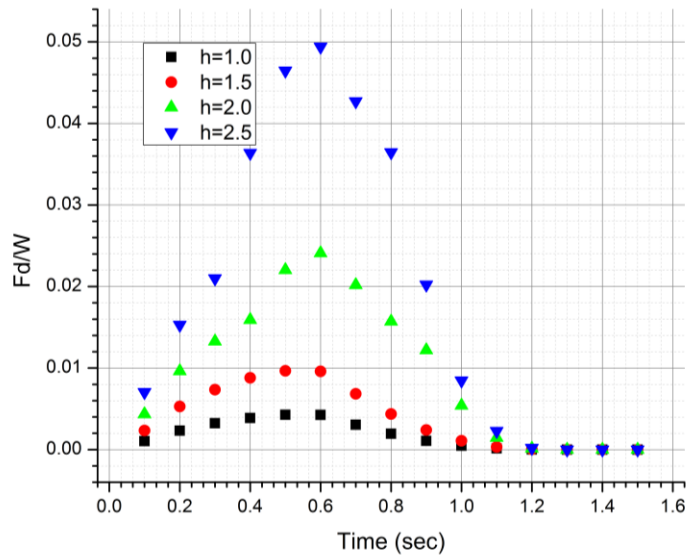


Figure 3.22. Computed vertical drag forces are shown for $T=3.0$ sec.
Note: The maximum occurs at approximately 0.6 seconds for all wave heights.

3.6.5.3 Vertical Inertia

For the first half cycle, the vertical component of the inertia force is negative, as indicated by the acceleration profile in Figure 3.14. For the second half the vertical component is positive, but because the bottom of the bridge girders are located above the SWL, the bridge is not loaded by this portion of the wave. Because the only contribution from the inertia is negative, it will be neglected for these simulations.

3.6.5.4 Vertical Drag Coefficient

The vertical drag coefficients were computed with same approach used to determine the horizontal drag coefficients. The resulting vertical drag coefficients, shown in Table 3.6 were exceptionally large, ranging from a minimum of 13.9 to a maximum of 56.7. Because these values are significantly larger than published data reviewed by the authors, it appears that the effect of lift due to wave drag forces and buoyancy does not capture the physics of the phenomena.

It is apparent that the physical basis of the proposed wave forces does not account for the totality of the measured vertical reaction forces. It is assumed that the remaining force is likely due to entrapped air. Proceeding under this assumption, and further taking the entrapped air forces to be in phase with the buoyancy, as a first estimate, a scale factor was added to the buoyancy force to account for the entrapped air force. Although the entrapped air would apply a surface force and the buoyancy force applies a body force, for the purposes of computing the reaction forces the two methods of force application would result in the same vertical reaction forces. Accurate computation of internal member force distributions would require a more physically based entrapped air force application approach.

In the revised approach, the vertical drag coefficient was taken to be the same value as the horizontal drag coefficient listed in Table 3.5, and the required buoyancy increase was computed. Table 3.7 shows the resulting buoyancy coefficients for all simulations. The coefficients averaged 2.98, with a standard deviation of 0.6. For the simulations that do not have experimental data, the value of 3.0 will be used.

Table 3.9 shows the resulting simulation maximum vertical reaction forces scaled by bridge weight compared to experimental results. The differences between the simulated and experimental results are much smaller than the expected accuracy of the experimentally determined reactions. The increase in the buoyancy forces suggests that the wave entrapped air loads range from 40 to 100% of the bridge span weight.

Table 3.7. The drag coefficients needed to match the measured maximums when only drag and buoyancy forces considered are exceptionally large

T (sec)	H (ft)	F_v/W	C_d
2	1.0	0.46	47.2
	1.5	0.57	31.0
	2.0	0.71	13.9
2.5	1.0	0.32	53.8
	1.5	0.66	41.3
	2.0	0.96	23.9
	2.5	1.30	17.3
3.0	1.0	0.29	50.7
	1.5	0.72	56.7
	2.0	1.12	40.7
	2.5	1.48	31.9

Table 3.8. Summary of buoyancy constant, C_b, needed to match the measured maximums

H (ft)	T=2.0 sec		T=2.5 sec		T=3.0 sec	
	C_d	C_b	C_d	C_b	C_d	C_b
1.0	4.7	2.91	4.4	2.92	4.0	2.31
1.5	2.5	3.09	3.0	3.37	3.5	3.41
2.0	1.6	2.30	2.2	2.55	2.9	3.04
2.5	---	--	1.9	3.19	2.9	4.53

Table 3.9. Maximum horizontal reaction forces from simulations and experiments

T (sec)	H (ft)	Run	Ry/W		% Diff
			Sim	OSU	
2.0	0.5	C01	---	---	---
	1.0	C02	0.364	0.364	4.40E-04
	1.5	C03	0.546	0.546	5.28E-04
	2.0	C04	0.728	0.729	1.39E-04
2.5	0.5	C05	---	---	---
	1.0	C06	0.380	0.380	3.98E-04
	1.5	C07	0.639	0.639	2.86E-04
	2.0	C08	0.944	0.944	2.45E-04
	2.5	C09	1.294	1.294	1.25E-04
3.0	0.5	C10	---	---	---
	1.0	C11	0.308	0.308	4.95E-04
	1.5	C12	0.676	0.676	2.81E-04
	2.0	C13	1.186	1.186	2.87E-06
	2.5	C14	1.838	1.838	1.48E-04

3.7 Summary

This chapter introduced a general framework that allows the finite element method to be used to evaluate the response of a structure to surge induced wave based loading. As a demonstration of the approach, linear gravity wave theory and simple wave force theories were implemented and the approach was used to simulate large scale wave load experiments conducted at Oregon State University. The results showed that accurate reproduction of the maximum reaction forces can be achieved using this approach, even with simple wave and force theories.

The wave force theory included a small number of coefficients that link wave particle kinematics with the resulting wave forces. It was found that to match the reaction forces experimentally determined at OSU, the size of the coefficients depended on the wave height and wave period. Table 3.5 summarizes the computed coefficients.

It was found that the vertical reactions measured during the OSU experiments were much larger than those resulting from reasonable drag or inertia force coefficient values. Thus a separate source of vertical lift must be involved, which was assumed to be due to entrapped air. To account for this additional lift, a buoyancy coefficient was introduced, and the values of the coefficients are summarized in Table 3.8. The force coefficients contained in Tables 3.5 and 3.8 will be used as the basis for wave load determination in the full scale simulations found in Chapter 4.

CHAPTER 4 – FULL SCALE SIMULATIONS

4.1 Overview of Full Scale Simulations

This chapter examines the FEM simulations of full scale bridge sections subjected to storm surge induced wave loading. The bridge section geometry considered is based on blueprints of the Biloxi Bay Bridge damaged during Hurricane Katrina. The storm surges considered include estimated wave profiles from Hurricane Katrina and Hurricane Ivan as well as predicted profiles for hurricane categories ranging from I to V.

4.2 Modeled Bridge Structure

The Biloxi Bay Bridge was located along one of the two main east-west corridors for the Mississippi Gulf Coast on US Highway 90 connecting Biloxi to Ocean Springs. Before damage by Hurricane Katrina, average daily traffic (ADT) counts were approximately 30,000 according to the Mississippi Department of Transportation (MDOT). The water depth surrounding the bridge is shallow (2 to 3 ft), with exception of a 11 to 12 ft deep shipping channel (Douglass et al. 2006).

The geometry of the Biloxi Bay Bridge was obtained using as-built blueprints provided by MDOT. Geometric simplifications were incorporated into the model as appropriate. The superstructure of the original bridge included pre-stressed concrete girders with a cast-in-place reinforced concrete deck shown in Figure 4.1. The deck was 52 ft long and 33.4 ft wide. The weight of the bridge span evaluated on the blueprints was 300 kips. Each girder's span length was 52 ft with a cross-sectional area of 3.06 ft²; detailed girder dimensions are provided in Figure 4.1. The Biloxi Bay Bridge had full depth diaphragms, which were spaced so that ten cavities were present within each span created by the connection of the girders and the diaphragms. The bridge sections were supported by pier caps at each end and no resistance to vertical lift was provided.

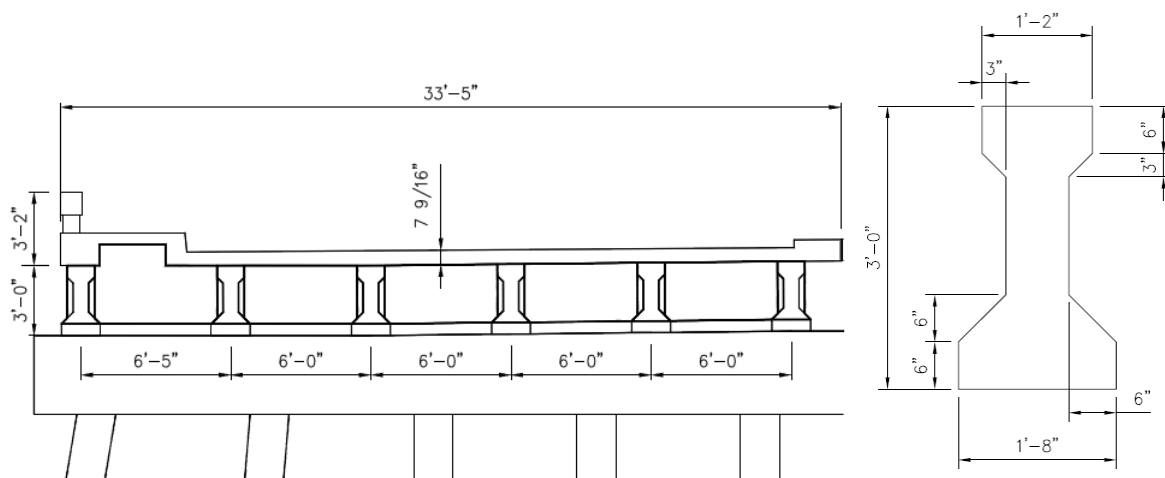


Figure 4.1. Biloxi Bay Bridge typical span and girder cross sections.

4.3 Finite Element Model

The finite element model is composed of a bridge geometry mesh, boundary conditions that specify and control bridge displacements at support locations, and applied loads. The following sections describe the finite element model.

4.3.1 Finite Element Mesh

The finite element model of the Biloxi Bay Bridge structure geometry is shown in Figure 4.2 with and without the deck present. For purposes of this evaluation, the deck geometry was simplified to a flat surface, and the exterior railing was removed. The bridge deck mesh and girders contained approximately 19,000 Hexahedral elements having isotropic, linear elastic, material properties.

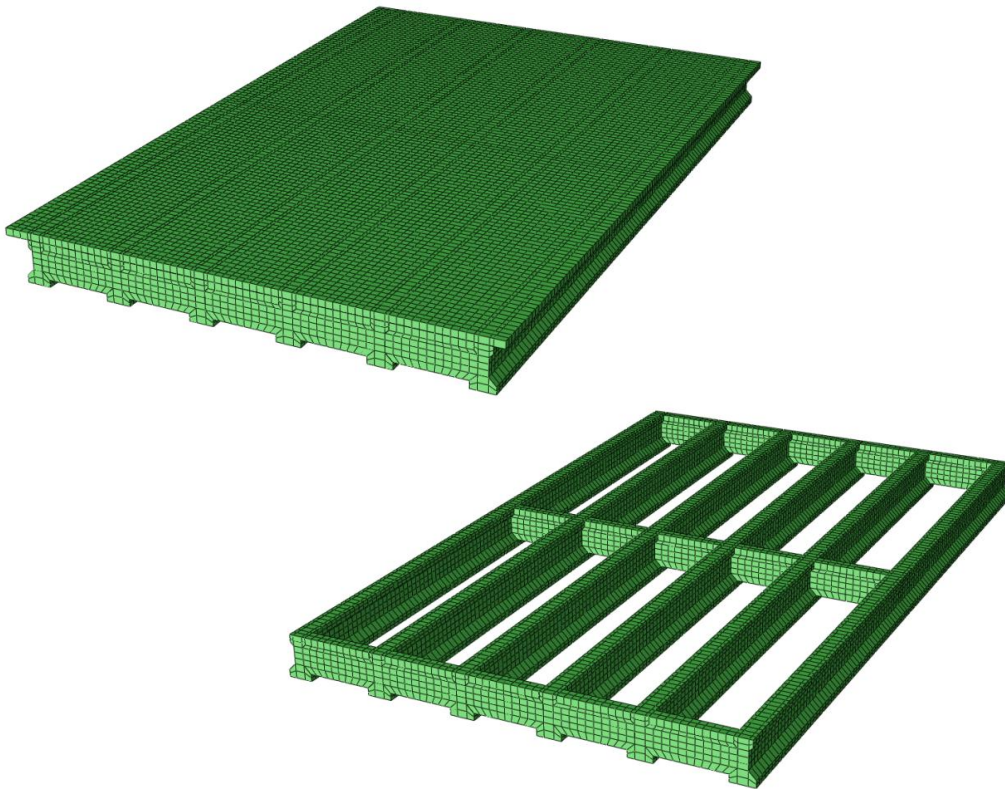


Figure 4.2. Biloxi Bay Bridge model.

4.3.2 Bridge Supports

The primary purpose of the FEM simulations was to predict wave induced reaction forces for use in bridge retrofit calculations. Reaction forces were considered for three support conditions:

- BC1 Girders pinned at both ends: no translations at either end.
- BC2 Girders simply supported: z translation (parallel to traffic) allowed at one end.
- BC3 Girders simply supported, with +y (vertical) motion allowed.

4.3.3 Wave Profiles

Wave profiles were established for a variety of storm intensity scenarios, ranging from Category I through Category V. Fourteen wave loading events were simulated. Four were from case studies of Hurricane Katrina and Hurricane Ivan, and ten were from a Texas Department of Transportation report (Jin et al. 2008) providing predicted wave parameters for a variety of storm strengths.

4.3.3.1 Wave Profiles for Recent Hurricanes

Wave profiles corresponding to recent storm events were used to compute reaction forces (Table 4.1). They include: Hurricane Katrina at US 90 over Biloxi Bay Bridge, with wave profile information from Douglass et al. (2006); Hurricane Ivan at I-10 over Escambia Bay from Krolak (2007); Hurricane Katrina at US 90 at Biloxi Bay from Krolak (2007); and Hurricane Katrina at US 90 over St. Louis Bay with profile information from Krolak (2007). Figure 4.3 shows the wave profiles superimposed on the bridge cross section. Wave induced surface and body loads were calculated using the WFS software assuming that surge SWE corresponded to the bottom of the bridge girders.

Table 4.1. Wave profiles for recent hurricanes

Load Case	Bridge/Storm	Source	T (sec)	D (ft)	H (ft)	L (ft)
1	U.S. 90 Biloxi Bay/Katrina	Douglass et al. 2006	6	16	10	130
2	U.S. 90 Biloxi Bay/Katrina	Krolak 2007	5	20	11	114
3	I-10 Escambia Bay/Ivan	Krolak 2007	3	12	13	49
4	U.S. 90 Bay St. Louis/Katrina	Krolak 2007	6	25	15	157

Note: T is wave period; D is SWE; H is wave height; L is wave length

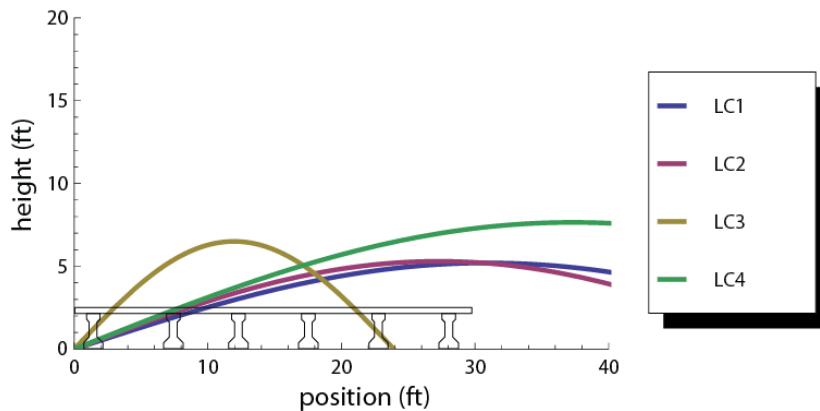


Figure 4.3 Wave profiles for recent hurricanes.

4.3.3.2 Predicted Profiles for Storm Categories

To examine reaction forces for a variety of storm strengths, simulations were performed using wave profile information produced by Jin et al. (2008). Site specific wave

profiles were available for several Texas coastal bridges vulnerable to hurricane induced wave forces. Numerical models were developed using the Advanced Circulation Model for Oceanic, Coastal and Estuarine Waters (ADCIRC) and the Simulating Waves Near Shore (SWAN) software in order to predict extreme wave heights and periods for hurricane Categories I through V. The wave profile information developed for the Galveston Causeway, as shown in Tables 4.2 and 4.3, forms the basis for the wave force simulations performed in this work.

Table 4.2. Galveston Causeway extreme wave heights (ft) as functions of surge height and storm category

Storm Category	Surge (ft)							
	0.0	3.3	6.6	9.8	13.1	16.4	19.7	23.6
I	5.4	7.5	9.5	12.0	13.0	14.0	15.0	15.5
II	5.5	7.8	9.8	13.0	14.0	16.0	17.0	18.0
III	5.8	8.3	10.0	12.5	14.5	17.0	19.0	21.0
IV	6.1	8.5	11.0	13.5	15.5	18.0	20.0	22.0
V	6.5	9.3	12.0	14.0	16.0	19.0	21.5	24.0

Table 4.3. Galveston Causeway extreme wave periods (sec) as functions of surge height and storm category

Storm Category	Surge (ft)							
	0.0	3.3	6.6	9.8	13.1	16.4	19.7	23.6
I	2.8	3.3	3.7	4.5	4.5	4.5	4.5	4.5
II	2.8	3.3	4.0	4.0	4.9	4.9	4.9	4.9
III	2.5	3.0	3.7	4.5	4.5	5.4	5.4	5.4
IV	3.0	5.4	3.3	3.7	4.5	4.9	4.9	5.9
V	4.0	4.9	5.9	6.5	7.2	4.5	4.9	5.4

Water depths for Category I through V storms were developed by assuming a SWE of 5 feet, and adding surge levels for categorized storms from the Saffir-Simpson Hurricane Intensity Scale (Table 2.2). This yielded minimum and maximum water depths for storm Categories I through V. Wave heights and periods were then determined by interpolation of tabulated data in Tables 4.2 and 4.3. The resulting wave profile data is provided in Table 4.4. The plots of the simulated wave profiles are superimposed over the bridge cross section in Figures 4.4 through 4.8.

Table 4.4 Extreme wave and storm surge estimations

Category	Load Case	T (sec)	H (ft)	D (ft)	L (ft)
I	5	3.4	7.9	9	53.8
	6	3.5	8.5	10	57.0
II	7	3.9	9.4	11	68.3
	8	4.0	10.7	13	73.1
III	9	4.2	12.0	14	80.4
	10	4.5	13.9	17	88.5
IV	11	4.4	15.5	18	89.5
	12	4.9	18.7	23	108.0
V	13	4.8	20.9	24	107.2
	14	5.3	23.5	28	127.9

Note: T is wave period; D is SWE; H is wave height; L is wave length

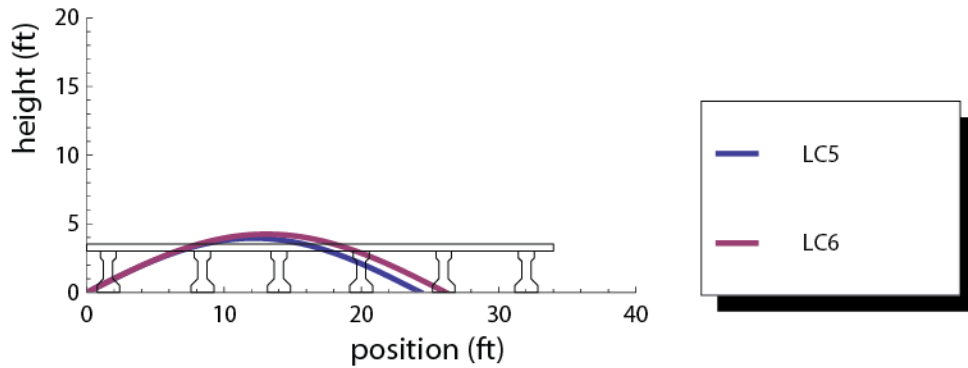


Figure 4.4. Modeled Category I predicted profiles.

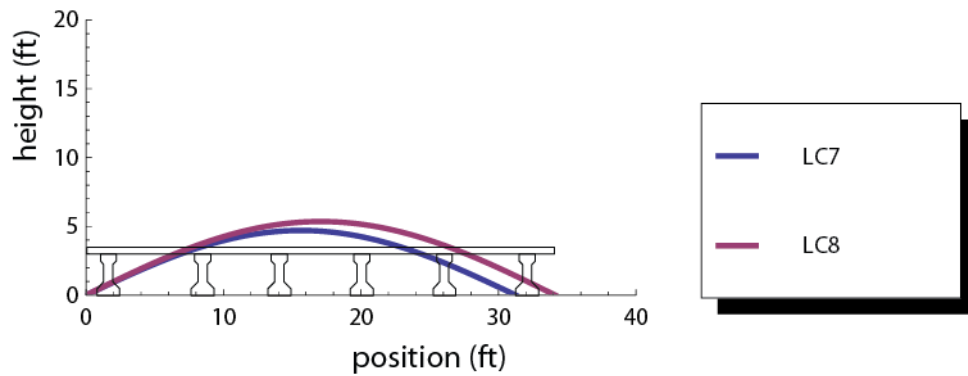


Figure 4.5. Modeled Category II predicted profiles.

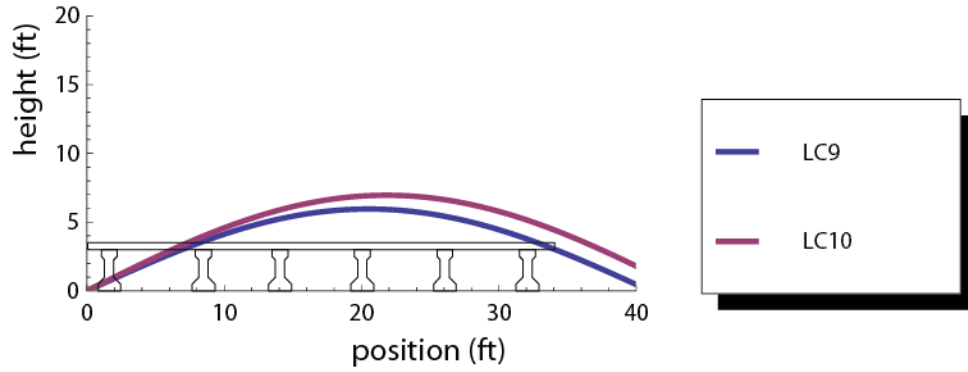


Figure 4.6. Modeled Category III predicted profiles.

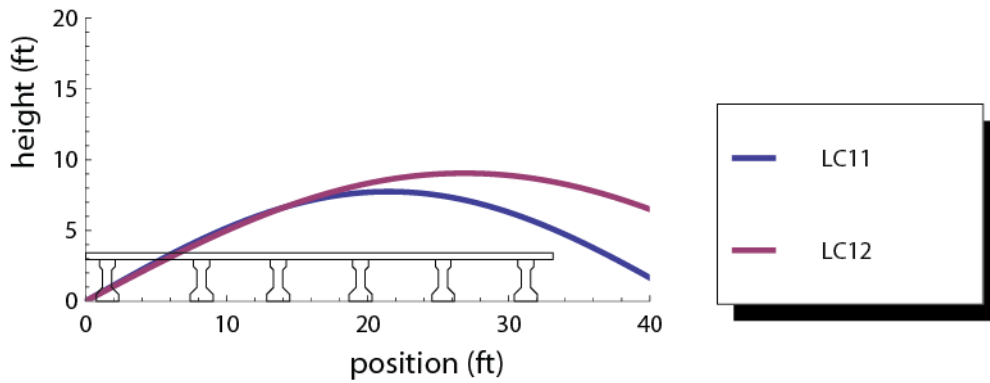


Figure 4.7. Modeled Category IV predicted profiles.

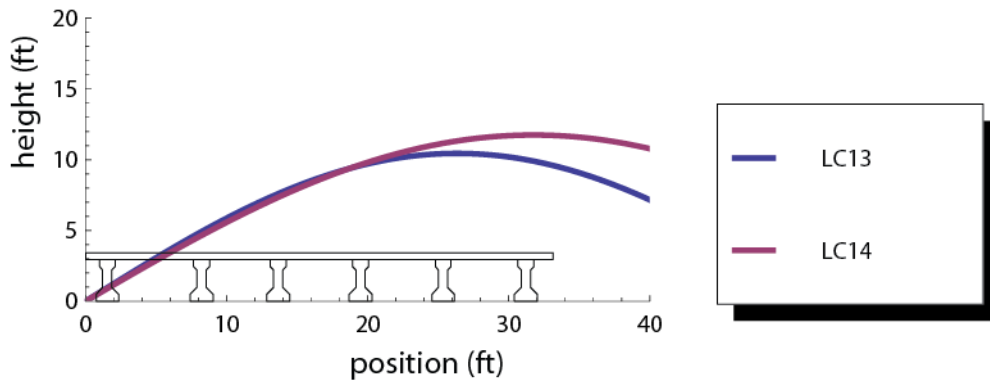


Figure 4.8. Modeled Category V predicted profiles.

4.3.4 Wave Force Coefficients

Section 3.6.4 demonstrated that the calibrated drag and inertia force coefficients depended on wave height and period. Therefore, the coefficients for the full scale simulations are assumed to vary with design wave height and period. The drag, inertia, and buoyancy coefficients used in the present simulations were developed using the calibrated values from Tables 3.5 and 3.8.

Figure 4.9 plots the OSU wave periods and heights for which coefficients were calibrated along with the full scale simulation wave periods (scaled down using Froude scaling) and heights for which drag and inertia coefficients are desired. Coefficients for the full scale simulations were determined from the OSU calibrated values by one of two methods:

1. If the desired wave period and height fell within the space of the OSU data (fully enclosed by blue), the coefficients were chosen using the natural neighbor interpolation (Sibson 1981).
2. If the desired wave period and height fell outside the space of the OSU data (blue on only three sides), simulation coefficients were assigned based on nearest neighbor interpolation (given same value as OSU data within the same blue region).

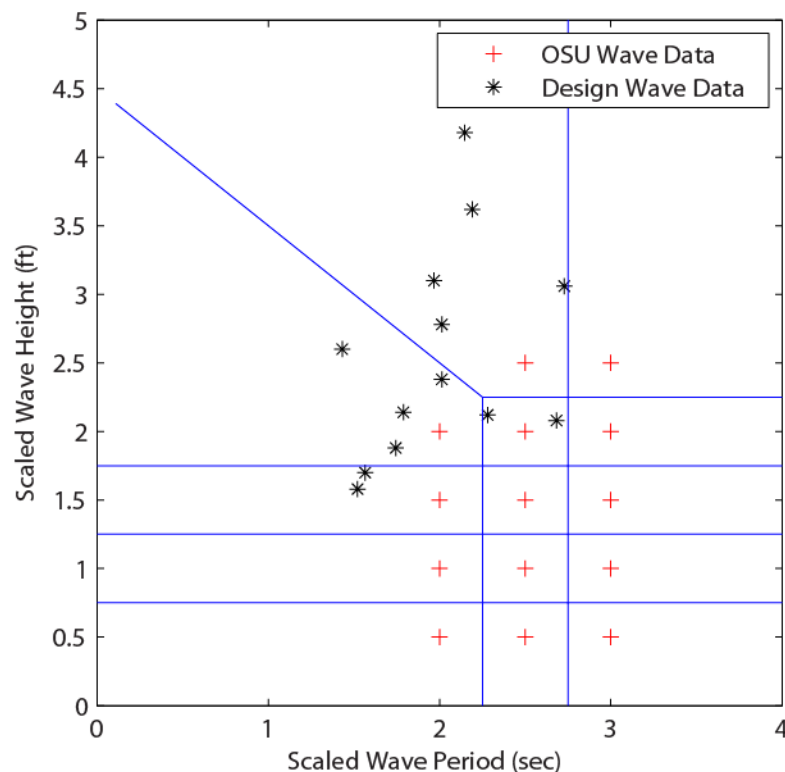


Figure 4.9. Shows the data used to determine wave forcing function coefficients for the full scale simulations.

Note: Force coefficients for full scale design wave simulations were set based on the coefficients of the nearest OSU wave data.

4.4 Maximum Total Reaction Forces

The FEM simulations provide detailed information regarding the response of the bridge structure to the wave loading. However, because the reaction forces are of primary concern in the design of support retrofits, only support reactions are presented. Table 4.5 presents the reactions extracted from simulation results and scaled by the bridge weight

(300,000 lb). The horizontal reaction R_x , is equal in magnitude to the horizontal load applied to the bridge structure by the wave action and varies from approximately 30% of the bridge weight for Category I and II storms to 125% for Category V storms. The horizontal reaction R_z , present for BC1 only, is oriented along the length of the bridge span and was not significant.

The vertical load is represented schematically in Figure 4.10. The vertical wave loading (F_y) represents the maximum vertical force due to the combined drag, inertia, buoyancy and entrapped air forces. Values vary from 50% to 225% of the bridge weight (150,000 to 675,000 lb) for Category I and Category V storms, respectively. The peak vertical reaction, R_y , is the difference between the vertical lift (F_y) and the bridge weight (W). Positive R_y values correspond to cases for which the vertical force due to wave loading is smaller than bridge weight and negative values when the vertical lift exceeds the span weight (i.e. positive values are desired). As an example, BC1 case 1 Max R_y/W is -0.29, which can be interpreted as 87,000 lb of additional restraint needed to maintain vertical equilibrium in a storm event.

The maximum vertical reactions for BC3 simulations, which allowed unrestricted vertical motion of the bridge, have been omitted from the table, because no vertical restraint was applied. It should be noted that maximum reaction forces for cases involving separation of the bridge superstructure may lead to significant transient dynamic impact forces between the bridge span with the pier cap. For cases run until impact occurred, the transient loading ranged from 4 (Case 3) to 30 (Case 10) times the bridge weight. These large forces are a result of the pier cap modeled as a ridge surface and the concrete girders as perfectly elastic members, and though they are unrealistically large, they suggest the potential for severe girder and pier cap damage due to impact.

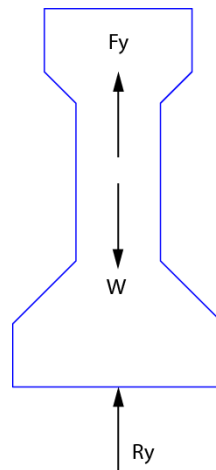


Figure 4.10. Illustrates the direction of vertical force components with respect to a single girder. F_y is the load caused by wave action, W is the weight and R_y is the reaction on the bottom surface of the girder.

Note: positive is upward.

Table 4.5. Scaled total reaction model results

	Category	Load Case	D (ft)	H (ft)	T (sec)	Scaled Horizontal		Scaled Vertical	
						Max R _x /W	Max R _z /W	Max F _y /W	Max R _y /W
BC1	---	1	16	10.4	6	0.39	0.00	1.29	-0.29
		2	20	10.6	5.1	0.28	0.00	1.16	-0.16
		3	11.7	13	3.2	0.47	0.00	0.84	0.16
		4	25	15.3	6.1	0.52	0.00	1.59	-0.59
	I	5	9	7.9	3.4	0.27	0.00	0.48	0.52
		6	10	8.5	3.5	0.30	0.00	0.57	0.43
	II	7	11	9.4	3.9	0.22	0.00	0.67	0.33
		8	13	10.7	4.0	0.28	0.00	0.82	0.18
	III	9	14	11.9	4.5	0.40	0.00	1.01	-0.01
		10	17	13.9	4.5	0.54	0.00	1.55	-0.55
	IV	11	18	15.5	4.4	0.67	0.00	1.69	-0.69
		12	23	18.1	4.9	0.88	0.00	1.89	-0.89
	V	13	24	20.9	4.8	1.09	0.00	2.09	-1.09
		14	28	23.5	5.3	1.24	0.00	2.25	-1.25
BC2	---	1	16	10.4	6	0.40		1.29	-0.29
		2	20	10.6	5.1	0.28		1.16	-0.16
		3	11.7	13	3.2	0.47	---	0.84	0.16
		4	25	15.3	6.1	0.52		1.59	-0.59
	I	5	9	7.9	3.4	0.27		0.48	0.52
		6	10	8.5	3.5	0.31	---	0.57	0.43
	II	7	11	9.4	3.9	0.23		0.67	0.33
		8	13	10.7	4.0	0.28	---	0.82	0.18
	III	9	14	11.9	4.5	0.40		1.01	-0.01
		10	17	13.9	4.5	0.55	---	1.55	-0.55
	IV	11	18	15.5	4.4	0.68		1.69	-0.69
		12	23	18.1	4.9	0.89	---	1.89	-0.89
	V	13	24	20.9	4.8	1.10		2.09	-1.09
		14	28	23.5	5.3	1.25	---	2.25	-1.25
BC3	---	1	16	10.4	6	0.40		1.29	
		2	20	10.6	5.1	0.29		1.16	
		3	11.7	13	3.2	1.42	---	0.84	---
		4	25	15.3	6.1	0.53		1.59	
	I	5	9	7.9	3.4	0.27		0.48	0.52
		6	10	8.5	3.5	0.30	---	0.57	0.44
	II	7	11	9.4	3.9	0.22		0.67	0.33
		8	13	10.7	4.0	0.36	---	0.82	0.20
	III	9	14	11.9	4.5	0.45		1.01	
		10	17	13.9	4.5	0.59	---	1.55	---
	IV	11	18	15.5	4.4	0.73		1.69	
		12	23	18.1	4.9	0.97	---	1.89	---
	V	13	24	20.9	4.8	1.21		2.09	
		14	28	23.5	5.3	1.32	---	2.25	---

Note: T is wave period; D is SWE; H is wave height; L is wave length

4.5 Maximum Force on a Single Beam

The distribution of girder forces was non-uniform across the bridge girders. As such a retrofit design must account for the extreme reaction values as well as the total lift forces. The peak girder loads were extracted for each beam for boundary condition 2 (BC2) and

listed in Table 4.6. In Table 4.6, the vertical load sign convention of the reaction forces follows that of Figure 4.10 with negative loads representing additional vertical restraint needed for vertical equilibrium. The maximum horizontal reaction force on a single beam varied from 6% to 26% of the bridge weight, and the extreme vertical forces on a single beam varied from 0% to 45% of the bridge weight.

Table 4.6. Scaled maximum beam reaction model results

	Category	Load Case	D (ft)	H (ft)	T (s)	Reactions		
						Max R_x/W	Min R_y/W	Max R_z/W
BC2	---	1	16	10.4	6	0.08	-0.08	0.00
		2	20	10.6	5.1	0.06	-0.06	0.00
		3	11.7	13	3.2	0.14	-0.13	0.00
		4	25	15.3	6.1	0.10	-0.17	0.00
	I	5	9	7.9	3.4	0.08	0.01	0.00
		6	10	8.5	3.5	0.09	0.00	0.00
	II	7	11	9.4	3.9	0.06	0.00	0.00
		8	13	10.7	4.0	0.07	-0.03	0.00
	III	9	14	11.9	4.5	0.09	-0.07	0.00
		10	17	13.9	4.5	0.12	-0.20	0.00
	IV	11	18	15.5	4.4	0.15	-0.25	0.00
		12	23	18.1	4.9	0.19	-0.32	0.00
	V	13	24	20.9	4.8	0.23	-0.41	0.00
		14	28	23.5	5.3	0.26	-0.45	0.00

Note: T is wave period; D is SWE; H is wave height; L is wave length

4.6 Comparison with AASHTO Loads

To evaluate the WFS load modeling approach, it was compared to more established wave load methods. Aguiñiga, et al. (2008) surveyed existing design guidelines through 2006 and found very limited data for development of wave loading for bridge structures. The Army Corps of Engineers, Coastal Engineering Manual (CEM 2006) was found to be the most common source of data for wave design load data.

CEM (2006) includes formula for the determination of structural loads, but the structural geometry it considered was that of a vertical wall extending to the seabed. Given the strong dependence of wave forces on geometry, correlation to bridge loads would be troublesome. The manual further recommended laboratory testing for important structures due to uncertainty in the design load development.

Overall, it appears that the *Guide Specifications* (AASHTO 2008) based design loads provide the most relevant source of comparison to the WFS. The *Guide Specifications* provides equations to develop vertical (Design Case I) and horizontal (Design Case II) loads to be used in the design of superstructure anchorage. Each design case provides vertical, horizontal, and overturning moments resolved at the far girder bottom trailing edge. Loads used for design of critical structures are multiplied by a 1.75 factor, while loads used for extreme limit state evaluation use a factor of 1.0. For the purpose of comparing the WFS, the extreme limit state is considered. The AASHTO vertical loads were calculated according to AASHTO (2008), Section 6.1.2.2, "Maximum Quasi-Static Vertical Force and Associated Forces and Moments".

Loads were computed using the *Guide Specifications* with percent air entrapments (%AIR) of 0, 20, 30, 50 and 100%. Table 4.7 shows the Design Case I maximum vertical, F_{V-AV}/W , vertical slamming F_S/W , associated horizontal F_{H-AV}/W , and associated moments M_{T-AV}/W .

Table 4.7. *Guide Specifications* Design Case I extreme event limit state loads by type at trailing edge far side girder.

Case	Category	F_{V-MAX}/W		F_S/W	F_{H-AV}/W	M_{T-AV}/W
		%AIR=0	%AIR=100			
1	---	0.68	1.57	0.73	0.24	48.28
2		0.71	1.71	0.64	0.24	50.98
3		0.23	0.77	0.17	0.07	24.10
4		1.08	2.33	1.25	0.29	71.73
5	I	0.18	0.59	0.18	0.11	19.45
6		0.21	0.66	0.21	0.13	21.83
7	II	0.23	0.70	0.30	0.18	24.50
8		0.30	0.85	0.36	0.20	29.39
9	III	0.34	0.91	0.50	0.25	33.31
10		0.43	1.13	0.58	0.25	39.79
11	IV	0.46	1.21	0.56	0.19	41.21
12		0.64	1.56	0.88	0.21	54.21
13	V	0.67	1.62	0.85	0.17	54.92
14		0.84	1.92	1.23	0.23	67.40

Table 4.8 compares the total *Guide Specifications* vertical loads of Table 4.7 with the WFS based wave loads of Table 4.5. For the categorized storm loads, the WFS vertical loads were enveloped by the *Guide Specifications*. This behavior is illustrated in Figure 4.11. The WFS loads were found to correspond most closely to the 20% entrapped air value. For surge and wave cases considered in cases 1 through 4, the WFS loads were enveloped for Case 3. For cases 1, 2 and 4 the WFS were lower than the *Guide Specification* AASHTO loads. In these cases the assumed storm category was III, but the predicted AASTHO load levels matched more closely to those of Categories IV and V, while WFS loads are similar to Category III, or III/IV levels.

Figure 4.11 shows that for (%AIR) = 20% the linear regression resulted in a 1:1 curve, showing that the 20% entrapped air case resulted in a close correspondence between the two methods. Another way to interpret the Figure 4.11 results is that the WFS prediction exceeded the AASHTO *Guide Specifications* prediction when %AIR of less than 20% was entered into *Guide's* Section 6.1.2.2 calculations, but when %AIR of more than 20% was entered into the *Guide's* Section 6.1.2.2 calculations, the WFS prediction was less than the *Guide Specifications*. This is significant as the WFS model was calibrated using data from Oregon State University and different data was used to develop the *Guide Specifications*. The WFS was enveloped by the *Guide Specifications* and showed that %AIR values on the lower end of the allowable scale provided in the manual were predicted by finite element modeling, and the finite element modeling showed the Biloxi Bay Bridge would fail in Hurricane Katrina as it did.

Table 4.8. AASHTO Case I extreme event vertical wave loads

Case	Category	AASHTO F_v/W @ (%AIR)					WFS F_y/W
		0	20	30	50	100	
1	---	1.42	1.63	1.74	1.95	2.31	1.29
2		1.35	1.59	1.71	1.95	2.35	1.16
3		0.41	0.54	0.60	0.73	0.95	0.84
4		2.34	2.64	2.79	3.09	3.58	1.59
5	I	0.36	0.46	0.51	0.60	0.77	0.48
6	II	0.41	0.52	0.58	0.69	0.87	0.57
7		0.53	0.64	0.70	0.81	1.00	0.67
8	III	0.65	0.79	0.85	0.99	1.21	0.82
9		0.84	0.98	1.05	1.19	1.41	1.01
10	IV	1.01	1.18	1.26	1.43	1.71	1.55
11		1.02	1.20	1.29	1.47	1.77	1.69
12	V	1.53	1.75	1.86	2.07	2.44	1.89
13		1.51	1.74	1.86	2.09	2.47	2.09
14		2.08	2.33	2.46	2.72	3.15	2.25

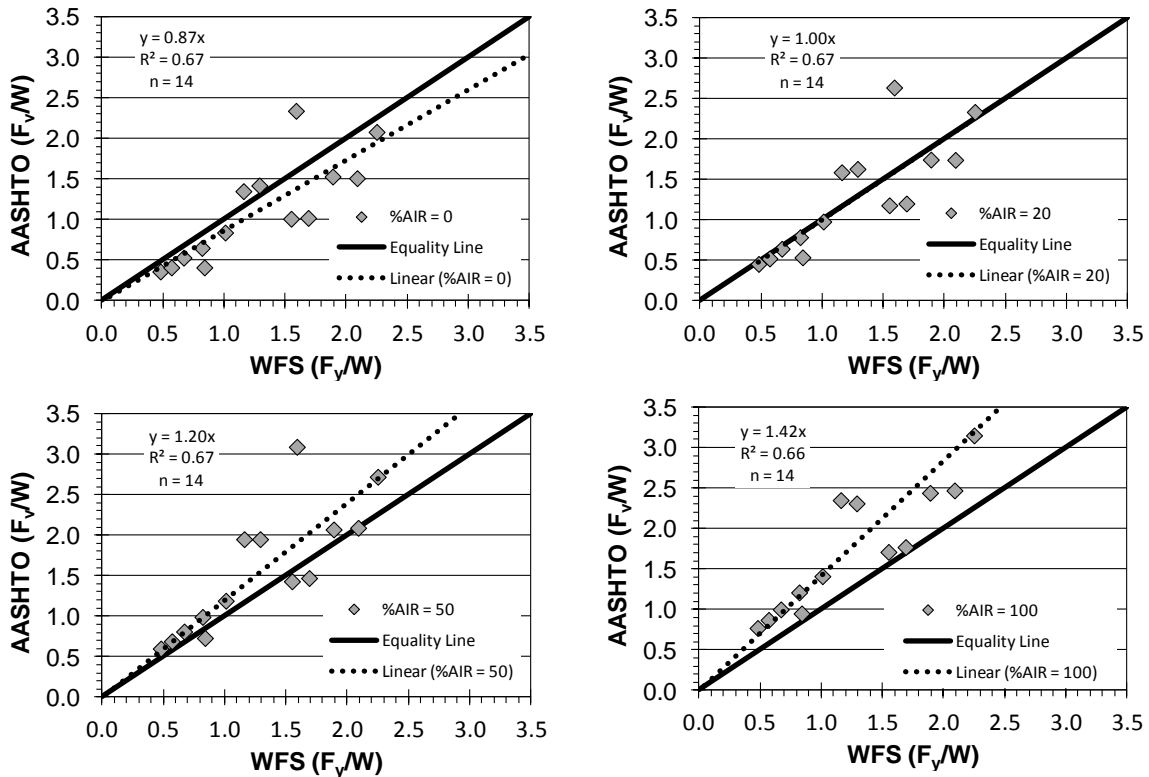


Figure 4.11. The relationship between AASHTO and WFS predicted vertical loads for various levels of percentage entrapped air are shown. The best agreement was found for %AIR = 20.

4.7 Comparison with AASHTO Single Girder Loads

The WFS maximum girder loads were also compared to the AASHTO *Guide Specification* values. The maximum WFS loads were taken directly for the dynamic simulation. In order to determine maximum AASTHO girder loads the bridge section was

assumed to act as a ridge body, and symmetric anchoring was considered for each girder. With these assumptions, the free body diagram shown in Figure 4.12 was developed to approximate the girder reaction loads. In this figure, W is the bridge weight, R_{y-Gi} is the vertical reaction at girder i , F_v is the total AASHTO vertical force acting on the entire span and M and F_h are the associated moment and horizontal loads.

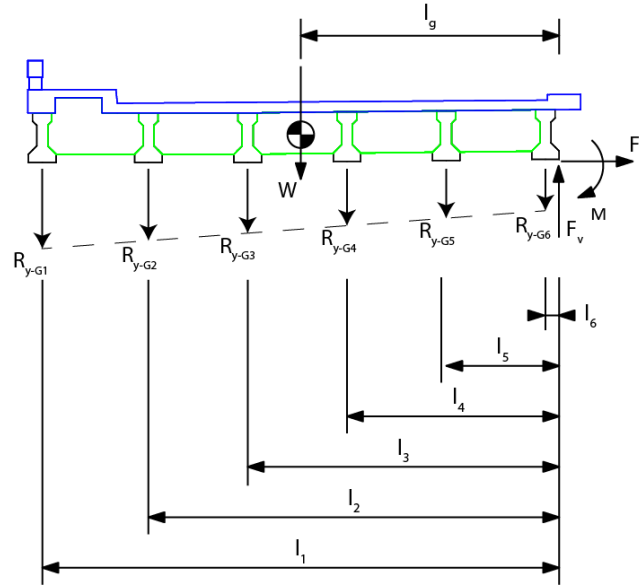


Figure 4.12. Shows the relationship between AASHTO *Guide Specification* and WFS predicted vertical loads for various levels of percentage entrapped air. The best agreement was found for %AIR = 20.

Static equilibrium in the vertical direction can then be expressed as:

$$\sum_{i=1}^n R_{y-Gi} = F_v - W \quad (4.1)$$

where n is the total number of girders. Moment equilibrium is:

$$\sum_{i=1}^n R_{y-Gi} l_i = M - W l_g \quad (4.2)$$

where l_i is the distance from the reaction to the trail edge girder location. With the assumed rigid behavior, the linear reaction variation may be written in the form:

$$R_{y-Gi} = m l_i + b, \quad (4.3)$$

where m is the slope and b the intercept at the point of the applied loads. Substituting Equation 4.3 into 4.1 leads to an expression for b :

$$\begin{aligned} \sum_{i=1}^n (m l_i + b) &= F_v - W \\ m \sum_{i=1}^n l_i + n b &= F_v - W \\ b &= \frac{1}{n} [F_v - W - m \sum_{i=1}^n l_i] \end{aligned} \quad (4.4)$$

Substituting Equation 4.3 into 4.2 yields an expression for m :

$$\sum_{i=1}^n (ml_i + b)l_i = M - Wl_g$$

$$m \sum_{i=1}^n l_i^2 + b \sum_{i=1}^n l_i = M - Wl_g \quad (4.5)$$

Combining Equations 4.4 and 4.5 leads to the following equations for the m and b :

$$m = \frac{n(M - Wl_g) - (F_v - W) \sum_{i=1}^n l_i}{n \sum_{i=1}^n l_i^2 - (\sum_{i=1}^n l_i)^2} \quad (4.6)$$

$$b = -\frac{n(M - Wl_g) \sum_{i=1}^n l_i - (F_v - W) \sum_{i=1}^n l_i^2}{n \sum_{i=1}^n l_i^2 - (\sum_{i=1}^n l_i)^2} \quad (4.7)$$

Thus the maximum AASHTO anchor force is given by Equations 4.3, 4.6 and 4.7, and occurs at Girder 1. The values were computed for %AIR = 20, and are shown for the load cases considered in Table 4.9. Figure 4.13, which plots Table 4.9 with the WFS load on the horizontal and the corresponding AASHTO load on the vertical, shows that for the small loads, the AASHTO loads are consistently larger, but as the WFS loads increase, the AASHTO loads are smaller. The latter behavior may be an artifact of the rigid body assumption, which would tend to break down as loading levels become large. This is significant as the *Guide Specifications* may be under predicting single girder loads for larger storm events due to the rigid body assumption. Loads increasing in a girder due to stiffness of surrounding members decreasing is intuitive as the surrounding members are not as equipped to transfer the loads. This behavior should be investigated further to more comprehensively quantify the effects.

Table 4.9. Comparison of AASHTO Case I extreme event, and WFS maximum single girder loading

Case	Category	%AIR = 20		AASHTO R_{v-G1}/W	WFS R_{v-max}/W
		F_v/W	M/W		
1	---	0.24	0.38	0.37	0.44
2		0.23	0.39	0.39	0.45
3		0.07	0.16	0.18	0.09
4		0.39	0.60	0.55	0.77
5	I	0.06	0.13	0.15	0.04
6		0.07	0.14	0.17	0.07
7	II	0.09	0.17	0.19	0.11
8		0.11	0.20	0.23	0.17
9	III	0.14	0.24	0.26	0.23
10		0.17	0.29	0.31	0.31
11	IV	0.17	0.30	0.32	0.32
12		0.25	0.41	0.42	0.50
13	V	0.25	0.41	0.42	0.51
14		0.35	0.53	0.52	0.70

-- $F_v = F_{V-MAX} + F_s$

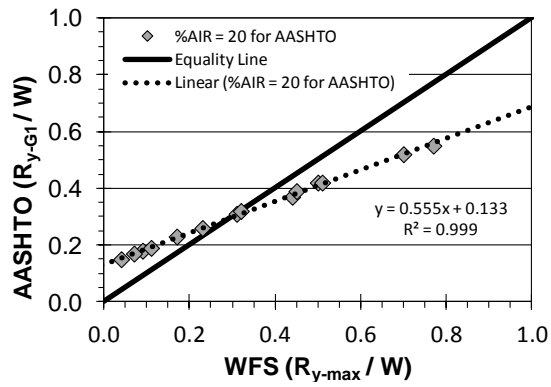


Figure 4.13. The relationship between AASHTO and WFS predicted single girder maximum loads for %AIR=20.

Note: The WFS predicted maximum girder loads were smaller for lower category I and II storms and larger for category IV and V storms.

CHAPTER 5 – RETROFIT DESIGN FOR STORM SURGE

5.1 Retrofit Design Overview

Time constraints are one of, if not the, most formidable challenges to rapidly retrofitting a bridge for storm surge as only a few hours to at most a few days will be available. The work presented in this chapter focused on rapid methods to temporarily retrofit bridges to withstand storm surge. The approach taken was to first review the *Retrofit Manual* (Modjeski and Masters 2008) and evaluate the options listed for feasibility in the aforementioned environment. The *Retrofit Manual* focuses on permanent retrofits based on a 100-year return period design event that are not performed in a rapid manner. *Retrofit Manual* options deemed feasible were evaluated; and where applicable, calculations were performed to assess their potential impact for a given storm. Construction guidance was provided for options deemed feasible.

5.2 Examination of *Retrofit Manual* Strategies for Rapid Deployment

The *Retrofit Manual* approach includes three steps: screening, evaluation, and retrofit. The screening procedure provides a simplified analysis to determine the vulnerability of a coastal bridge to storm induced surge and wave loading. Vulnerable bridges are then evaluated using one or more analysis approaches designated as Levels I, II, and III. The analysis difficulties range from Level I, which allows for simplified determination of wave parameters and loads from empirical equations, to Level III which requires an extensive computer modeling and analysis effort (e.g. Jin et al. 2008). Vulnerabilities assessed during the evaluation process may be mitigated using several approaches described in the manual:

1. Reduction of buoyancy loads
2. Reduction of wave loads
3. Connection of adjacent spans
4. Connection of bridge superstructure to substructure
5. Strengthening substructure
6. Strengthening the geotechnical capacity of the substructure
7. Accepting loss of superstructure to protect substructure

Of these six approaches, 5 and 6 are not related to bridge decks being lost in storm events, so they are not discussed further. The remainder of this section discusses approaches 1 to 4 and their attributes with respect to the goals of this study; approach 7 is indirectly considered later in this chapter.

5.2.1 Reduction of Buoyancy Loads

The information presented in Section 3.6.5.4 indicated buoyancy forces due to air entrapped between bridge girders and compressed by wave action may comprise a significant portion of the maximum vertical lift. The simulations of the OSU experiments suggest that the lift force due entrapped air varied 40% to 100% of the span weight, with 8 out of 11 cases between 60% and 100% of the bridge span weight. These results translate to vertical loads

ranging from 90,000 to 300,000 lb for the typical Biloxi Bay Bridge span. These computational results are in good agreement with entrapped air load estimates included in the *Retrofit Manual* and presented in Section 2.6 of this report. Rising surge levels can result in gradual buoyancy force increases, while wave action can generate transient buoyancy forces. The *Retrofit Manual* suggests three measures for air venting: cored deck vents, diaphragm vents (where applicable), and/or replacing concrete diaphragms.

Cored deck vents allow evacuation of inter-girder air displaced by rising surge levels as well as wave motion. Because vents can be cored from the bridge deck surface, access for retrofit can be accomplished via lane closure. As such, cored deck venting may provide an effective means of rapid retrofit.

Diaphragm vents allow movement of entrapped air along the length of the bridge. Rising surge levels may entrap air uniformly along the length of the bridge. The approach may be most effective for reducing wave-induced trapped air loads. Because the retrofit requires construction from the underside, diaphragm modifications may not be as well suited for rapid repair as cored deck vents. Solid diaphragm replacement represents a significant construction effort and while effective for longitudinal venting, would not be feasible for rapid construction.

5.2.2 Reduction of Wave Loads

Reduction of loads imparted by waves to the bridge structure may be accomplished by means of wave alteration (e.g. introduction of artificial reefs) or significant modification to the bridge structure (e.g. raising bridge elevation). Because this approach is likely to involve significant evaluation and construction efforts, rapid, economical deployment of such measures may not be feasible, and is outside the scope of this investigation.

5.2.3 Connection to Adjacent Spans

The *Retrofit Manual* suggests continuous spans are less vulnerable to storm damage than simple spans because adjacent spans are not likely to experience maximum loading simultaneously. Therefore by connecting spans, the horizontal and vertical wave load on highly loaded sections will be resisted by the weight of multiple spans. Examples for two means of connecting adjacent spans are provided: connecting adjacent girders with restraint cables, and connecting adjacent diaphragms with shear keys. Both measures would require access from below the bridge, and may not be well suited for rapid retrofit.

5.2.4 Connection of Bridge Superstructure to Substructure

Connection between the bridge superstructure and substructure prevents horizontal and/or vertical displacement of the superstructure relative to the supporting substructure. While many approaches are possible, earwalls, shear blocks, or cable restraints are specifically addressed in the *Retrofit Manual*.

Earwalls and shear blocks represent physical barriers to lateral and sometimes vertical motion of girders at the pier cap locations. Earwalls generally refer to structural components connected to the axial ends of pier caps that provide bearing supports to the outside girders. Shear blocks refer to structural components connected to the top of the pier caps and located

in between girders. For bridge superstructures with diaphragms at the ends of the girders, introduction of shear walls would require the partial removal of girder diaphragms, and would not be well suited for rapid retrofit.

Cable restraints, tie the bridge structure to the pier caps and restrain motion in the vertical and lateral directions. Cables are looped around the pile caps and threaded through holes in bridge girders and/or diaphragms. Where the capacity of the pier cap is in question the manual suggests tying the cables directly to the piles. Because of the relative simplicity, Cable restraints may be feasible for rapid retrofit.

5.3 Rapid Retrofit Options

Approaches 1 and 4 of Section 5.2 were deemed suitable for further rapid retrofit consideration in this study based on discussion provided in Sections 5.2.1 to 5.2.4. Deck venting could reduce buoyancy loads, and connection of the substructure to the superstructure could provide added lateral and uplift stability. Guidance for each of these approaches is provided in the remainder of this section.

5.3.1 Deck Venting Performed from Deck

Deck venting requires no construction materials. Coring drills with bits (e.g. 4 in and 6 in diameter) are readily available and are part of routine construction operations. Much larger core diameters are possible (e.g. 12 to 14 in diameter), though these bits are probably not as readily available to a Department of Transportation (DOT). A drill suitable for coring a bridge deck would weigh on the order of 100 lb.

Coring holes into a bridge deck can be performed from the top of the bridge deck with equipment easily transportable with light to medium duty trucks, and the process would be fairly fast. Several fairly small crews (e.g. three people per crew) could work simultaneously. The time required to vent a deck would be a function of several variables (e.g. deck thickness, concrete properties, distance between core locations) but it should be feasible with a moderate number of coring drills and corresponding construction crews (traffic control will also be needed). An estimated coring rate for a 6 in diameter hole is 30 min, which includes time for set-up, alignment, and coring (approximately half this time would be coring the concrete at approximately 0.5 in/min). Bridge deck thicknesses were ≈ 8 to 10 in for Escambia Bay and Biloxi Bay Bridges based on Figure 3.10 (1:5 scale) and Figure 4.1. With these numbers, one crew and one coring drill producing 15 holes per day is a reasonable planning estimate.

The Escambia Bay and Biloxi Bay Bridges (Figures 3.1, 3.9, 3.10, 3.11, 4.1, 4.2, and 4.3) were used as examples for construction estimates. The Escambia Bay Bridge girder and diaphragm combinations resulted in fifteen cavities that could entrap air per span (spans were 57 to 60 ft long), indicating at least fifteen cores would be needed per span to provide an outlet for all air that could be entrapped during an overtopping event. The Biloxi Bay Bridge had ten cavities (albeit larger cavities than Escambia Bay) per span (52 ft spans), indicating at least ten cores would be needed per span to provide an outlet for all potentially entrapped air. As a planning estimate, one crew of three people with one coring drill could vent one bridge deck span per day with one hole per cavity produced by girder and diaphragm intersections. The cost to core one span should be a few thousand dollars.

The number of core holes required for a particular bridge and wave combination is unknown. Additional information regarding the reduction in uplift forces that occurs with a given coring size and pattern is needed. The data presented in Table 4.8 (and in Section 5.2.1), however, makes it apparent that entrapped air effects are a first order problem and deserve serious consideration. One core per cavity is suggested as a beginning point for further investigation.

The coring pattern used should account for reinforcing steel in the bridge deck, to avoid compromising the integrity of the deck. Locating reinforcing steel for multiple core locations is the largest drawback for rapid deck venting. This approach is more feasible if performed in a controlled fashion a noticeable period prior to hurricane season. The drawback of performing the approach a noticeable period before hurricane season is more bridges would have to be cored, which could come at a fairly large expense.

5.3.2 Connection Between Substructure and Superstructure Installed from Deck

Providing a connection between the superstructure and substructure that can be installed from the bridge deck seems promising. In this section the simulation generated wave loads from Chapter 4 were used to evaluate a straightforward, installed from above, connection scheme. Figure 5.1 shows one of many possible approaches to connect the substructure to the superstructure. In Figure 5.1 a hole is cored through the deck just to the edge of but not through the diaphragm and the pile cap is also cored to a depth sufficient to embed the rod for anchorage. A plate is fastened to the top of the deck, completing the anchoring approach.

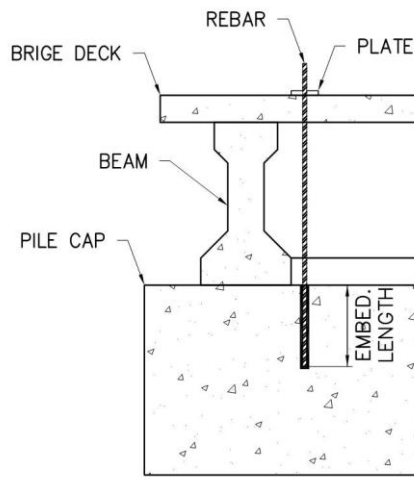


Figure 5.1. Example retrofit schematic.

Many combinations of the Figure 5.1 concept are possible. Generally speaking, a long slender object such as a threaded rod, rebar, cable, or tendon is fastened to the top of the bridge deck and also to the bridge superstructure. Attachment of the threaded rod, rebar, cable, or tendon to the existing bridge is only considered in general terms in this report as this will depend on bridge geometry, owner preferences, bridge condition, and several other factors. In some cases, the limiting factor will be the bridge itself and not the retrofit method. With known design loads, bridge attachment details would be straightforward for a

given bridge provided an assessment of the in-situ properties were available. A series of options are presented in the remainder of this section that provide situation dependent retrofit guidance.

Option 1: If the concrete deck and substructure are of a quality to handle the design storm surge loading, a minimum number of large rods, tendons, or cables should be used for expediency. This is the most desired case, but requires higher loads per anchor location to be carried by the bridge deck and substructure.

Option 2: If the concrete deck and substructure are of a quality to handle the design storm surge loading so long as it is distributed more evenly, several smaller rods, tendons, or cables could be used. This will require more time than Option 1, but could provide for an effective retrofit in some situations if enough time is available.

Option 3: If the concrete deck and substructure cannot handle but a portion of the design storm surge loading that is anticipated using rods, tendons, or cables that could be installed within the time available, fuse elements (e.g. Figure 2.1) could be installed to protect the bridge superstructure if the actual event is smaller than the design event, but also prevent damage to the substructure if the loads that would damage the substructure do occur. This option has some merit for some applications, but probably is more valuable if installed a fair amount of time before an anticipated disaster event.

Option 4: Install anchorage locations for the deck and substructure well ahead of any anticipated storm event, and leave the rod, tendon, or cable un-connected at one end. Immediately before the event, the free end of the system could be connected, thus mobilizing its load carrying capacity. There are numerous approaches that could be used in this case. Examples include, but are in no way limited to: two threaded rods where a turnbuckle (or fuse element) is installed between them immediately before the anticipated surge event; a cable that is tensioned from the bridge deck immediately before the anticipated surge event, or a connection with a shear pin that is placed immediately before the surge event. Option 4 requires the most initial investment, but could be deployed the fastest prior to a surge event.

5.3.2.1 Design Loads

Table 5.1 shows the maximum anchorage forces for a span superstructure weighing 300,000 lbs. The total shear and lift reactions represent the forces to be transmitted from the superstructure to the substructure by the retrofit anchors. The shear forces are the maximum horizontal load applied to the entire span by the wave action. No decrease due to frictional resistance was considered. The lift forces represent the difference between the upward lift applied to the span by the wave action and the downward gravitational force. In Cases 3, 5, 6, 7, and 8, the gravity load exceeds the wave load, resulting in no retrofit anchor axial loads.

Table 5.1. Maximum calculated total anchorage and girder anchorage for simply supported span

Case	Category	Total Reaction (kips)		Max Girder (kips)	
		Shear	Lift	Shear	Lift
1		117	87	24	24
2		84	48	18	18
3	--	141	0	42	39
4		156	177	30	51
5	I	81	0	24	3
6		90	0	27	0
7	II	66	0	18	0
8		84	0	21	9
9	III	120	3	27	21
10		162	165	36	60
11	IV	201	207	45	75
12		264	267	57	96
13	V	327	327	69	123
14		372	375	78	135

--1 kip = 1,000 lb

5.3.2.2 Design Load Evaluation

A meaningful contribution of this research to rapid retrofit is believed to be using the maximum reaction forces calculated by the WFS (Table 5.1) to determine the amount of capacity needed for a rapidly deployable system so end users could have a feasibility assessment. Rebar was used for the investigation. The investigation assumes that a specific design detail can be developed such that the connection strength is controlled by ductile failure of the rebar steel (i.e. Option 1 or Option 2 presented earlier).

Table 5.2 shows the number of ASTM A615, Grade 60 reinforcing bar anchors required to transmit the wave loads from the deck to the pier cap. The calculation is based on ACI 318-11 Appendix D requirements, and assumes total load is distributed evenly among all anchors, and that the maximum lift and shear are assumed to act simultaneously.

For all Category I and II storms (Cases 5 to 8) and Category III, Case 3, the lift forces due to wave loading do not exceed the weight of the bridge span. Thus, the anchor count represents the number to transmit the entire shear load assuming no frictional forces. These generally vary from 4 to 6.

For all other cases, the size of the maximum wave and surge lift forces exceed the weight of the bridge span. As such, the anchors are required to transmit both tensile and shear forces. The required number of anchors increases with storm category and varies from eight #8 bars for Category III storms to twelve #10 bars for a Category V storm. While these results indicate that steel anchors can provide the necessary tie down strength for a wide variety of storm loadings, the number of anchors required may be prohibitive in some cases.

Because of bridge flexibility, the distribution of the anchor loads may differ significantly from the uniform distribution assumption. The maximum anchor size required will depend on the number and placement of anchors, as well as the structural details of the bridge superstructure. In the present case, for example, suppose twelve #7 bars (two per girder) were chosen to retrofit a Category III storm such as Case 10 of Table 5.2. From Table 5.1, the uniform assumption results in approximately 13.5 kip lift and shear loads for each

anchor (162 to 165 kips divided by 12). The maximum single girder load shows that some anchors will be subject to 30 kip lift and 18 kip shear loads. The maximum single girder load would require installation of #9 rebar.

Table 5.2. The approximate number of anchors required based on steel strength

Case	Category	Bar Size							
		#3	#4	#5	#6	#7	#8	#9	#10
1	--	38	22	14	10	8	6	6	4
2		26	16	10	8	6	4	4	4
3		40	22	16	10	8	6	6	4
4		56	32	20	14	12	8	8	6
5	I	24	14	10	6	6	4	4	2
6		26	14	10	8	6	4	4	4
7	II	20	12	8	6	4	4	4	2
8		24	14	10	6	6	4	4	4
9	III	34	20	12	10	8	6	4	4
10		56	32	20	14	12	8	8	6
11	IV	70	38	26	18	14	10	8	6
12		90	50	32	24	18	14	10	8
13	V	112	62	40	28	22	16	14	10
14		128	70	46	32	24	18	14	12

--Generally speaking, the bar diameter (in) is the bar size divided by 8.

For the Biloxi Bay Bridge, twelve anchor locations would provide one anchor at each end of each girder (six girders were present per span as shown in Figure 4.1.) Installing twelve anchors per bridge span would be more time consuming than coring the decks to relieve entrapped air forces. Based on the estimates provided in Section 5.3.1, it would take one crew of three people over one day to anchor one bridge span. If the number of anchors required were reduced to six (one anchor on each end of three of the six girders placed in a somewhat symmetric pattern), the process becomes more feasible.

Using tie down anchors to protect against Category IV and V storms may not be feasible unless Option 4 is used. The approach, however, appears feasible for smaller storm events such as Category I and perhaps Category II. A rapid retrofit anchoring approach beyond Category II should be approached with caution based on the information collected in this report.

5.4 Rapid Retrofit Summary

The rapid retrofit evaluation in this chapter indicates that deck venting and superstructure anchoring may be effective options that merit closer evaluation. When comparing the relative merits of coring and anchoring, deck coring presents a much more compelling rapid retrofit option. The calculations performed in Chapter 3 provide support for the generally accepted notion that entrapped air is a first order effect on the response of bridge spans subject to wave loading. Effective venting can reduce deck vertical loads by 40

to 100% of the span weight. The effect of such reductions loosely transforms Category V hurricane lift loads to the more realistically manageable Category III levels. In turn, Category III wave loading with venting is reduced and no longer overcomes gravity loads. On the other hand, at this point it is hard to envision a rapidly deployable anchoring design that would provide effective bridge protection for low-lying bridges with dozens and dozens of spans found along the Gulf Coast. Installation of a single #9 ASTM A615, Grade 60 rebar anchor, assuming sufficient embedment to ensure ductile anchor failure, provides approximately 32 kips pure shear and 58 kips pure tensile strength. The aforementioned level of anchoring is required to carry the local maximum girder loads for Category III surge and wave loading, making the sufficiency of rapidly anchoring for more severe storms unlikely.

CHAPTER 6 – SUMMARY CONCLUSIONS AND RECOMMENDATIONS

6.1 Summary

The primary objective of the research presented in this report was to perform finite element modeling to determine forces on highway bridges as a result of storm surge and use these forces to investigate the feasibility of rapid retrofit techniques to prevent failure. Both objectives were met. The retrofit evaluation performed is a fairly traditional assessment that makes use of fundamental principles. The finite element modeling (FEM) approach, however, is fairly unique and has applications beyond those presented in this report.

The Texas, Louisiana, Mississippi, Alabama, and Florida DOT's were contacted to obtain information to aid in meeting the research objectives. A variety of approaches and philosophies related to storm surge were identified, and the feedback from bridge engineering experts within state DOT's was very helpful and provided direction for the research. In addition, the *AASHTO Subcommittee on Bridges and Structures* was contacted, and they provided additional guidance beyond the published *Guide Specifications* (AASHTO 2008), including the *Retrofit Manual* (a working document presented in Modjeski and Masters (2008) provided to the research team for use). The *Guide Specifications* were used as the primary evaluator of the FEM performed in this project, while the *Retrofit Manual* was the primary document used to guide rapid retrofit guidance.

A three component FEM approach (Figure 3.2) was developed and used in this research; the components are a structural model, a wave load model, and an element data transfer model. The structural model is comprehensive but is not unique and can be performed with a variety of commercially available FEM software packages (Abaqus was used in this project). The wave load model (named wave load software (WLS) by the authors) is much more unique and is a key component to this project. The WLS was written in Fortran (other languages could be used) and is a set of software routines that generates wave based surface and body forces based on a wave theory model that has core functionality that is independent of the FEM model. The element data transfer model was also written in Fortran (other languages could be used) to communicate problem specific information between the FEM structural model and the WLS. A third program (Python) was used to submit the multiple load cases and to extract numerical results in an automated manner.

The FEM based wave load modeling approach shown in Figure 3.2 approach was applied to test data from the 1:5 scale replication of a typical Escambia Bay Bridge span made available by Oregon State University. These simulations were used to select wave force model constants that were subsequently applied to a full scale representation of a Biloxi Bay Bridge span for fourteen storm events representing five storm categories. Results of these simulations were very promising, and they compared favorably with predicted load envelopes predicted by the *Guide Specifications*. Results from the WLS simulations were then used for retrofit design where the *Retrofit Manual* was initially used as a guide.

The FEM based numerical modeling developed in this report is a very efficient computational tool for a multi-phase transient problem in three dimensions. Computational time per simulation is measured in minutes on a personal computer (e.g. the fourteen load cases in Tables 4.1 and 4.5 were performed in a single job submittal through Python and all computations were performed on a personal computer in approximately two hours). The

Figure 3.2 computational framework could prove very useful for state DOT's when coupled with scaled testing at a facility such as the O.H. Hinsdale Wave Research Laboratory (or equivalent).

Results from the first generation models within the WLS are very promising, but equally (if not more) useful is that the wave theory models can be modified with moderate effort as more information becomes available from ongoing and future research efforts. One drawback of some numerical modeling efforts is they are totally dependent on the body of knowledge at the time the modeling was conducted. The WLS can be updated over time within the same operational framework as more information becomes available. An additional advantage of the modular nature of this project is that different groups can implement the same overall framework with user specific preferences on software types, wave theory models, and similar. This could be important as, generally speaking, all state DOT's have a similar mission but they each operate under different policies, laws, and they serve people with varying positions on social, environmental, and similar issues. A modular approach could allow different DOT's to utilize the computational tool in a manner that is feasible for and compatible with their system.

6.2 Conclusions

- Guidance for wave loading on coastal bridges is less mature than that for wave loading on other structures such as offshore platforms. Coastal bridge engineers could benefit from additional research on wave loading due to storm surge. It is noteworthy, however, that considerable efforts have occurred in the past few years.
- The computational framework represented by Figure 3.2 was successful and the results are very promising. Use of this computational framework alongside scaled testing has the potential to enhance understanding of coastal bridges subjected to storm surge.
- The WFS software approach was developed using fundamental, but well established, concepts of wave motion and wave loading, and was calibrated using experimental data from a set of 11 OSU experiments. The resulting approach with no special calibration was then compared to the AASHTO (2008) *Guide Specification* design equations that were developed based on experimental work and wave load formulations besides that conducted by OSU. The computed results were found to be in very reasonable agreement, providing strong indication of the relevance of the modeling approach.
- The computational approach demonstrated that physics based relationships used in Chapter 3 did not fully capture the vertical loads measured by Oregon State University when typical inertia and drag coefficients were used. Behaviors were captured through introduction of an entrapped air factor which on average resulted in a peak uplift equal to 80% of the span weight.
- Rapid retrofit of a highway bridge to resist uplift forces due to storm surge appears to be feasible for some storm events depending on the retrofit method employed. Venting the bridge deck to reduce forces due to entrapped air appears to be the most viable rapid retrofit approach. Anchoring the superstructure to the substructure in a rapid manner appears more useful for lower category storms (i.e. Category I and Category II) than for higher category storms.

- The WFS and AASHTO *Guide Specifications* approaches were in agreement based on a linear regression fit of data produced by each method when the *Guide Specification* equations used $\%AIR = 20\%$. The WFS exceeded AASHTO when $\%AIR$ was less than 20% and AASHTO exceeded WFS when $\%AIR$ was more than 20%. The WFS was enveloped by the *Guide Specifications* and showed that $\%AIR$ values on the lower end of the allowable AASHTO scale were predicted by finite element modeling. The same finite element modeling showed the Biloxi Bay Bridge would fail in Hurricane Katrina as it did.

6.3 Recommendations

- State DOT's should consider the rapid retrofit guidance provided in Chapter 5 for storm events that are likely to separate bridge spans from their substructure due to lateral and uplift forces. Rapid retrofit has the potential to prevent bridge failure for some storm events.
- Perform scaled testing of bridge decks to further assess the feasibility of rapid venting for disaster mitigation. Testing at a facility such as the O.H. Hinsdale Wave Research Laboratory (or equivalent) where bridge decks are subjected to a series of simulated storms without vented decks and the experiment is repeated for the same deck configurations with differing amounts of venting due to coring circular holes is suggested. The decks should be instrumented to determine the reduction in vertical reaction forces due to deck venting, as well as the load distribution change resulting from deck venting. A test plan where different coring patterns, different vented areas, and different girder-diaphragm cavity volumes are investigated is recommended.
- Use the full scale data collected in the previous recommendation to improve understanding of the physics based relationships currently in the WFS and if warranted, update the WFS to improve the drag and inertia coefficient formulations.
- Use the WFS model to investigate the rigid body assumption used by the *Guide Specifications* when calculating the *Guide's* Design Case I extreme event maximum single girder loading. Modeling a series of different deck stiffnesses, girder stiffnesses, girder spacings, and diaphragm spacings is recommended.
- Evaluate impact loads for vertically unconstrained retrofit approaches. Specifically investigate impact load effects on pre-stressed concrete girders. Impact forces could be quite large based on the modeling performed for this report.

CHAPTER 7 – REFERENCES

- AASHTO. (2010). *AASHTO LRFD Bridge Design Specifications*, 5th Edition. American Association of State Highway and Transportation Officials, Washington, DC.
- AASHTO. (2008). *Guide Specifications for Bridges Vulnerable to Coastal Storms*. American Association of State Highway and Transportation Officials, Washington, D.C.
- ACI 318 (2011). *Building Code Requirements for Structural Concrete and Commentary (ACI 318-11)*. American Concrete Institute, Farmington Hills, MI.
- Aguiniga, F., Matakis, K., Estrada, H., Sai, J., Leelani, P., Sheldon, J. (2008). *Synthesis of Wave Load Design Methods for Coastal Bridges*. Report FHWA/TX-07/0-5516-1, pp. 83.
- Bea, R.G., Xu, T., Stear, J., and Ramos, R. (1999). "Wave Forces on Decks of Offshore Platforms," *Journal of Waterway, Port, Coastal, and Ocean Engineering*, 125(3), 136-144.
- Bea, R.G., Iversen, R., Xu, T. (2001) "Wave-in-Deck Forces on Offshore Platforms," *Journal of Offshore Mechanics and Arctic Engineering*, 125:10-21
- Bergeron, A. (2007). "Contractor Ahead of Schedule on Biloxi Bay Bridge Erection," *Engineering News Record*. (Accessed March 2, 2010).
<<http://enr.construction.com/news/transportation/archives/070503.asp>>
- Bradner, C. (2008). *Large-Scale Laboratory Observations of Wave Forces on a Highway Bridge Superstructure*. MS Thesis, Oregon State University, pp. 150.
- Bradner, C., Schumacher, T., Cox, D., and Higgins, C. (2008), "Large-Scale Laboratory Measurements of Wave Forces on Highway Bridge Superstructures," *Proceedings of Coastal Engineering 2008-31st International Conference*, Aug 31-Sept 5, Hamburg, Germany.
- Bradner, C., Schumacher, T., Cox, D., Higgins, C. (2011). "Experimental Setup for a Large-Scale Bridge Superstructure Model Subjected to Waves," *Journal of Waterway, Port, Coastal, and Ocean Engineering*, 137(1), 3-11.
- CEM (2006). *Coastal Engineering Manual*. U.S. Army Corps of Engineers, EM1110-2-110.
- Chen, Q., Wang, L., Zhao, H. (2009). "Hydrodynamic Investigation of Coastal Bridge Collapse during Hurricane Katrina." *Journal of Hydraulic Engineering*, 135(3), 175-186.
- Coastal Engineering Research Center (1984). *Shore Protection Manual*. Fourth Edition, Vol. 1 and 2, Waterways Experiment Station, Vicksburg, MS.
- Dean, R.G., Dalrymple, R.A. (1991). *Water Wave Mechanics for Engineers and Scientists*. Singapore; Teaneck, NJ, World Scientific.

Denson, K.H. (1978). *Wave Forces on Causeway-Type Coastal Bridges*. Final Report, Water Resources Research Institute, Mississippi State University.

Denson, K.H. (1980). *Wave Forces on Causeway-Type Coastal Bridges: Effects of Angle of Wave Incidence and Cross-Section*. Final Report MSHD-RD-80-070, Water Resources Research Institute, Mississippi State University.

Denson, K.H. (1981). *Pressures on Coastal Bridges Due to Normal Incidence Waves*. Final Report, Water Resources Research Institute, Mississippi State University.

DesRoches, R. (2006). *Hurricane Katrina: Performance of Transportation Systems*. Monograph No. 29, Technical Council on Lifeline Earthquake Engineering, American Society of Civil Engineers, pp. 62.

Douglass, S.L., Chen, Q., Olsen, J.M., Edge, B.L., Brown, D. (2006). *Wave Forces on Bridge Decks*. Final Report Prepared for U.S. Department of Transportation and Federal Highway Administration Office of Bridge Technology, Washington, D.C.

Douglass, S.L., Krolak, J. (2008). *Highways in the Coastal Environment*. Final Report FHWA-NHI-07-096 Prepared for U.S. Department of Transportation and Federal Highway Administration Office of Bridge Technology, Washington, D.C.

FEMA. (2005). *Coastal Construction Manual*, 3rd Edition. Federal Emergency Management Administration, Jessup, MD.

Isaacson, M., Prasad, S. (1994). "Wave Slamming on a Horizontal Circular Cylinder." *International Journal of Offshore and Polar Engineering*, 4(2), 81-88.

Jin, J., Jeong, C., Chang, K.A., Song, Y.K., Irish, J., and Edge, B. (2008). *Site Specific Wave Parameters for Texas Coastal Bridges: Final Report*. Report 0-6063-1, Texas Department of Transportation, Austin, TX.

Kaplan, P. and M. Silbert (1976). *Impact forces on platform horizontal members in the splash zone*, Offshore Technology Conference, 3 May – 6 1976, Houston, Texas.

Kaplan, P. (1992). *Wave Impact Forces on Offshore Structures: Re-Examination and New Interpretations*, Offshore Technology Conference, 4 May – 7 May 1992, Houston, TX.

Kaplan, P., J.J. Murray, et al. (1995). *Theoretical analysis of wave impact forces on platform deck structures*, 14th International Conference on Offshore Mechanics and Arctic Engineering, Copenhagen, Denmark.

Kjeldsen, S.P., Myrhaug, D. (1979). "Breaking Waves in Deep Water and Resulting Wave Forces." *Proceedings of the Offshore Technology Conference*, Society of Petroleum Engineers, Richardson, TX.

Krolak, J. (2007). "FHWA/AASHTO Wave Task Force-Plan of Action", *A Briefing for Federal Highway Administration*, 14 Feb 2007, Washington, DC.

McConnell, K.J., Allsop, N.W.H., Cuomo, G., Cruickshank, I.C. (2003). "New Guidance For Wave Forces on Jetties in Exposed Locations," *Proceedings of the Sixth Conference on Coastal and Port Engineering in Developing Countries*, Colombo, Sri Lanka, pp. 1-20.

Modjeski and Masters. (2008). *Handbook of Retrofit Options for Bridges Vulnerable to Coastal Storms*. Report Submitted to Federal Highway Administration for Task Order DTFH61-06-T-70006, 90% Complete, Limited Use Document, pp. 60.

Morison, J.R., O'Brien, M.P., Johnson, J.W., and Schaaf, S.A. (1950). "The Force Exerted by Surface Waves on Piles," *Petroleum Transactions*, 189, 149-157.

NRF. (2008). *National Response Framework*. US Department of Homeland Security, Washington, DC, pp. 82.

O'Connor, J. (2005). *US 90 over Biloxi Bay Between Harrison and Jackson Counties, Mississippi*. Multidisciplinary Center for Earthquake Engineering Research-MCEER, University of Buffalo. (Accessed February 24, 2012)
<<http://mceer.buffalo.edu/research/Reconnaissance/Katrina8-28-05/05BiloxiBay/>>

Ramey, G., Sawyer III, A., Melville, J. (2008). *Hurricane Surge/Surface Wave Forces on Deck-Girder Bridges and Design/Retrofit Options for These Bridges*. Final Report. Alabama Department of Transportation, Auburn, AL.

Robertson, I.N., Riggs, H.R., Yim, S.C.S., and Young, Y.L. (2007). "Lessons from Hurricane Katrina Storm Surge on Bridges and Buildings." *Journal of Waterway, Port, Coastal, and Ocean Engineering*, 133(6), 463-483.

Sarpkaya, T., M. Isaacson, et al. (1981). *Mechanics of wave forces on offshore structures*, Van Nostrand Reinhold New York.

Sarpkaya, T. (2010). *Wave Forces on Offshore Structures*. Cambridge University, New York, NY.

Schumacher, T., Higgins, C., Bradner, C., and Cox, D. (2008). "New Innovative Large-Scale Laboratory Setup for Experiments on Highway Bridge Superstructures Exposed to Wave Forces," *Proceedings of the 2008 Concrete Bridge Conference*, May 4-7, St. Louis, MO.

Schumacher, T., Higgins, C., Bradner, C., Cox, D. Yim, S. (2008b). "Large-Scale Wave Flume Experiments on Highway Bridge Superstructures Exposed to Hurricane Wave Forces," *Proceedings of the Sixth National Conference on Bridges & Highways-Seismic Technologies for Extreme Loads*, July 27-30, Charleston, S.C.

Sheppard, D.M., and Marin, J. (2009). *Wave Loading on Bridge Decks*. Final Report BD545-58, Florida Department of Transportation, Tallahassee, FL.

Sibson, R. (1981). *A Brief Description of Natural Neighbor Interpolation*. Interpreting multivariate data V. Barnett. New York, John Wiley & Sons. 21: 21-36.

White, T.D., Truax, D.D., McAnally, W.H., Eamon, C.D., Gullett, P.M., Cole, H., Fitzpatrick, P., Jackson, R., Lau, Y., Li, Y. Bhat, S. and Skalko, S.V. (2006). *Coast in the Eye of the Storm-Hurricane Katrina: August 29, 2005*. Technical Report No. CMRC 06-1, Construction Materials Research Center, Mississippi State University.



"An Industry, Agency & University Partnership"

